MULTI-DIMENSIONAL IMAGING OF CELL AND EXTRACELLULAR MATRIX INTERACTIONS DURING CORNEAL WOUND HEALING

APPROVED BY SUPERVISORY COMMITTEE

W. Matthew Petroll, Ph.D.

Robert Eberhart, Ph.D.

David Schmidtke, Ph.D.

Venkateswara Mootha, M.D.

Chet Xu, Ph.D.

DEDICATION

I would like to thank my Ph.D. advisor and mentor, Dr. W. Matthew Petroll, for his patience, mentorship, and kindness throughout my Ph.D. studies. I would also like to thank the members of my Graduate Committee, Dr. Robert Eberhart, Dr. David Schmidtke, Dr. Vinod Mootha, and Dr. Chet Xu, for their time, feedback, and expertise in guiding me during my Ph.D. research. I also would not have been able to complete the following dissertation work without Kyle and Miguel, who have been incredibly helpful with experiments, or Rossella and Vindhya, whom I've been able to confide in and have as part of my lab "family."

I would also like to thank my dearest friends Anna and Joanne for making sure I never doubt myself from high school to now. AG, thank you for giving me your endless support throughout my research; your love, thoughtfulness, and generosity have been invaluable. My mother Marjan and sister Sanam for being lending ears, and encouraging my endeavors.

I want to dedicate this dissertation to my Dad, whose love, loyalty, and support has been more than I ever could have asked for. I couldn't have made it this far without you. Thank you for always believing in me.

MULTI-DIMENSIONAL IMAGING OF CELL AND EXTRACELLULAR MATRIX INTERACTIONS DURING CORNEAL WOUND HEALING

by

POURISKA BIGVAND KIVANANY

DISSERTATION

Presented to the Faculty of the Graduate School of Biomedical Sciences

The University of Texas Southwestern Medical Center at Dallas

In Partial Fulfillment of the Requirements

For the Degree of

DOCTOR OF PHILOSOPHY

The University of Texas Southwestern Medical Center at Dallas

Dallas, Texas

May, 2018

MULTI-DIMENSIONAL IMAGING OF CELL AND EXTRACELLULAR MATRIX INTERACTIONS DURING CORNEAL WOUND HEALING

Pouriska Bigvand Kivanany, Ph.D.

The University of Texas Southwestern Medical Center at Dallas, 2018

Supervising Professor: Walter Matthew Petroll, Ph.D.

Corneal haze is a leading cause of blindness, and may occur after injury, surgery, or chemical burns. The cornea's thickest layer, the stroma, accounts for two-thirds of the eye's refractive power, and contains highly aligned collagen fibrils needed for transparency. Stromal cells, or keratocytes, help maintain the extracellular matrix (ECM). After injury or surgery, keratocytes within the wound undergo apoptosis, while keratocytes in the wound margin transform and activate into fibroblasts and myofibroblasts, leading to contraction, deposition of fibrotic ECM, and haze. Thus, spatial and temporal investigations of cell/ECM interactions are needed for further insight into this healing process. In this research, freeze-injury (FI), lamellar keratectomy (LK), and photorefractive keratectomy (PRK) in vivo rabbit

models are used, and cell/ECM interactions are tracked using an in vivo confocal microscope as well as second harmonic generation (SHG) and multiphoton imaging. These in vivo models revealed that in the short term, intrastromal cells migrated in parallel to the collagen lamellae, while cells over the stromal wound bed transformed to myofibroblasts and were randomly arranged. Stromal haze initially increased after injury, but gradually decreased over time. Long term, collagen became more organized, more quiescent cells replaced myofibroblasts, and normal stromal thickness regenerated (after keratectomy) below the ablation surface. Punctate F-actin labeling was detected along cells that co-aligned with native and regenerated collagen, suggesting critical involvement of cell/ECM interactions in stromal remodeling and regeneration. Collagen lamellae appeared to provide a template for fibroblast patterning during both intrastromal migration and stromal regrowth. Overall, cells appear to regenerate and remodel the ECM to produce a lamellar structure similar to the native stroma. These results provide novel insights into the mechanisms of cell/ECM interactions involved in various stages of wound healing in the cornea, and may lead to potential therapies that prevent or reverse fibrosis in the clinic.

TABLE OF CONTENTS

PRIOR PUBLICATIONS

Kivanany, PB, Grose, KC, Tippani, M, Su, S, Petroll, WM. Assessment of Corneal Stromal Remodeling and Regeneration after Photorefractive Keratectomy. Invest Ophthalmol Vis Sci. *Submitted.*

Kivanany, PB, Grose, KC, Petroll, WM. Temporal and spatial analysis of stromal cell and extracellular matrix patterning following lamellar keratectomy. Exp Eye Res, 2016.153: p. 56-64.

Petroll, WM, **Kivanany, PB**, Hagenasr, D, Graham, EK. Corneal Fibroblast Migration Patterns During Intrastromal Wound Healing Correlate With ECM Structure and Alignment. Invest Ophthalmol Vis Sci, 2015. 56(12): p. 7352-61.

Miron-Mendoza, M, Graham, E, **Kivanany, P**, Quiring J, Petroll WM. The Role of Thrombin and Cell Contractility in Regulating Clustering and Collective Migration of Corneal Fibroblasts in Different ECM Environments. Invest Ophthalmol Vis Sci, 2015. 56(3): p. 2079-90.

LIST OF FIGURES

LIST OF TABLES

LIST OF SUPPLEMENTAL FILES

LIST OF DEFINITIONS

EBM – Epithelial Basement Membrane

ECM – Extracellular Matrix

PRK – Photorefractive Keratectomy

LASIK – Laser Assisted In Situ Keratomileusis

TGF-β – Transforming Growth Factor-Beta

FI – Freeze Injury

LK – Lamellar Keratectomy

UV – Ultraviolet Light

PDGF – Platelet Derived Growth Factor

TSCM –Tandem Scanning Confocal Microscope

HRT-RCM – Heidelberg Retinal Tomograph with Rostock Corneal Module

NA – Numerical Aperture

CMTF – Confocal Microscopy Through-Focusing

SHG – Second Harmonic Generation

ARVO – Association for Research in Vision and Ophthalmology

DMSO – Dimethyl Sulfoxide

PBS – Phosphate Buffered Saline

DAPI – 4',6-diamidino-2-phenylindole

ANOVA – Analysis of Variance

RCFM – Retrocorneal Fibrous Membrane

OCT – Optical Coherence Tomography

PMMA – poly(methyl methacrylate)

PDMS – polydimethylsiloxane

MEM – Minimal Essential Media

NaOH – Sodium Hydroxide

DMEM – Dulbecco's Modified Eagle's Medium

RPMI – Roswell Park Memorial Institute

NRK – Primary Rabbit Corneal Keratocytes

α-SMA – Alpha-Smooth Muscle Actin

FITC – Fluorescein Isothiocyanate

DIC – Differential Interference Contrast

SEM – Scanning Electron Microscopy

Na – Sodium

kV – Kilovolts

OI – Orientation Index

SF – Serum Free

SR – Slow Release

Pre-Op – Pre-Operative

Epi – Epithelium

BL – Basal Lamina

Endo – Endothelium

DTAF – (5([4,6-dichlorotriazin-2yl]amino)fluorescein)

FT – Fourier Transform

OCTS – Optimal Cutting Temperature Solution

TRITC – Tetramethylrhodamine

IL-1 – Interleukin-1

FGF-1 – Fibroblast Growth Factor-1

FGF-2 – Fibroblast Growth Factor-2

TUNEL – Terminal Deoxynucleotidyl Transferase-Mediated dUTP Nick End Labeling

MMPs – Matrix Metalloproteinases

CHAPTER ONE
Introduction

1.1 BACKGROUND

1.1.1 Cornea Structure and Function

The cornea is the transparent, outermost tissue of the eye, and is responsible for two-thirds of the eye's refractive power.[4] The cornea is composed of three primary layers: the epithelium, stroma, and endothelium (Figure 1.1).[5] The epithelium acts as a barrier against antigens and microbes, and consists of stratified squamous cells (anterior) and columnar, or basal, cells (posterior).[6, 7] An acellular epithelial basement membrane (EBM), consisting of a variety of proteins such as collagen, laminin, and proteoglycans, connects the epithelium with the stroma.[8, 9] The Bowman layer (posterior to the EBM), found only in primates, is acellular and composed of random collagen fibrils.[10]

The corneal stroma is 90% of the total cornea thickness, and is a target for vision correction procedures.[4] Keratocytes reside in between the lamellae, and are primarily responsible for maintaining the extracellular matrix (ECM) in the cornea.[11-13] The corneal stroma consists mostly of Type I collagen fibers (about 25 to 35 nm in diameter), which are uniformly sized and spaced, and are organized into approximately 200 lamellae, or layers of collagen fibers, throughout the stroma (Figure 1.1).[14, 15] The highly organized arrangement of the collagen fibers is important for transparency and proper light scattering for transmittance

to the retina. The endothelium is composed of a single cell layer that is bound to a basement membrane called Descemet's membrane, and maintains dehydration of the cornea.[7, 10]

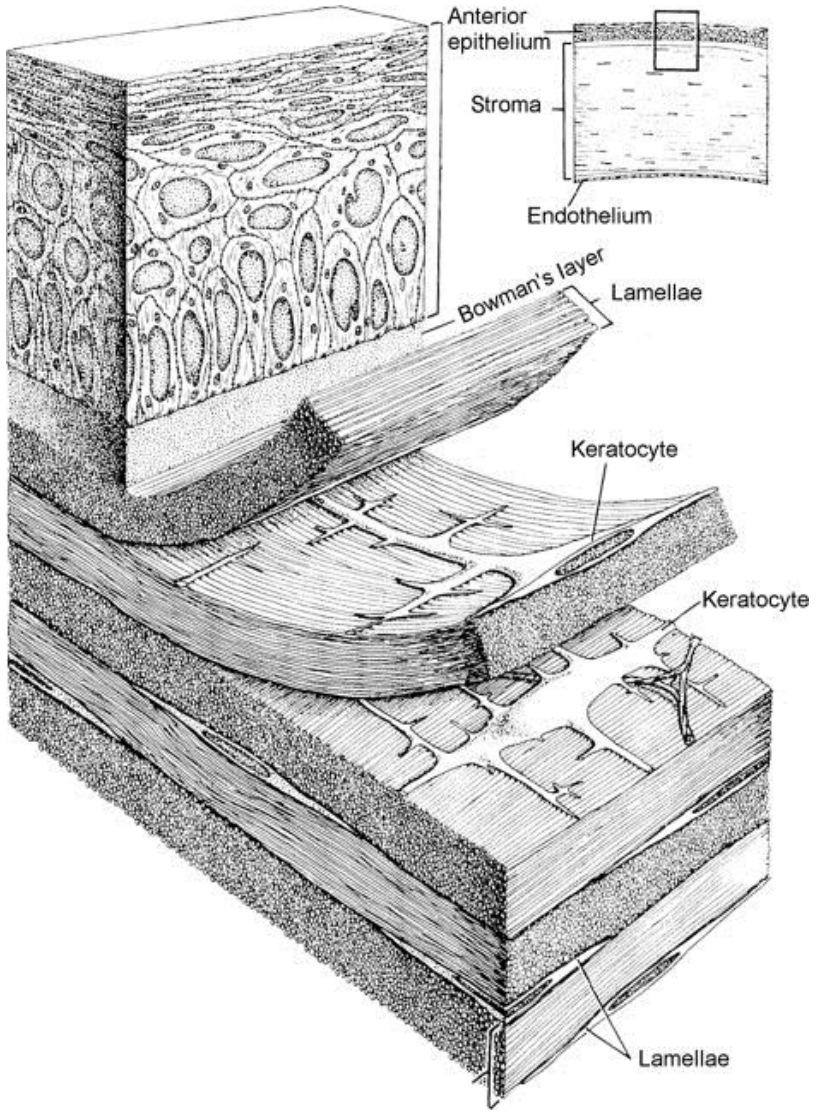

Figure 1.1. Corneal structure revealing collagen lamellae and cell organization.[1]

1.1.2 Corneal Wound Healing

Stromal keratocytes play a central role in mediating the corneal response to injury or refractive surgery.[4] During wound healing, quiescent corneal keratocytes surrounding the area of injury generally become activated, proliferate, and transform into a fibroblastic phenotype.[16, 17] In certain wound types, fibroblasts further differentiate into myofibroblasts, which generate stronger forces and synthesize a disorganized fibrotic extracellular matrix.[18, 19] Following vision correction procedures such as photorefractive keratectomy (PRK) or laser assisted in situ keratomileusis (LASIK), cellular force generation and fibrosis can alter corneal shape and reduce corneal transparency. In addition, a decrease in the concentration of keratocyte-specific "corneal crystallin" proteins has been associated with an increase in cellular light scattering during wound healing, which also contributes to clinical haze.[20, 21]

The transparency of the cornea is heavily dependent on its highly organized collagen structure.[22] Cell-matrix mechanical interactions likely play a key role in development, maintaining corneal transparency, and facilitating wound healing.[23, 24] In vitro studies conducted previously in Dr. Petroll's lab reveal growth factors found during wound healing and changes in ECM stiffness can modulate cell phenotype, migration rate, and morphology.[25-27] Growth factors also have been shown to influence cell-induced ECM reorganization.[27] Multiple studies have reported that myofibroblast transformation of corneal keratocytes during wound healing is mediated by transforming growth factor beta (TGF-β) in combination with other growth factors;[16, 18, 28-32] however, there is a gap in understanding of how different biophysical signals regulate cell patterning and mechanical differentiation

during different phases of corneal wound healing. The goal of this dissertation is to address this gap by using novel multi-dimensional imaging techniques to determine the temporal and spatial relationship between cell and ECM patterning during the migratory, fibrosis, remodeling, and/or regeneration phases of wound healing. These imaging techniques include in vivo confocal microscopy and second harmonic generation (SHG) and multiphoton imaging. In vivo confocal microscopy allows time-dependent assessing of cell reflectivity and morphology as well as measurements of corneal sub-layer thickness and stromal haze. SHG and multiphoton imaging allows for simultaneous 3-D imaging of collagen and cell patterning within in situ labeled corneal tissues using laser scanning confocal microscopy. To assess these processes, the following in vivo rabbit wound healing models are used: freeze-injury (FI), lamellar keratectomy (LK), and photorefractive keratectomy (PRK). Preliminary studies using an in vitro model of aligned collagen have also been implemented to better isolate specific growth factor effects on keratocyte morphology, behavior, and patterning.

1.2 NEED FOR MULTIPLE WOUND HEALING MODELS

1.2.1 Intrastromal Migration Models

1.2.1.1 In Vivo Transcorneal Freeze Injury (FI)

Both PRK and LASIK result in a region of keratocyte death at and beneath the laser-treated area.[33-35] Stromal cell death can also be induced by toxic injury [36, 37] as well as UV cross-linking of the cornea in keratoconus patients.[38-40] Ideally, repopulation of damaged stromal tissue following these insults should occur via intra-stromal migration of keratocytes

from the surrounding stromal tissue without generation of contractile forces that could disrupt the organized collagen architecture or the production of fibrotic ECM, which can reduce transparency. To better understand how topography and patterning of the ECM affects cell migratory patterns into the wound site within the stroma, a FI model will be used to induce cell death in the stroma without removal of the EBM or ECM. The EBM inhibits growth factors from the tears and epithelium from penetrating into the stroma, allowing cell migratory patterns to be assessed purely in response to the scaffolding and topography of the ECM.

1.2.1.2 Aligned Collagen In Vitro Model

During corneal wound healing, several growth factors are involved, including platelet derived growth factor (PDGF) and TGF-β, from the tears and epithelial cells.[41-44] Previous studies reveal that PDGF induces a migratory phenotype and dendritic, narrow cell morphologies in stromal keratocytes.[27] TGF-β has been shown to transform corneal keratocytes into myofibroblasts, leading to tissue contraction and deposition of fibrotic matrix.[45, 46] However, these growth factors have not been studied previously with respect to varying mechanical and topographic cues that mimic the stroma via fabrication of aligned fibrillar collagen channel substrates. Since many growth factors are involved during corneal wound healing in vivo, it is challenging to isolate the effects of individual growth factors and their role in cellular patterning. In vitro models that mimic the stromal architecture are needed to isolate the effects of individual growth factors.

The stroma consists of aligned collagen fibrils; therefore, fabrication of aligned collagen is needed to model this arrangement. Previous studies describe fabrication of self-assembled aligned fibrillar collagen substrates using a microfluidics device.[47] With this technique, fiber density and collagen concentration are controlled, and channel size of the aligned collagen substrate can be customized to desired dimensions.[48] Additionally, the biocompatibility and controllable patterning of these substrates allows for in vitro modeling of biological processes, including corneal wound healing. Adopting this approach to producing aligned collagen substrates and seeding with primary keratocytes allows isolation and investigation of specific growth factor and topographical effects on cell behavior, phenotype, and patterning.

1.2.2 Lamellar Keratectomy (LK)

With the FI and in vitro aligned collagen models, intrastromal migration can be investigated deeply; however, a model that induces fibrosis is also needed. One model which is used to investigate fibrosis formation during wound healing is LK, in which the epithelium, EBM, and part of the anterior stroma is mechanically removed. Healing following keratectomy wounds in the rabbit has several phases: stromal repopulation (migration), fibrosis, and regeneration and/or remodeling.[49, 50] Specifically, using in vivo confocal microscopy, Jester and coworkers demonstrated that following PRK, corneal fibroblasts migrated into the wounded stromal tissue by 7 days after injury, without transforming into myofibroblasts.[49] By 21 days, significant sub-epithelial haze, myofibroblast transformation, and associated fibrosis were detected. Following initial fibrosis, interestingly,

both stromal thickness and haze values returned to near pre-operative levels by 17 weeks, suggesting regeneration and/or remodeling of corneal tissue. In addition to changes in cell phenotype and backscatter during stromal wound healing, others have studied changes in ECM composition following keratectomy wounds;[49, 51-54] however, the temporal and spatial correlation between cell alignment and ECM patterning during the migratory, fibrosis, remodeling and/or regeneration phases of wound healing has not been established.

1.2.3 Photorefractive Keratectomy (PRK)

Although the LK model allows investigation of wound healing after corneal tissue removal, temporal and spatial assessment of cell/ECM interactions in the stroma also needs to be investigated using a more clinically relevant model. PRK is a common refractive procedure in which lasers are used to photoablate and re-shape the cornea for vision correction. Unlike the LK model, the PRK model is more consistent, since removal of tissue is automated and not heavily reliant on surgeon consistency. Tracking cell/ECM interactions, patterning, regeneration, and remodeling following PRK long term is essential for a better understanding of how the cornea heals after routine refractive procedures in the clinic.

1.3 MICROSCOPY TECHNIQUES

1.3.1 In Vivo Confocal Microscopy

In vivo confocal microscopy has been used in a variety of corneal research and clinical applications since its development over 25 years ago (for review see [55-65]), and is ideally suited to monitoring the cellular events of wound healing.[61, 64, 66-69] Three main confocal

systems have been developed for in vivo corneal imaging: the Tandem Scanning Confocal Microscope (TSCM), [70-72] the Confoscan 4,[73, 74] and the Heidelberg Retinal Tomograph with Rostock Corneal Module (HRT-RCM).[61] The HRT-RCM is a laser scanning confocal microscope, which operates by scanning a 670 nm laser beam in a raster pattern over the field of view.[75] The system uses a high numerical aperture 63x objective lens (0.9 NA), and produces images with high contrast and better axial resolution (7.6 µm) than other in vivo confocal systems (9 µm for the TSCM and 24 µm for the Confoscan).[72, 76, 77] This has led to the expansion of its development and use in recent years.[65]

Figure 1.2. HRT-RCM in vivo confocal microscope in Dr. Petroll's lab, modified to allow for automated scanning via motor drive and slit lamp stand for facilitating positioning of the objective on the cornea as previously described.[2]

To collect and quantify 3-D information from the cornea, a technique termed confocal microscopy through-focusing (CMTF) was developed for the TSCM by Jester and coworkers.[78, 79] This technique is based on the observation that different corneal sub-layers

generate different reflective intensities when imaged using confocal microscopy.[80] CMTF scans are obtained by scanning through the cornea from the epithelium to endothelium at a constant lens speed, while continuously acquiring images. One important limitation of the HRT-RCM is that although volume scans of approximately 80 µm can be generated using a motorized internal lens drive,[30, 44, 45] a manual thumbscrew drive must be used to change the focal plane position over larger distances, which requires rotating the objective housing by hand. Because CMTF imaging requires continuous focal plane movement at a known speed, *quantitative* high resolution 3-D imaging of the full-thickness cornea is not possible with the standard HRT-RCM system. In a recent study, however, the HRT-RCM hardware and software were modified to address this limitation and allow quantitative CMTF imaging of the normal rabbit cornea (Figure 1.2).[2, 65]

1.3.2 Second Harmonic Generation (SHG)

SHG signals are created when two near-infrared photons interact with a non-centrosymmetric material, such as fibrillar collagen, and emit a single visible photon with half the wavelength and double the frequency of one of the original photons.[81] Collagen fibrils within the cornea have been shown to emit SHG signals in multiple species.[82, 83] Previous SHG studies in the human cornea reveal that collagen lamellae in the anterior stroma is interwoven (Figure 1.3A), and becomes more aligned and orthogonal in the mid (Figure 1.3B) and posterior stroma (Figure 1.3C).[3] Since SHG signals from the cornea are intense, SHG imaging is an ideal method to use for detection of collagen patterning in the cornea using the aforementioned wound healing models.[84] Additionally, SHG imaging of collagen can be combined with multiphoton imaging using a laser scanning confocal

microscope, allowing for simultaneous z-stack acquisition with fluorescently labeled components, like phalloidin for F-actin in the cornea. By combining these imaging techniques, cell and collagen patterning/interactions can be assessed in the cornea.

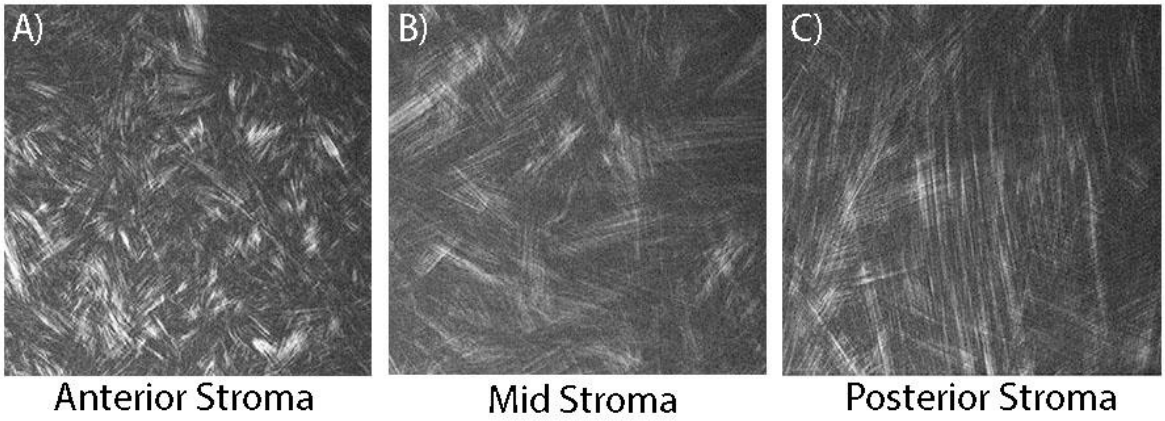

Figure 1.3. SHG signals in the anterior (A), mid (B), and posterior (C) stroma. Images are 220 µm x 220 µm. Modified from Morishige, N., Petroll, W.M., Nishida, T., Kenney, M.C., and Jester, JV, *Noninvasive corneal stromal collagen imaging using two-photon-generated second-harmonic signals*, J Cataract Refract Surg, 2006. 32: p. 1784-1791.[3]

1.4 SIGNIFICANCE

This research will provide the first assessment and quantification of cell and collagen alignment following corneal wound healing using a combined temporal and spatial analysis. To accomplish this, several wound healing models in the cornea as well as advanced imaging modalities will be used to analyze cell and ECM interactions. For the first time, studies using a unique, aligned collagen in vitro model will be implemented to isolate the effects of topography on cell migration and patterning after stimulating with wound healing growth factors following in vitro FI.

1.5 HYPOTHESES AND SPECIFIC AIMS

Based on previous studies using SHG and initial findings using in vivo confocal microscopy, it is hypothesized that collagen organization in the stroma will correlate with cell patterning during intrastromal migration. **Specific Aim 1: Determine if collagen organization in the stroma regulates keratocyte patterning following FI in vivo.**

Based on pilot data, it is hypothesized that a) PDGF will stimulate corneal keratocyte migration with dendritic morphologies that are co-aligned with collagen fibrils, and b) TGF-β will induce myofibroblast transformation without alignment to collagen fibrils. **Specific Aim 2: Determine how the interplay between topography and selected growth factors present during corneal wound healing affect cell alignment and patterning in an in vitro stromal model.**

Based on previous studies and preliminary data, it is hypothesized that keratocytes accumulating on top of a stromal wound (where there are no topographic cues) will assume a random alignment, contain more prominent stress fibers, and will transform into myofibroblasts. **Specific Aim 3: Examine effects of collagen topography on elements of cell phenotype, patterning, and morphology during the development of haze and fibrosis after keratectomy injuries in vivo.**

Based on preliminary data, it is hypothesized that over time, keratocytes will transform into a regenerative phenotype, and remodel the fibrotic ECM to produce a lamellar structure that is similar to the native corneal stroma in both structure and transparency. **Specific Aim 4: Temporally track specific cell/ECM interactions that contribute to long term regeneration/remodeling in the cornea after keratectomy injury.**

CHAPTER TWO
In Vivo and In Vitro Models of Intrastromal Migration

Portions of this chapter are reproduced with permission from: Petroll, W. M., Kivanany, P.B., Hagenasr, D., and Graham, E.K., Invest Ophthalmol Vis Sci, 2015. 56: p. 7352-7361, ARVO.

2.1 INTRASTROMAL MIGRATION IN THE CORNEA

2.1.1 Investigation of Intrastromal Migration of Keratocytes post-FI

Following transcorneal FI, a modified HRT-RCM system was used to assess keratocyte backscattering, alignment, morphology, and connectivity during intrastromal wound healing in vivo in the rabbit. These findings were correlated with en bloc 3-D confocal fluorescence imaging of cellular patterning, and SHG imaging of the corneal collagen lamellae. Using this combined approach, a unique pattern of keratocyte alignment and connectivity was identified during wound healing which is highly correlated with the structural organization of the lamellae, suggesting contact guidance of intrastromal cell migration. While biophysical cues have been shown to impact fibroblast behavior in in vitro models,[85-87], this is the first demonstration known to show that ECM structure mediates the pattern of intrastromal corneal fibroblast migration during in vivo wound healing.

2.2 IN VIVO FI METHODS

2.2.1 Animal Model for FI

Studies were performed using 22 New Zealand white rabbits (3-4 kg). All procedures adhered to the ARVO (Association for Research in Vision and Ophthalmology) Statement

for the Use of Animals in Ophthalmic and Vision Research. For transcorneal FI, a 3 mm diameter stainless steel probe cooled with liquid nitrogen was applied to the anterior, central corneal surface of one eye per animal three times for 10 seconds each time. This created a region of cell death through the full thickness of the central cornea (epithelium, stroma and endothelium).[14, 88] After each surgery, one drop of gentamicin antibiotic solution was applied twice a day for 3 days.

2.2.2 In Vivo Confocal Microscopy

To collect and quantify 3-D information from the cornea, CMTF was performed with an HRT-RCM (HRT II with Rostock Cornea Module, Heidelberg Engineering, GmBH, Dossenheim, Germany) that was custom modified in Dr. Petroll's laboratory.[2, 78, 79] This system uses a joystick-controlled lens drive system, and incorporates software from Heidelberg Engineering that allows real-time "streaming" of images to the hard drive during an examination. Rabbits were scanned one week prior to surgery, and at 1, 3, 7, 14 and/or 28 days post-operatively. Prior to confocal imaging, rabbits were anesthetized with 50 mg/kg intramuscular ketamine and 5.0 mg/kg xylazine. A drop of topical anesthetic (proparacaine) was also applied to each eye. For confocal imaging, a drop of Genteal was placed on the tip of the HRT-RCM objective lens. The objective lens was then positioned so that flat-field images were observed at a central region of the cornea (confirming proper alignment). For CMTF, scans were made from the endothelium to the epithelium at a constant speed of 60 μm/sec, while collecting images using the HRT streaming software function with the acquisition rate set to 30 frames/second. Scans were made with the "automatic brightness"

function in the HRT II software turned off (by unchecking the corresponding box). The gain level was controlled using the horizontal slider above the "automatic brightness" box. Images were collected at gains of both 6 and 10 (corresponding to the number of mouse clicks the slider was moved to the right). A minimum of 4 CMTF scans were performed at each gain setting, in the central region of each cornea. Each scan had a step size of approximately 2 μm between images. The field of view for each 384x384 pixel image was 400 μm x 400 μm, resulting in a voxel size of 1.04 μm x 1.04 μm x 2 μm (x, y, z).

For analysis of HRT-RCM data, in-house CMTF software was used in which ".vol" files can be directly loaded for 3-D visualization and analysis. CMTF intensity curves were generated by calculating the average pixel intensity of each image and plotting versus z-depth.[78, 79] Using intensity peaks corresponding to basal lamina and endothelium, measurements of stromal thickness were made as previously described.[78] A relative estimate of stromal cell and ECM backscattering was obtained by measuring the area under the CMTF curve (intensity x distance). Area was measured from the beginning of the basal lamina peak to the end of the endothelial peak (3 images past the endothelium). A baseline intensity of 17 was used for the area calculations, which was above the background intensity obtained from the anterior chamber (12–14), and below the average image intensity of baseline stromal images.

2.2.3 In Situ Imaging

At 3 and 7 days post-operatively, both eyes from six rabbits were collected for in situ imaging. Corneas were fixed via anterior chamber perfusion with 1% paraformaldehyde solution consisting of 1% dimethyl sulfoxide (DMSO), 1% Triton X 100, and 5% Dextran for 10 minutes immediately after sacrificing, as previously described.[89] Corneas were removed and fixed in the same solution for an additional 10 minutes. Corneal blocks were washed in PBS for 20 minutes (10 minutes per wash), placed in Alexa Fluor 488 phalloidin (Molecular Probes, Thermo Fisher Scientific, Waltham, MA) in PBS (1:20) for 3 hours at 37^{o}C, then washed in PBS 3 times (30 minutes per wash). In some samples, nuclei were labeled by adding DAPI (4',6-diamidino-2-phenylindole, Molecular Probes, Waltham, MA) at a 1:500 concentration in PBS for 1 hour at room temperature.

Samples were mounted epithelial side down on MatTek (MatTek Corporation, Ashland, MA) glass bottom dishes in glycerol:PBS (1:1), and imaged using laser scanning confocal microscopy (Leica SP8, Heidelberg, Germany). An Argon (488 nm) laser was used for imaging F-actin, and a UV laser (405 nm) was used to image DAPI. Stacks of optical sections (z-series) were acquired using a 25x water immersion objective (0.95 NA, 2.4 mm free working distance). Sequential scanning was used to image double-labeled samples to prevent cross-talk between fluorophores. To expand the effective field of view, montages of overlapping images were created using the programmable motorized stage and image tiling feature within the Leica software. Multiphoton fluorescence and second harmonic generation imaging was also performed on some samples, using a Zeiss LSM 510 confocal microscope

(Carl Zeiss Microscopy, Thornwood, N.Y) with a Chameleon multiphoton laser (Coherent, Santa Clara, CA) set at 900 nm. Z-series of the forward and backscattered SHG signal from the collagen lamellae were acquired simultaneously along with F-actin images, using a 40X water immersion objective (0.8 NA, 3.6 mm free working distance).

2.2.4 Quantification of Cell/ECM Alignment

Alignment of cells and collagen was quantified from F-actin and SHG images using the "directionality" plug in within Image J, which uses a Fourier Transform algorithm to determine the percent of image content aligned at each radial angle within the image. Plots showing both cell and matrix directionality were generated to allow direct comparison of the angle distributions.

2.2.5 Statistics

All statistical analysis was carried out using the analysis tool box in SigmaPlot (version 12.5, Systat Software, Inc., San Jose, CA). Analysis of variance (ANOVA) was used to compare group means. Post-hoc multiple comparisons between groups were performed using the Holm–Sidak method. Linear regression analysis was used to assess the correlation between cell and ECM directionality.

2.2.6 Scientific Rigor and Reproducibility

For the in vivo assessment, multiple scans were used to calculate the means for epithelial and stromal thickness as well as stromal backscatter. Structures observed in the in

vivo backscatter scans were validated using fluorescent labeling in *in situ* images. Additionally, images of cells captured simultaneously as collagen images using SHG and multiphoton from the UTSW Core Microscopy Facility were also captured using the laser scanning confocal microscope in Dr. Petroll's lab for comparison.

2.3 IN VIVO FI MODEL RESULTS

2.3.1 In Vivo Confocal Microscopy Imaging post-FI

CMTF scans were successfully obtained using the HRT-RCM at all of the time points studied. Raw images are shown in Figure 2.1; images with contrast adjusted for better visualization are shown in Figure 2.2. As detailed in the Methods, scans were collected using gains of both "6" and "10". The signal from wound healing fibroblasts was often saturated when using a gain of 10, so scans with a gain of 6 were used for all reconstructions and analyses. Consistent with previous studies, in pre-operative scans, the primary signal in the stroma was derived from the keratocyte nuclei (Figure 2.1A;a-c, Supplemental Movie 1). Corneal stromal nerves were also visualized in some regions (not shown). Endothelial images looked similar to those obtained using specular microscopy (Figure 2.1A;d). Note that the superficial epithelium is obscured in these image stacks by the bright reflection from the Tomocap.

Three days after transcorneal FI, an acellular region was observed in the central cornea, as was significant stromal edema. Closer to the edge of the wound, the acellular region was limited to the anterior stroma (Figure 2.1B;a). Beneath this area, highly reflective structures

were observed (Figure 2.1B;b.c). The morphology of these structures was consistent with that of polarized migratory corneal fibroblasts.[24, 90] Interestingly, these structures were generally arranged in long, parallel lines. Distinct groups of these aligned structures were consistently observed, particularly in the posterior stroma (Figure 2.2, Supplemental Movie 2). Elongated, reflective cells were observed at the level of the corneal endothelium (Figure 2.1B;d). F-actin labeling confirmed that these were fibroblastic endothelial cells, as indicated by a loss of cortical F-actin and expression of intracellular stress fibers (Figure 2.3). This is consistent with previous studies demonstrating that migrating endothelial cells undergo fibroblastic transformation following FI in the rat, rabbit and cat.[14, 91-93] To better visualize the 3-D relationship between structures, images from the posterior 100 μm of the stroma were automatically aligned using the *linear stack alignment* plug-in in Image J (Fiji version), in order to compensate for movements that occur during in vivo imaging. As shown in Supplemental Movie 3, distinct "layers" of parallel linear structures were more clearly revealed in these reconstructions. Interestingly, the alignment of these structures shifted from one layer to the next.

Seven days post-operatively, highly reflective, interconnected cells were observed in the anterior stroma (Figure 2.1C;a & Figure 2.2C;a). In the mid and posterior stroma, parallel groups of presumptive corneal fibroblasts were consistently observed (Figure 2.1C, Supplemental Movie 4). Reflective areas were often observed at the level of the endothelium in the center of the wound (Figure 2.1C;d). These areas were generally thicker than the adjacent normal endothelium, consistent with previous studies demonstrating that a

retrocorneal fibrous membrane (RCFM) forms after FI in the rabbit and cat.[14, 88, 91] This RCFM results from transformation of the endothelium to a fibroblast and/or myofibroblast phenotype.[94-96] Similar to 3 days after FI, aligned stacks from the posterior stroma showed distinct "layers" of parallel linear structures, with the alignment changing from one layer to the next (Supplemental Movie 5).

Beginning at 14 days after injury, the amount of cell activation began to decrease (not shown), and by 28 days the corneal stroma images looked similar to those obtained pre-operatively (Figure 2.1D;a-c, Supplemental Movie 6). The endothelium appeared to have a more cobblestone-like appearance than it did pre-operatively (Figure 2.1D;d), suggesting that the cell-cell junctions had not completely reformed. These cells covered the posterior surface of the RCFM, which persisted in some areas, consistent with previous studies.[14, 91]

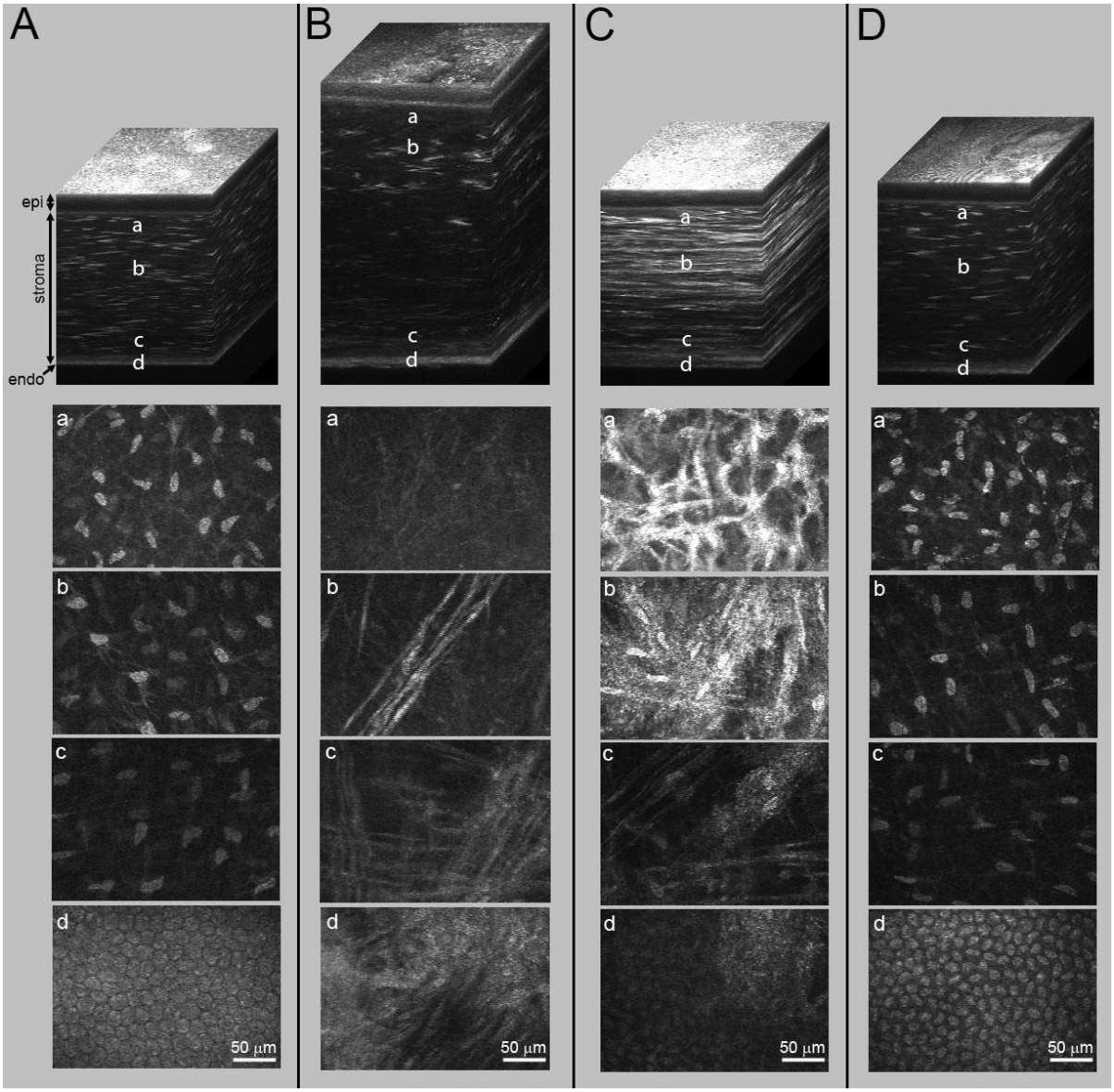

Figure 2.1. 3-D stacks of images from CMTF scans collected using the HRT-RCM, before and after transcorneal FI. A. Preoperative scan. B. 3 days after FI. C. 7 days after FI. D. 28 days after FI. The top row shows 3-D reconstructions of the confocal z-stack. a-d show selected en face images from each stack.

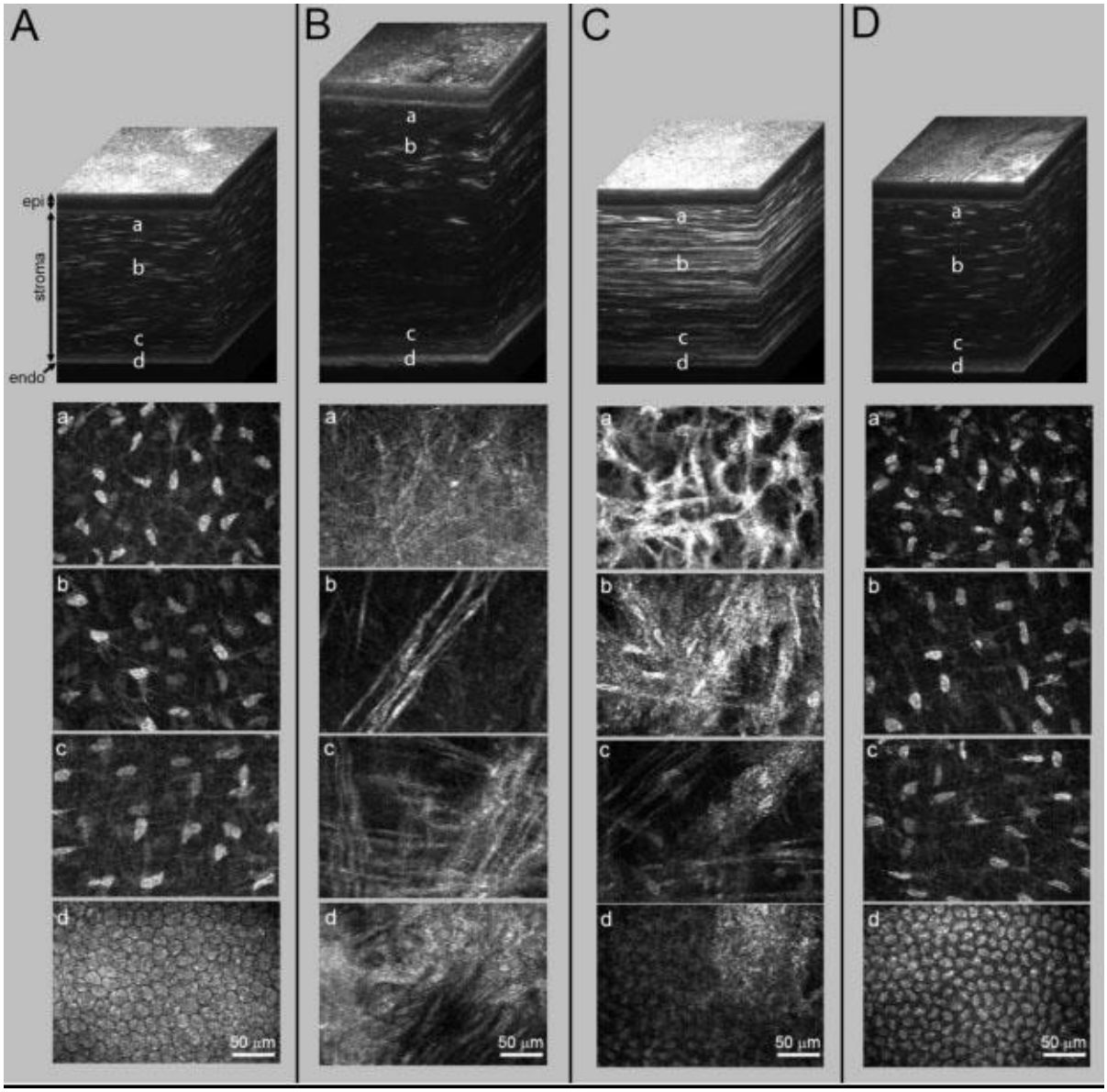

Figure 2.2. 3-D stacks of images from CMTF scans collected using the HRT-RCM, before and after transcorneal FI with enhanced contrast. Contrast was enhanced digitally to allow better visualization of cellular patterning. A. Preoperative scan. B. 3 days after FI. C. 7 days after FI. D. 28 days after FI. The top row shows 3-D reconstructions of the confocal z-stack. a-d show select en face images from each stack.

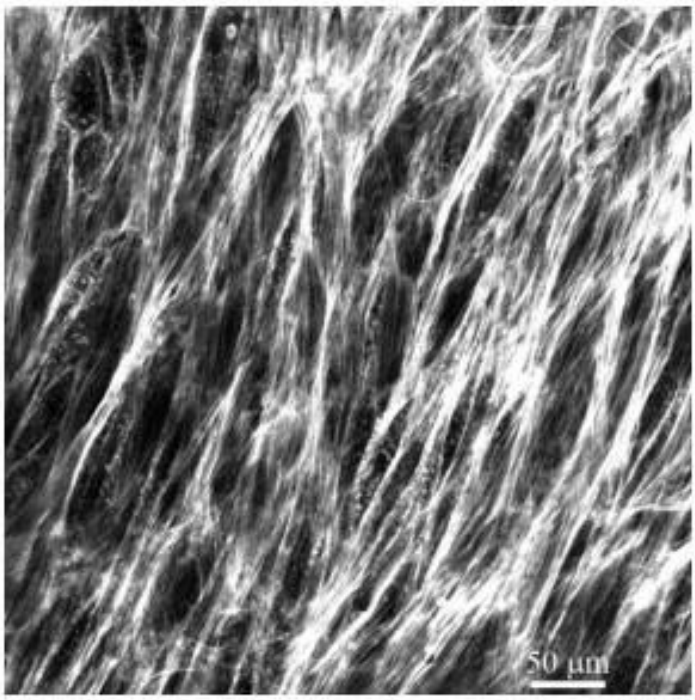

Figure 2.3. Confocal image collected in situ from a cornea labeled with phalloidin, 3 days after transcorneal FI. Fibroblastic endothelial cells were detected on the posterior surface of the cornea, as indicated by a loss of cortical F-actin and expression of intracellular stress fibers.

2.3.2 Quantitative Analysis using CMTF Scans

Quantitative analysis was also carried out using the modified CMTF software. As shown in Figure 2.4, CMTF curves had a strong peak derived from the Tomocap, which obscured the peak from the superficial epithelium normally observed when using the TSCM or Confoscan 4 system. However, the basal lamina and endothelium were easily identified at all of the time points, which allowed measurements of corneal stromal thickness to be obtained. A significant increase in stromal thickness was observed 7 and 14 days after injury, as compared to pre-operative values (Figure 2.4C). Furthermore, a striking increase in stromal backscattering was measured from the CMTF curves at days 7 and 14 (Figure 2.4D,

also compare Figure 2.4A and B). At 28 days, stromal backscattering was reduced to near baseline levels, and no haze was noted by gross examination (Figure 2.4D), although a small amount of stromal edema persisted.

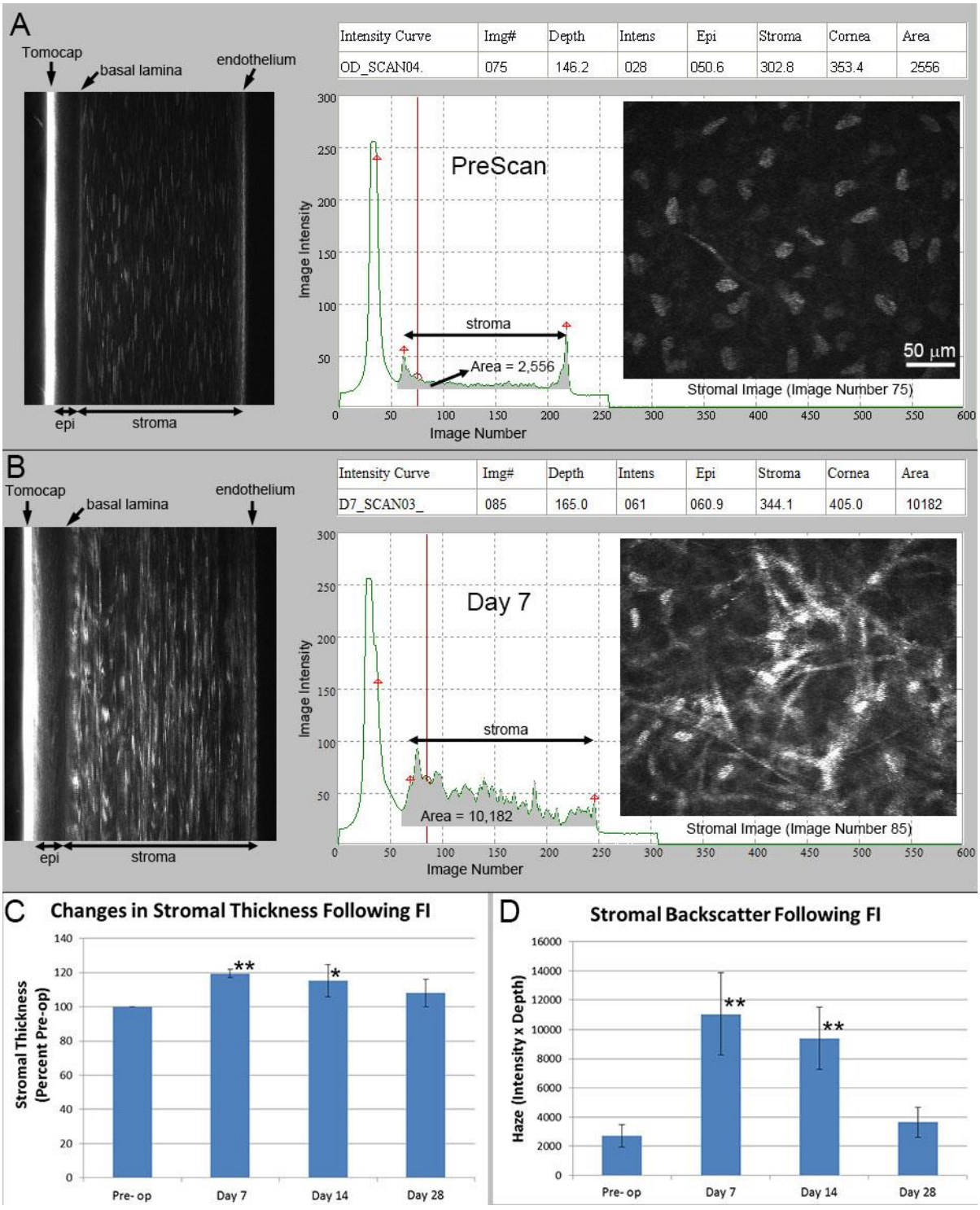
A
Tomocap
basal lamina
endothelium
epi
stroma
Intensity Curve | Img# | Depth | Intens | Epi | Stroma | Cornea | Area
OD_SCAN04. | 075 | 146.2 | 028 | 050.6 | 302.8 | 353.4 | 2556
PreScan
stroma
Area = 2,556
50 µm
Stromal Image (Image Number 75)
Image Intensity
Image Number
B
Tomocap
basal lamina
endothelium
epi
stroma
Intensity Curve | Img# | Depth | Intens | Epi | Stroma | Cornea | Area
D7_SCAN03_ | 085 | 165.0 | 061 | 060.9 | 344.1 | 405.0 | 10182
Day 7
stroma
Area = 10,182
Stromal Image (Image Number 85)
Image Intensity
Image Number
C
Changes in Stromal Thickness Following FI
Stromal Thickness (Percent Pre-op)
Pre- op
Day 7
Day 14
Day 28
D
Stromal Backscatter Following FI
Haze (Intensity x Depth)
Pre- op
Day 7
Day 14
Day 28

Figure 2.4. In vivo CMTF data collected from rabbit corneas using the modified HRT-RCM system preoperatively (A) and 7 days after transcorneal FI (B). Corneal stromal thickness was measured by marking the location of the top of the stroma and the corneal endothelial peak. A relative estimate of stromal cell and ECM backscattering was obtained by measuring the area under the CMTF curve (shaded areas under curves, "area" on top right of each image). C. Graph showing changes in stromal thickness over time (mean + S.D). A significant increase was found at 7 and 14 days after injury. D. Graph showing changes in stromal backscatter over time (mean + S.D.). Significant increases were identified 7 and 14 days after injury. (** $P < 0.01$; * $P < 0.05$)

2.3.3 In Situ Labeling and Imaging of post-FI Corneas

In order to verify that the aligned structures identified in the in vivo images were corneal fibroblasts, and to further investigate their organization, corneas were fixed and labeled in situ with phalloidin (for F-actin) and DAPI (for nuclei). As shown in Figure 2.5A, in control (unoperated) corneas, keratocytes had a stellate morphology and were interconnected by dendritic cell processes.[89] Three days after FI, an abrupt transition was found in the anterior stroma between dendritic keratocytes adjacent to the wound (Figure 2.5B, left side) and activated corneal fibroblasts migrating into the wounded stroma (Figure 2.5B, right side). Fibroblasts were characterized by an elongated, polarized morphology and more intense F-actin labeling. Fibroblasts formed an interconnected network that extended from the wound edge to the leading edge of the migratory front, and trains of cells moving along the same path were often observed (see Supplemental Movie 7). In the posterior stroma, long, interconnected lines of cells were observed (Figure 2.5C, wound is on bottom right of image). Parallel groups of these cell chains were consistently detected (Supplemental Movie 8), with the orientation shifting from one layer to the next. At 7 days, the central cornea was completely repopulated with corneal fibroblasts. Fibroblasts continued to be arranged in parallel streams in the mid and posterior cornea (Figure 2.5D and E). These

fibroblasts were thin and elongated, and did not have the broad morphology and prominent stress fibers that are characteristic of myofibroblast transformation.

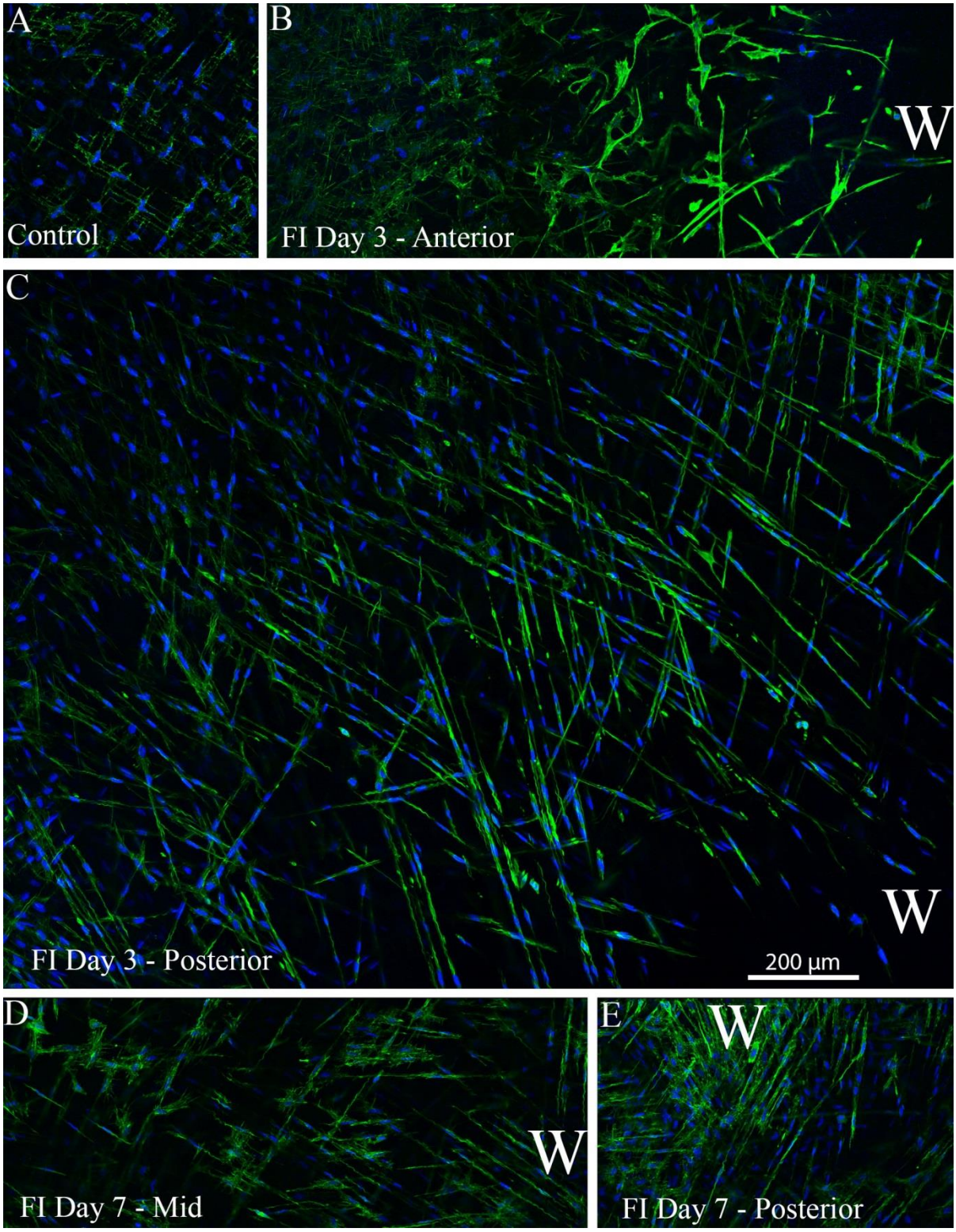
A
Control
B
W
FI Day 3 - Anterior
C
W
FI Day 3 - Posterior
200 µm
D
W
FI Day 7 - Mid
E
W
FI Day 7 - Posterior

Figure 2.5. Confocal images collected in situ from corneal blocks labeled with phalloidin (green) and DAPI (blue). A. Control (uninjured) cornea, B. Montage of tiled images from the anterior stroma, 3 Days after FI. C. Montage of tiled images from the posterior stroma, 3 days after FI. D and E. Montages of images from the mid and posterior cornea, 7 days after FI. "W" indicates the image area closest to the center of the wound.

2.3.4 SHG Imaging to Investigate Cell/ECM Patterning in the Cornea after FI

In order to investigate whether corneal fibroblast patterning correlated with the alignment of the corneal collagen lamella, SHG imaging was performed. In control corneas, corneal keratocytes had a stellate morphology and the cell bodies were not polarized, thus no preferential alignment was detected qualitatively or quantitatively (Figure 2.6, Top Row). However, the dendritic processes connecting corneal keratocytes in the posterior cornea often appeared to be aligned parallel with the collagen lamellae. This is consistent with a recent study by Quantock and coworkers which demonstrated that dendritic keratocyte processes are closely associated with orthogonally arranged stromal collagen fibrils in the developing chick cornea.[23]

At both 3 and 7 days after FI, a complex pattern of cell and matrix organization was found in the anterior stroma (Supplemental Movie 9). In en face image slices, no predominant alignment of either cells or collagen lamella could be identified qualitatively or quantitatively (Figure 2.6, Middle Row). In contrast, distinct, aligned layers of lamellae were observed in the posterior cornea qualitatively and quantitatively (Figure 2.6, Bottom Row). Corneal fibroblasts were consistently aligned parallel with the collagen lamella, resulting in high correlations between cell and ECM directionality (Supplemental Movie 10).

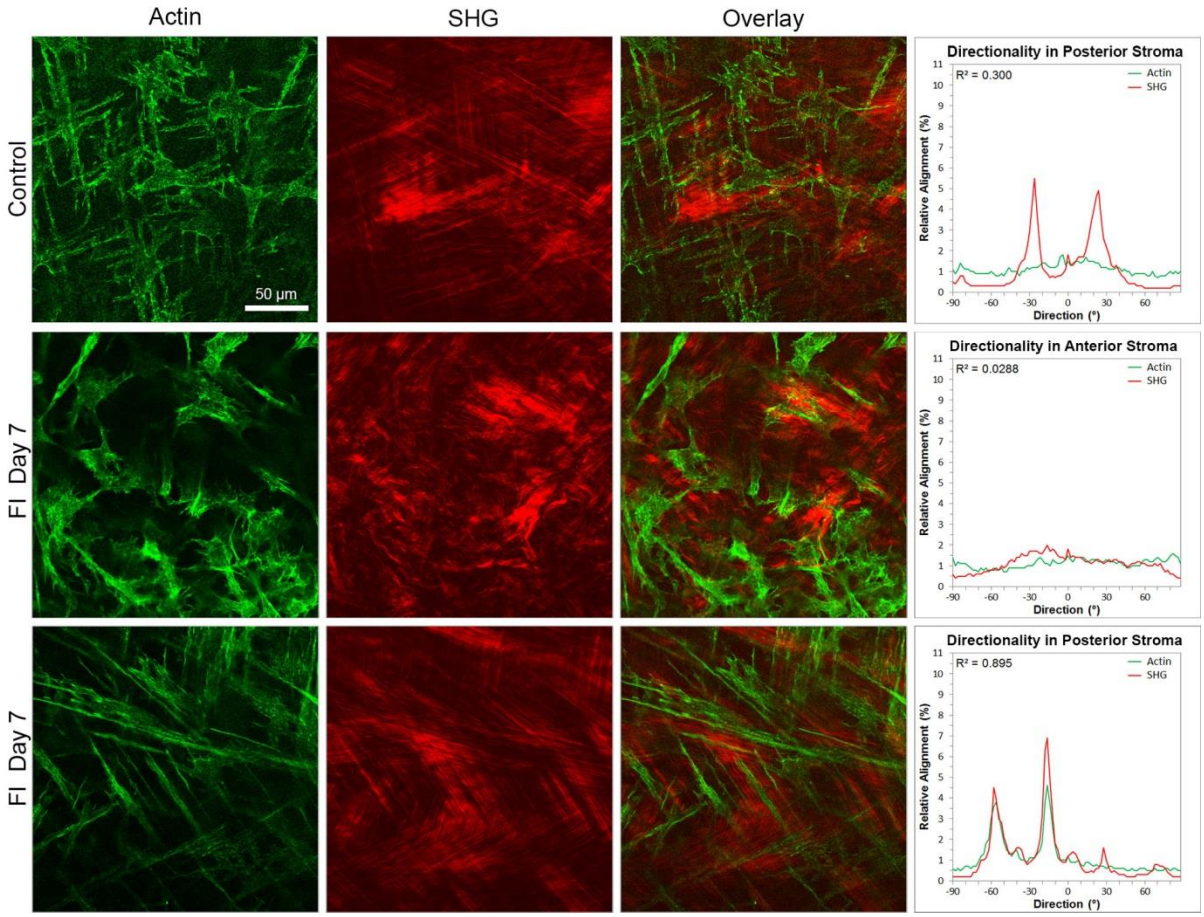

Figure 2.6. Multiphoton confocal images collected in situ showing fluorescent signal from phalloidin (green) and forward scattered SHG signal from stromal collagen lamellae (red). Graphs on right show the percent of image content aligned at each radial angle within the image for both cells and collagen. *Top Row*. Images from posterior of control (un-operated) cornea. *Middle Row*. Images are from anterior stroma (10 microns below basal lamina), collected 7 days after FI. *Bottom Row*. Images are from posterior stroma (20 microns above endothelium), collected 7 days after FI.

2.4 DISCUSSION OF FI STUDIES

2.4.1 In Vivo Confocal Microscopy for FI Analysis

In vivo confocal microscopy is ideally suited for studying corneal wound healing in vivo. CMTF has been used for quantitative assessment of sub-layer thickness and depth-dependent cell and ECM backscatter following injury, toxic insult, contact lens wear, infection and refractive surgery using the TSCM system. [55-69, 78, 79] The HRT-RCM produces corneal images with better resolution and contrast than the TSCM (which is no longer commercially available), and this has led to growing use of this instrument in recent years. Hardware and software modifications to the HRT-RCM were recently reported, which allow CMTF scans to be collected from the full thickness rabbit cornea in vivo.[2] In the current study, this system was used to assess the stromal wound healing response following transcorneal FI in the rabbit. For the first time, repopulation of keratocytes post-injury within the corneal stroma has been shown to occur with direct association to the ECM patterning. Additionally, multi-dimensional imaging tools were used simultaneously to assess in vivo cell morphology and reflectivity.

Quantitative CMTF analysis demonstrated a significant increase in stromal thickness at 7 and 14 days after injury, as compared to pre-operative values. Furthermore, a fourfold increase in stromal backscattering was measured from the CMTF curves at days 7 and 14. Unlike other 3-D imaging technologies such as optical coherence tomography (OCT) or high frequency ultrasound, CMTF scans provide a series of high resolution en face images which allow assessment of depth-dependent changes in cell morphology, density and reflectivity.[64,

[67, 68] Previous studies have demonstrated that when keratocytes transform to a migratory fibroblast phenotype, they assume a polarized morphology, and have increased light scattering due in part to a downregulation of crystalline protein expression.[97, 98] Consistent with these studies, highly reflective linear structures were observed in the corneal stroma beginning 3 days after FI. Subsequent labeling of corneal tissue for F-actin and in situ confocal imaging verified the cellular origin of these structures. Specifically, corneal fibroblasts were characterized by an elongated, polarized morphology and more intense F-actin labeling. In situ imaging also verified the unique pattern of organization identified in the in vivo confocal images. In the anterior stroma, cells were randomly organized. However, in the mid and posterior cornea, long parallel trains of cells moving along the same path were often observed. Interestingly, the alignment of these structures shifted from one layer to the next.

2.4.2 SHG Imaging post-FI Reveals Collagen Lamellae Patterning and Intrastromal Migration via Topographical ECM Cues

Previous studies using SHG imaging in the rabbit have shown that in the anterior stroma, there is significant interweaving of the collagen lamella; whereas in the mid and posterior cornea, there is less interweaving and the lamella form more distinct orthogonal layers.[3, 99] Based on the data from both in vivo and in situ imaging in the current study, it is hypothesized that corneal fibroblasts migrate into the wounded, acellular stroma in a pattern that corresponds with the lamellar organization of the tissue. To test this hypothesis, cell and matrix organization were directly compared by using SHG imaging. During wound healing, a

complex pattern of cell and matrix organization was found in the anterior stroma, and no predominant alignment of either cells or collagen lamella was found. In contrast, distinct, aligned layers of collagen were observed in the posterior cornea, and corneal fibroblasts were consistently aligned parallel with these lamellae.

Overall, these results suggest that the collagen lamellae provide contact guidance of intrastromal fibroblast migration during wound repopulation. This is consistent with in vitro studies demonstrating that topographical parameters (i.e. height, depth, width and spacing) can have a significant impact on cell morphology, differentiation and migration mechanisms.[85, 86, 100, 101 102] Individual Type I collagen fibers in the cornea are approximately 30 nm in diameter and have a center to center spacing of approximately 65 nm.[103] However, it is not clear if the pitch of individual fibers is responsible for the lamellar guidance of cell migration observed in this study. Murphy and coworkers demonstrated that corneal fibroblasts spread and migrated parallel to collagen coated ridges and grooves with a pitch of greater than 1 μm, whereas spreading and migration was randomly oriented on planar substrates or substrates with smaller topographic features. Interestingly, cells also migrated faster when moving parallel to the aligned substrate features.[104] Aligned substrates also increase the alignment of cells and matrix within each layer of self-assembled sheets derived from corneal fibroblasts.[87, 105-109] Within 3-D matrices, migrating cells can establish tracks for spreading and migration by aligning fibrils via mechanical force generation.[110-115] Similarly, strain-induced tension applied to 3-D matrices also can establish aligned tracks for cell migration.[116, 117]

Cell and collagen alignment has been assessed previously using SHG imaging following PRK in the rabbit.[54] Two weeks after surgery, wound healing was characterized by myofibroblast transformation of corneal keratocytes and the development of fibrotic tissue on top of the photoablated stroma. Both cells and matrix were randomly aligned within this fibrotic tissue layer, i.e. no specific pattern of organization was found. The data presented here suggest that, in contrast to this fibrotic layer that forms on top of the stroma, cells migrating within the stroma following FI in the current study were exposed to topographic cues from the native lamellae. These cues apparently led to cell alignment via contact guidance of migration.

In addition to developing a pattern of alignment that mirrored the lamellar structure of the corneal stroma, fibroblasts also appeared to form long streams of interconnected cells that extended from the wound edge to the leading edge of the migratory front. This pattern of collective cell migration is called "multicellular streaming",[118] and is thought to be involved in directional guidance of neural crest cells during embryonic development. Recently, a similar pattern of migration was identified by corneal fibroblasts invading 3-D fibrin matrices using a nested matrix model.[119, 120] Initially, fibroblasts extend their leading edge into the fibrin while remaining connected to cells behind them. Other cells follow along the same paths, producing long lines of interconnected cells. Lateral protrusions between adjacent cells also become interconnected, resulting in the formation of a mesh-like structure. Fibrin fibrils were randomly organized in the nested matrix model, whereas the corneal stroma lamellae

are made up of highly aligned collagen fibrils. In the current study, cells migrating within the mid and posterior corneal stroma were highly polarized, and did not appear to develop lateral processes. Thus, interconnections between the streams of aligned cells were not observed. In fibrin, cells at the leading edge of the migratory front appear to create tracks through the matrix that are used by the cells behind them.[119-121] Future studies are needed to determine whether similar tracks are created during intrastromal migration in vivo.

2.4.3 Limitations with CMTF Scanning

Although 3-D CMTF scans were successfully obtained using the HRT-RCM, there are still some limitations to this system. One issue encountered when performing repeated CMTF scans using the HRT-RCM was that the layer of Genteal between the objective and the back surface of the Tomocap progressively dissipated and shifted downward over time. If this Genteal layer moved below the optical axis, the image intensity decreased. This could generally be avoided by checking the layer carefully before and after scanning each eye. In cases where the Genteal layer was found to shift, scans were discarded and repeated with a new cap. Another issue is that the flat applanating tip (Tomocap) can produce compression artifacts which can distort cellular structures during clinical imaging. However, these artifacts are not generally observed when scanning the rabbit cornea. In addition, the reflection from the Tomocap generally obscures images of the superficial epithelial cells. Zhivov et al reported that a thin PMMA (poly(methyl methacrylate)) washer can be placed on the Tomocap to eliminate these reflections.[77] Using a similar device, full thickness scans

were obtained through the rabbit cornea that had clear images of the superficial epithelium, with no apparent change in the cellular backscattering detected (Figure 2.7).

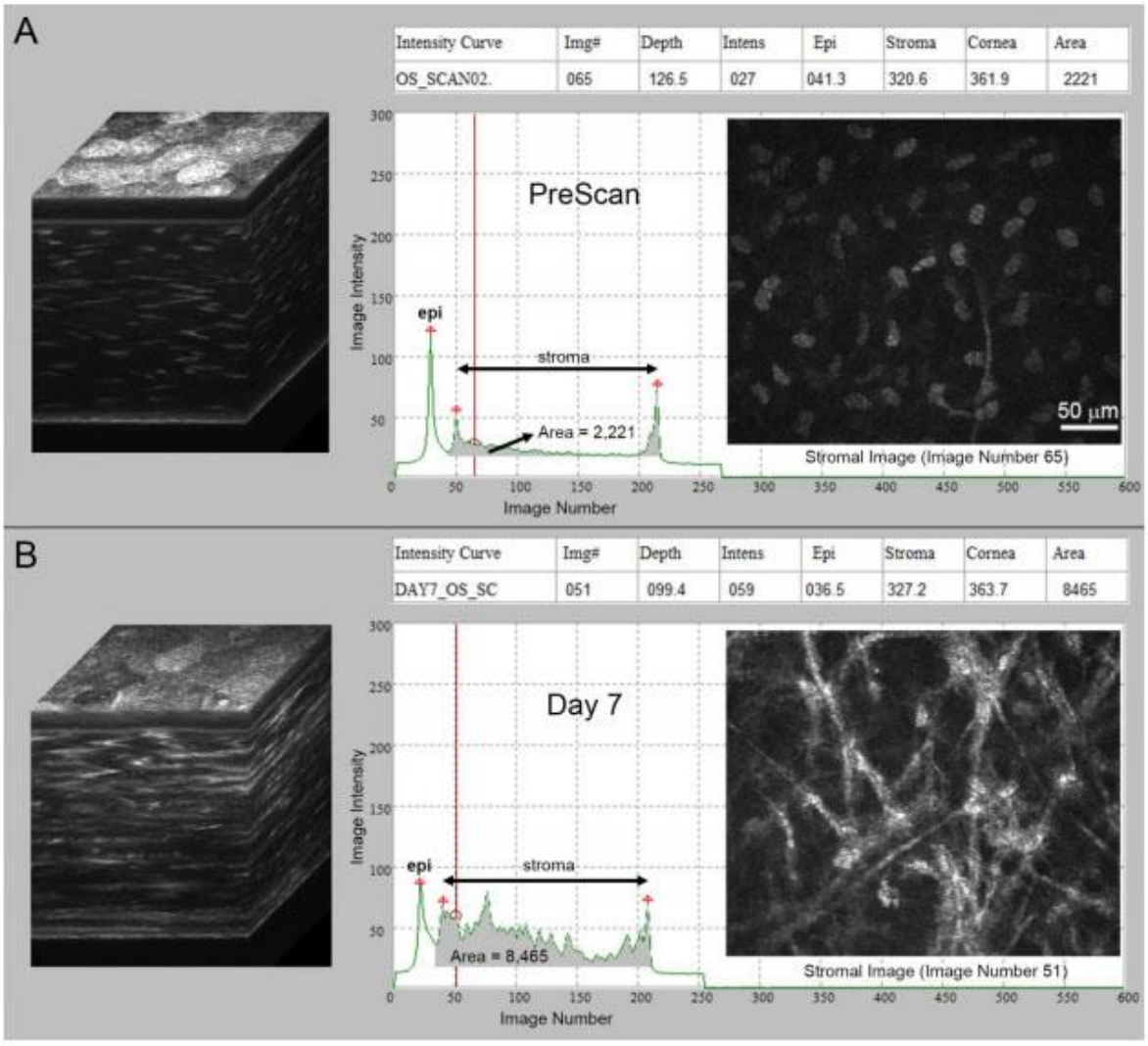

Figure 2.7. 3-D stacks of images from CMTF scans collected using the HRT-RCM, before and after transcorneal FI. A thin PMMA washer was applied to the tip of the Tomocap to reduce reflection and allow superficial epithelial imaging. A. Preoperative scan. B. 7 days after FI. The left column shows 3-D reconstructions of the confocal z-stack. Cellular patterning and backscattering was similar to what was observed without the PMMA washer.

2.5 INTRODUCTION TO PRELIMINARY STUDIES USING IN VITRO MODELS

2.5.1 Application of Aligned Collagen for Simulating Wound Healing in the Cornea

Previous findings using a rabbit model indicate that following transcorneal freeze-injury, keratocytes transform into fibroblasts and migrate into the wound site parallel to the collagen topography of the stroma.[122] Interestingly, cells do not transform into myofibroblasts or contain stress fibers, indicating phenotype dependence on mechanical cues from the stromal ECM. Furthermore, similar findings were also observed in Dr. Petroll's lab from preliminary studies using ex vivo organ culture models, where cells within the stroma post-FI lacked myofibroblastic transformation even after incubation with TGF-β over several days. Earlier in vitro studies using aligned electrospun Type I collagen fibers revealed a reduction in myofibroblastic transformation of corneal fibroblasts after stimulation with TGF-β compared to fibroblasts seeded on unaligned fibers, collagen gels, and tissue culture plates.[123] However, studies by Myrna and co-workers showed that myofibroblastic transformation also depended on the "pitch" (groove + ridge width) of the aligned topography within substrates, with a higher "pitch" reducing myofibroblastic transformation.[85] It is likely that a combination of ECM alignment, collagen structure type (fibrillar vs. gel, etc.), and growth factors affect cell behavior, patterning, and phenotype.

After injury, growth factors, such as TGF-β and PDGF (as mentioned in Chapter 1), are secreted by the epithelial cells and tears.[41-44] In this study, these growth factors were selected to study their effects on cell morphology, differentiation, alignment and orientation

using keratocytes seeded on aligned, random, and collagen coated substrates. Also a FI was applied to study contact guidance between cells and collagen fibers during migration and wound closure after stimulation with PDGF and TGF-β.

2.6 METHODS FOR IN VITRO STUDIES

2.6.1 Fabrication of Microfluidics Device

Slygard 184 Elastomer kit (Dow Corning, Michigan) was used to create a PDMS (polymethylsiloxane) solution (10:1 elastomer to curing agent), according to manufacturer instructions. PDMS solution was poured over a silicon wafer spun-coated, which contained channels with the following dimensions: 22000 µm x 1500 µm x 60 µm. Inlet and outlet elbow openings were added to allow collagen flow through the channel. The solution was then desiccated for 1 hour and oven-cured at 80^{o}C. Stamps were created from cured PDMS solution.

To complete the microfluidic device, PDMS stamps were attached to Aquasil-coated glass slides. Glass slides were soaked in 28.8% Nitric Acid Solution for 1 hour, oven-dried, washed 3 times with Millipore water, and placed into a 1% Aquasil solution (Thermo Fisher Scientific, Waltham, MA) for 15 seconds. To ensure a tight seal over the coated glass slides for collagen infusion through the channel, PDMS was cut from the wafer and cleaned in a PlasmaFlo chamber (High RF, 300 mTorr for 1 min) before glass attachment.

2.6.2 Fabrication of Collagen Substrates

On ice, 8 parts bovine Type I collagen solution (3.0 mg/ml, PureCol, Advanced BioMatrix, San Diego, CA) was mixed with 1 part 10x MEM and 1 part NaOH to adjust the pH to physiological levels for collagen preparation. 1x MEM was also added to adjust the final concentration of collagen to 1.6 mg/ml.

The solution was drawn into a 1 ml syringe connected to tubing (Silastic, Dow Corning), ensuring no bubbles. Immediately after, the tubing was connected to the PDMS device, and collagen solution was gently flowed through the channel prior to starting the flow (Figure 2.8). Once collagen had reached the outlet of the channel within the device, the syringe was quickly placed into a syringe pump, which was set at a flow rate of 7.5 μl/min (or 150 s^{-1}). The device was placed on a hot plate set at 37°C to initiate collagen polymerization. After 30 minutes, PDMS was removed from the glass and the newly formed collagen was rinsed carefully with Millipore water. Slides with aligned collagen were left to dry at room temperature. After the channel dried, a 30-mm diameter PDMS ring (cleaned in a PlasmaFlo chamber with high RF, 300 mTorr for 1 min) was inserted on top of the slide, creating a well for the cell suspension.

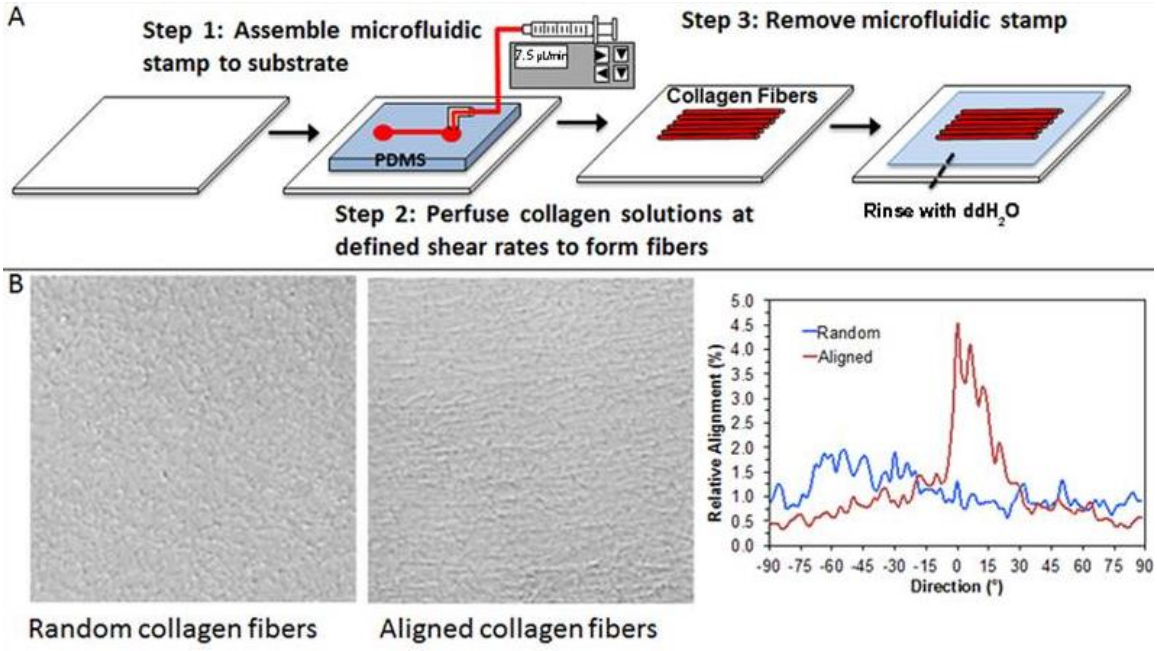

Figure 2.8. Schematic of Aligned Collagen Fabrication.

For random collagen, a PDMS ring (cleaned in a PlasmaFlo chamber High RF, 300 mTorr for 1 min) was placed on top of the Aquasil coated glass slide. The neutralized collagen solution (1.6 mg/ml) was placed into the well (while on ice to prevent polymerization), and immediately positioned over the hot plate at 37°C for 30 minutes.

For collagen-coated substrates, a 50 μg/ml neutralized solution of bovine Type I collagen solution (3.0 mg/ml, PureCol, Advanced BioMatrix, San Diego, CA) was dispensed into a glass bottom 30-mm diameter poly-d-lysine coated MatTek dish and placed in a humidified incubator (37°C, 5% CO2) for 30 minutes as previously described.[119] Dishes were rinsed twice with Dulbecco's modified Eagle's medium (DMEM; Sigma-Aldrich, St. Louis, MO) supplemented with 1% RPMI vitamin mix (Sigma-Aldrich, St. Louis, MO), 100

μM nonessential amino acids (Invitrogen), 100 μg/ml ascorbic acid, and 1% penicillin/streptomycin (Invitrogen) prior to adding cells.

2.6.3 Cell Culture

To study individual cell behavior on the collagen substrates, primary rabbit corneal keratocytes (NRK) cells extracted from New Zealand white rabbit eyes (Pel-Freez, Rogers, AR) were used. Cells were cultured in DMEM serum-free media for at least 3 days in a humidified incubator (37^{o}C, 5% CO_2) prior to experiment use.

2.6.4 Plating for Cell Spreading and Migration Experiments

For analysis of cell morphology and alignment following spreading on different topographic substrates, cells were seeded at a density of 20,000 cells/ml (allowing for acquisition of images with isolated cells) with either PDGF-BB (50 ng/ml), TGF-β1 (5ng/ml), or DMEM serum-free media (as described above) for 48 hours in a humidified incubator (37^{o}C, 5% CO_2). Experimental design for conditions used for assessment is displayed in Table 2.6.4.

Table 2.6.4. Experimental Design for Specific Aim 2

Experimental Group (Growth Factor)	Freeze Injury or No Injury	Collagen Orientation
Serum Free (control)	Freeze Injury	Random
		Aligned
		Collagen-coated
	No Injury	Random
		Aligned
		Collagen-coated
PDGF	Freeze Injury	Random
		Aligned
		Collagen-coated
	No Injury	Random
		Aligned
		Collagen-coated
TGF-β	Freeze Injury	Random
		Aligned
		Collagen-coated
	No Injury	Random
		Aligned
		Collagen-coated

To study the effects of topography on cell migration, a FI model was used. For FI experiments, cells were seeded at a density of 50,000 cells/ml with either PDGF-BB (50 ng/ml), TGF-β1 (5ng/ml), or DMEM serum-free media (as described above) for 24 hours. To conduct the FI, media was removed, and a 1 mm stainless steel probe was dipped in liquid nitrogen for 10 seconds. In the center of the dish (for random collagen and collagen-coated) and half-channel (width-wise) for aligned collagen, the probe was placed on the back (glass) side of the device for 10 seconds immediately after dipping in liquid nitrogen. Any detached or partially detached cells were then washed away with DMEM serum-free media, and the slide was checked for cell detachment in the wound area. If no cells detached, then the injury was created again in the same location. Following injury, media containing PDGF, TGF-β1, or DMEM serum-free media was re-added, and the cells were left for 4 additional days in a humidified incubator (37^{o}C, 5% CO_2) to allow for migration. In a subset of samples, time-lapse imaging was conducted for 72 hours.

2.6.5 Immunocytochemistry

Cells were fixed using a 3% paraformaldehyde solution for 10 minutes, washed two times for 10 minutes each, permeabilized using 0.5% Triton X-100 in PBS (phosphate buffered saline) for 15 minutes, washed once for 10 minutes, and incubated with Alexa Fluor 488 Phalloidin (1:100, Molecular Probes, Eugene, OR) for 1 hour at 37^{o}C. For alpha-smooth muscle actin (α-SMA) labeling, primary anti-mouse α-SMA (1:600, Sigma, St. Louis, MO, USA) was added to the cells and incubated for 2 hours at 37°C. Cells were then washed three times, 20 minutes per wash, and then incubated with secondary anti-mouse FITC (1:200) and

Alexa Fluor 546 Phalloidin (1:150) at 37°C for 1 hour. The collagen and cells were imaged using a Nikon TE300 inverted microscope (TE300; Nikon, Tokyo, Japan) with differential interference contrast (DIC), phase, and fluorescent capabilities using a 40x water immersion objective.

2.6.6 Scanning Electron Microscopy (SEM)

For SEM imaging, samples were fixed with a 2.5% glutaraldehyde in 0.1M Cacodylate buffer solution for 2 hours at room temperature. Samples were then rinsed in 0.1M Cacodylate buffer three times, and fixed again with 2% Osmium in 0.1M Na Cacodylate buffer. After rinsing five times with Millipore water, samples were dehydrated using an increasing concentration of ethanol (50%-100%). Following dehydration, samples were placed into a critical point dryer, and sputter-coated. Collagen fibers were viewed using a field emission SEM Zeiss Sigma at 3 kV.

2.6.7 Orientation Index

DIC and phase images sized at 1024 pixels x 1024 pixels were run through in-house MATLAB software for determination of orientation index (OI) along a given angle to quantify vertical alignment. The following equation was used:

$$OI\ (\theta) = \{2 < \cos^2 \theta > - 1\}100\%$$

Where,

$$< \cos^2 \theta > = \frac{\int_{-90}^{90} I(\emptyset)\{\cos^2(\emptyset - \theta)\} d\emptyset}{\int_{-90}^{90} I(\emptyset)\, d\emptyset}$$

and θ=0° is the x axis within the image.[124] In this study, the angle selected was 90°, which indicates the direction of the collagen fibers. For cells completely aligned with collagen, the OI is equal to 1; whereas for cells completely perpendicular to the collagen fibers, the OI is equal to -1, and for randomly aligned fibers the OI is equal to 0. Analysis was conducted on the entire image, and assessed for each region (wounded vs. unwounded). Values for each image were averaged with results from images in comparable areas. For each growth factor group, at least 5 experiments with two samples per region were used for calculations.

2.6.8 Assessment of Cell Morphological Changes

Fluorescent images of cells seeded at 20,000 cells/ml were used to calculate morphological changes in MetaMorph (Molecular Devices, LLC., San Jose, CA). Cells were traced using the multiline tool and painted white. Next, using the Integrated Morphometry Analysis Module, shape factor and length/breadth of cells were analyzed. Shape factor measured the circularity of the cell and ranged from 0 to 1, where a perfect circle has a shape factor of 1. Length/breadth values were also used to determine cell shape; the higher the ratio, the more elongated the cell.

2.6.9 Scientific Rigor and Reproducibility

Aligned collagen substrates were fabricated in both Dr. Petroll's and Dr. Schmidtke's lab. These substrates were also fabricated by different lab members, and imaged using DIC microscopy in Dr. Petroll's and Dr. Schmidtke's lab. In all cases, similar results were obtained. Aligned substrates were also fabricated using a microscope incubator as well as a hot plate, and each method had similar results. Experiments were conducted multiple times with multiple samples per condition.

2.7 INITIAL RESULTS USING IN VITRO MODELS

2.7.1 Outcomes for Substrate Fabrication

Collagen substrates were fabricated to create aligned and random collagen fibers, and collagen-coated dishes (Figure 2.8B). For random substrates, collagen fibers appeared tangled and orientated without preference to a specific direction after 30 min of polymerization (Figure 2.8B, left). After 30 min of collagen infusion at a flow rate of 7.5 µl/ min, aligned fibers started to develop throughout the collagen channel using the PDMS microfluidics device (Figure 2.8B, right). Collagen-coated substrates contained soluble, monomeric collagen, where no collagen fibers were present; therefore, collagen was not detectable using DIC microscopy.

2.7.2 SEM Imaging for Verification of Collagen Polymerization

SEM imaging was conducted on substrates to observe collagen fibers at a higher magnification and to verify collagen polymerization (Figure 2.9) seen with DIC. In the aligned collagen substrate, SEM imaging revealed collagen fibers that appeared to have a

twisted, rope-like structure (Figure 2.9A-C), similar to what has been shown before by Saeidi and associates.[48] In aligned substrates, alignment was seen at a global level at 10x (Figure 2.9A). There was no obvious difference detected in collagen structure between the non-injured (Figure 2.9A, B) and injured regions (Figure 2.9C). In random collagen substrates, collagen fibers were randomly oriented and did not have a twisted appearance in both non-injured (Figure 2.9D, E) and injured (Figure 2.9F) regions. There was also no difference detected between collagen fibers in the non-injured and injured regions of the random substrate. Interestingly, a thin, smooth layer of collagen appeared to form over the collagen fibers in some regions of the random substrates (Figure 2.9D-F). SEM imaging was not conducted on collagen-coated substrates since no fibers were formed. Cell processes extended on top of collagen fibers are shown in (Figure 2.9B, C, and F, arrows).

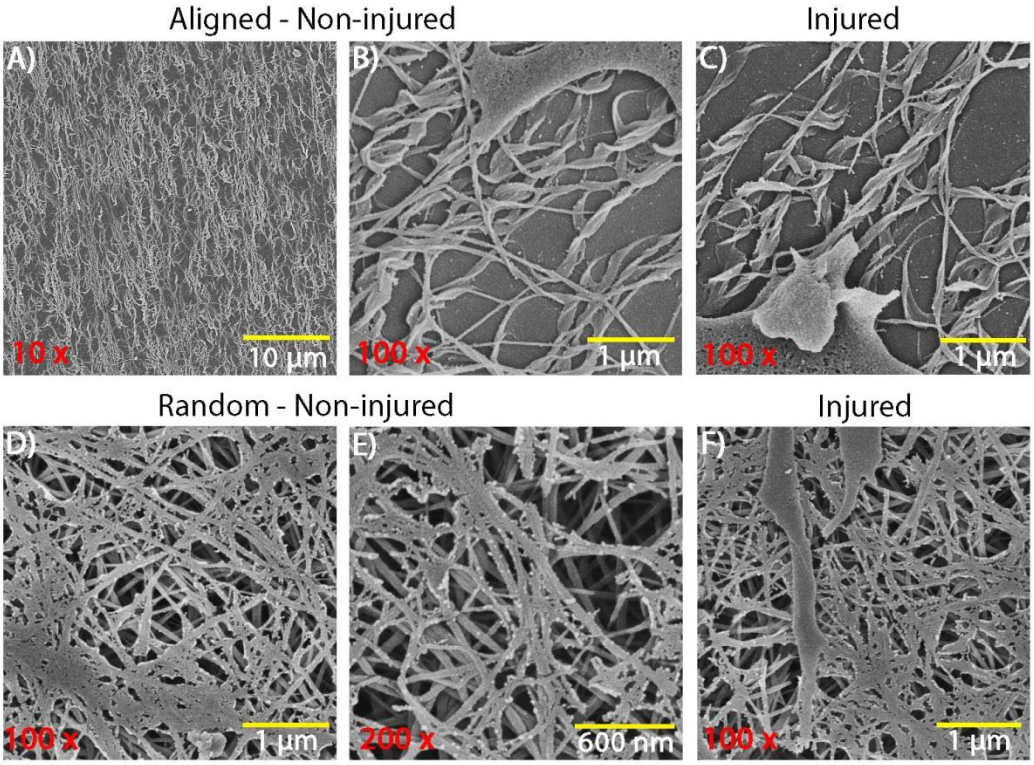

Figure 2.9. SEM images of collagen substrates in non-injured and injured regions. Aligned collagen fibers in non-injured (A, B) and injured regions are shown. Random collagen fibers in non-injured (D, E) and injured (F) regions are shown. Image A is at 10x magnification, while images B, C, D, and F are at 100x magnification. Image E is at 200x magnification. Arrows indicate cells.

2.7.3 DIC and Fluorescent Imaging

Cells were fixed and imaged using DIC and/or fluorescent microscopy for collagen and cell (F-actin) imaging, respectively. With aligned collagen substrates, cells in PDGF-containing media were narrow, elongated, and highly aligned to the collagen fibers (Figure 2.10A). In random and collagen-coated substrates, cells in PDGF were randomly oriented and elongated (Figure 2.10B and C, respectively).

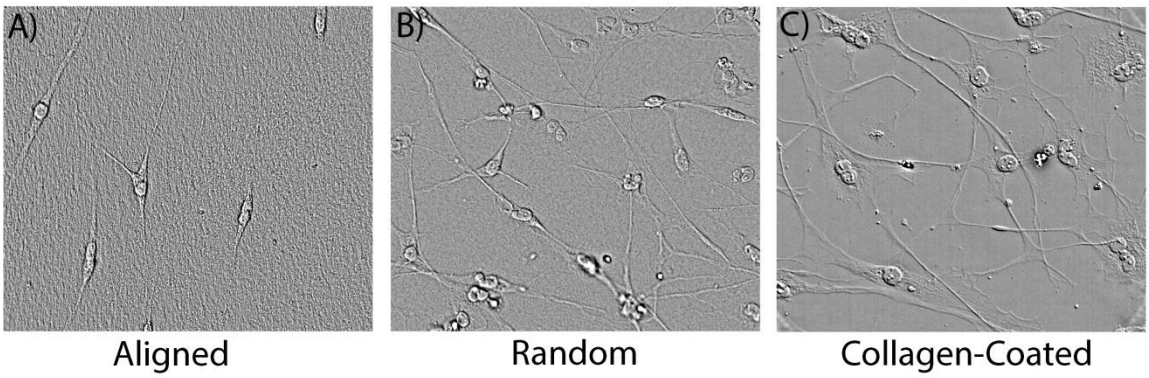

Figure 2.10. DIC images of PDGF treated primary keratocytes on vertically aligned (A), random (B), and collagen-coated (C) substrates. Images are 200 µm x 175 µm.

Similar to FI in vivo, cells surrounding the injured site began to migrate and repopulate the acellular region after injury in vitro. In the PDGF aligned collagen condition, cells in the non-injured region were generally aligned (Figure 2.11A), but cell processes became more co-aligned with collagen during migration into the injured site at the leading edge (Figure 2.11D and 2.12A). Cells were not observed to migrate against fiber alignment (Figure 2.12B). In initial experiments, wound areas were found to completely repopulate with cells plated on aligned substrates in PDGF (not shown). In the PDGF random collagen substrate, cells were randomly oriented in both the non-injured (Figure 2.11B) and injured regions

(Figure 2.11E). Similar to the random substrates, cell patterning in the collagen-coated dishes was random in both non-injured (Figure 2.11C) and injured regions (Figure 2.11F). Cells in PDGF did not completely repopulate the wound site on random or collagen-coated substrates in initial experiments. These early findings are thus far consistent with previous studies that indicate cells migrate faster while on aligned substrates.[125]

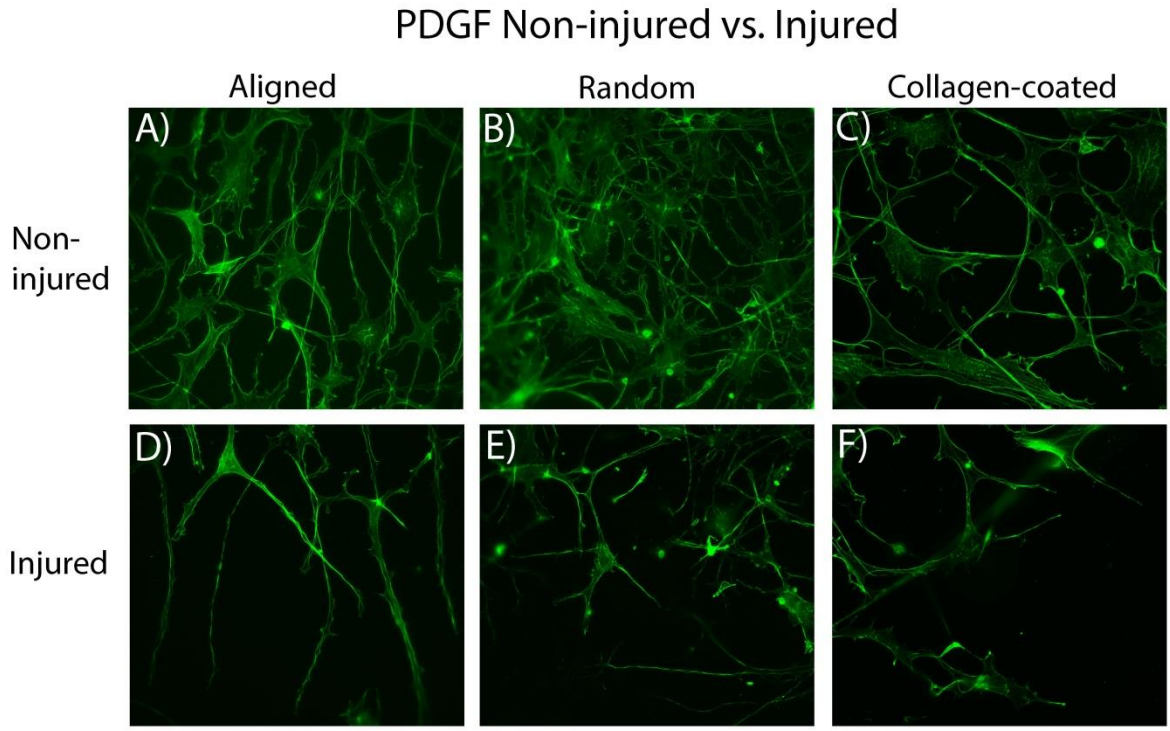

Figure 2.11. Fluorescent images of PDGF treated primary keratocytes on aligned (A, D), random (B, E), and collagen-coated (C, F) substrates. The non-injured regions (A-C) and leading edge of injured regions (D-F) are shown. The injured regions are at the bottom of images D-F. Collagen is patterned vertically in the aligned substrates. Images are 200 μm x 175 μm.

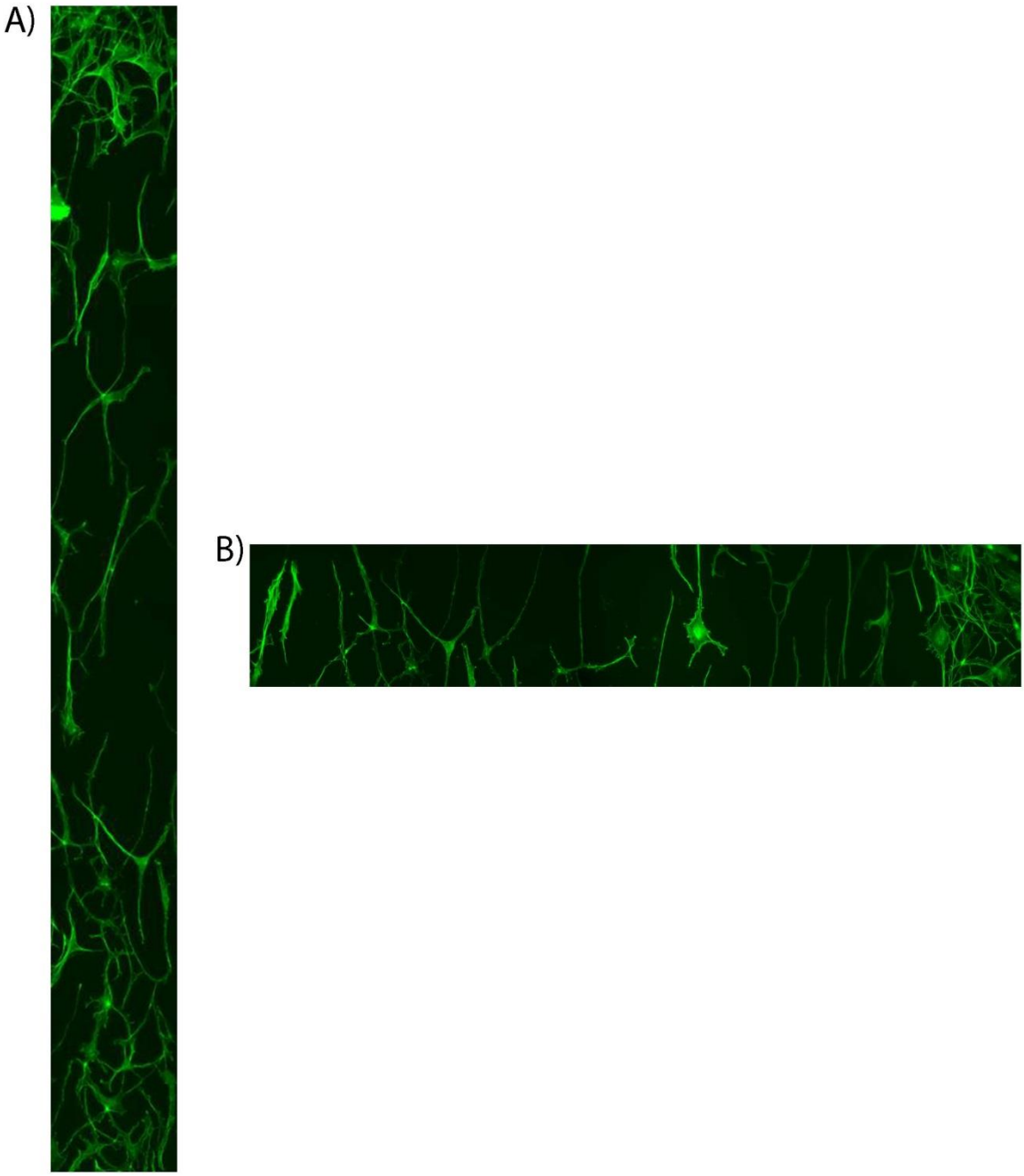

Figure 2.12. Fluorescent images of cells at the leading edge of the FI on aligned substrates. Image (A) shows the wound area length-wise along the collagen channel, while image (B) shows the wound area width-wise across the collagen channel. Collagen is patterned vertically in (A) and (B). Image (A) is 20 µm x 185 µm and image (B) is 245 µm x 45 µm.

Cells in TGF-β containing media expressed prominent stress fibers that were organized in parallel to the collagen fibers in non-injured (Figure 2.13A) and injured regions (Figure 2.13C) of aligned collagen substrates; cell membranes were also aligned to the direction of the collagen fibers. While conducting the experiments with random substrates in the PDGF condition, there were some challenges in obtaining consistency in substrate fabrication. Since the collagen-coated substrates yielded the same results as the random substrates in the PDGF condition and could be consistently fabricated, these substrates were used in place of random substrates thereafter for the TGF-β and serum free media conditions. Cells in TGF-β on collagen-coated substrates were also randomly oriented in non-injured (Figure 2.13B) and injured (Figure 2.13D) regions, and contained stress fibers. Cells with TGF-β did not appear to completely repopulate the wound area in either substrate in initial experiments.

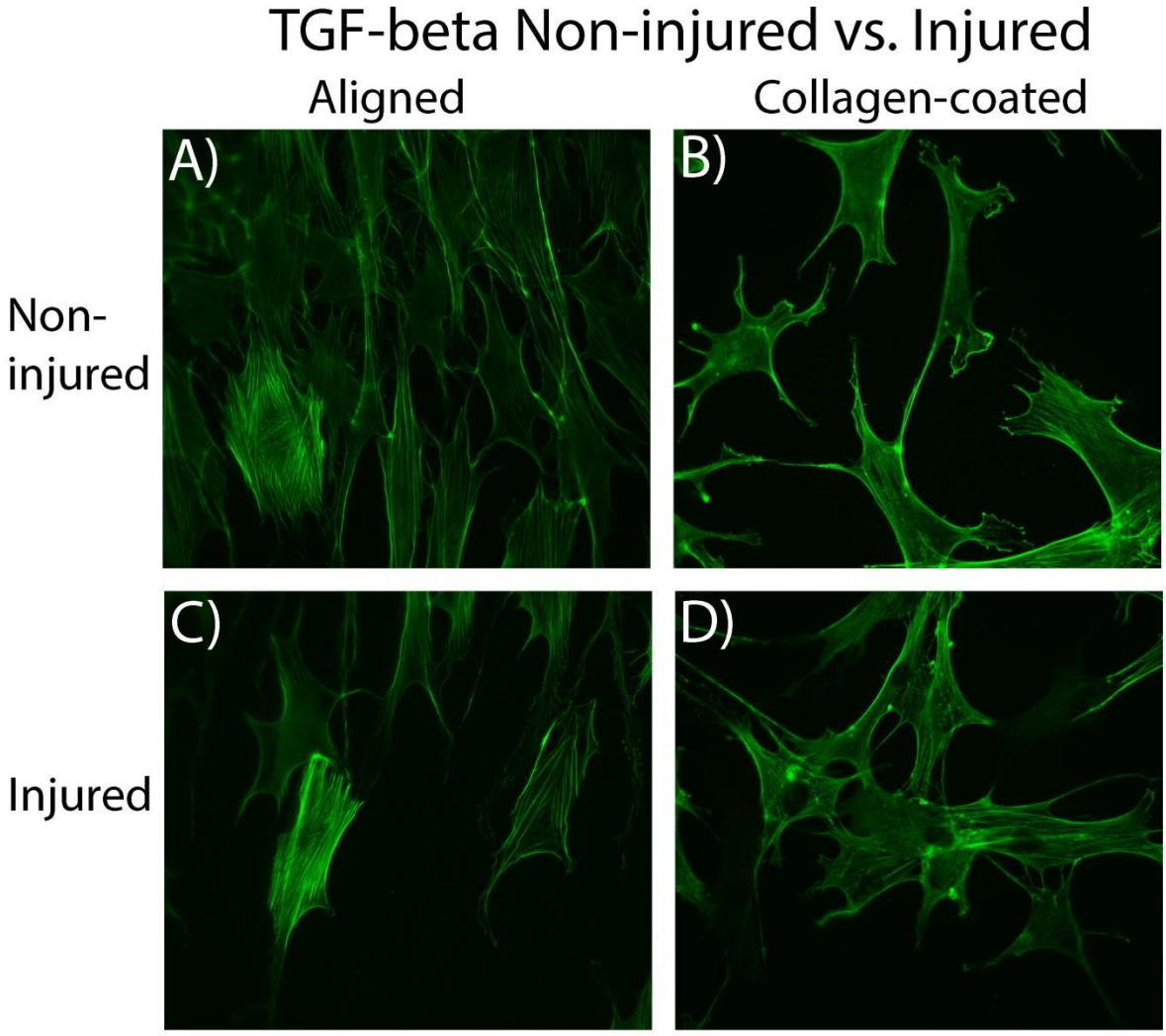

Figure 2.13. Fluorescent images of TGF-β treated primary keratocytes on aligned (A, C) and collagen-coated (B, D) substrates. The non-injured regions (A, B) and leading edge of injured regions (C, D) are shown. The injured regions are at the bottom of images C, D. Collagen is patterned vertically in the aligned substrates. Images are 200 μm x 175 μm.

Verification of myofibroblast transformation on cells plated in TGF-β media was conducted by labeling for α-SMA and phalloidin (Figure 2.14, in green and red, respectively). Generally, cells in the non-injured region of the aligned collagen expressed strong α-SMA signaling (Figure 2.14A), while migrating cells in the injured region did not show strong α-SMA signaling (Figure 2.14C). In the collagen-coated substrates, cells in the non-injured region expressed α-SMA (Figure 2.14B), and α-SMA signaling was also observed in the wound margin (Figure 2.14D). However, it is unclear if cells were migrating. In comparison with aligned collagen substrates, cells in the injured region of collagen-coated substrates had more α-SMA signaling.

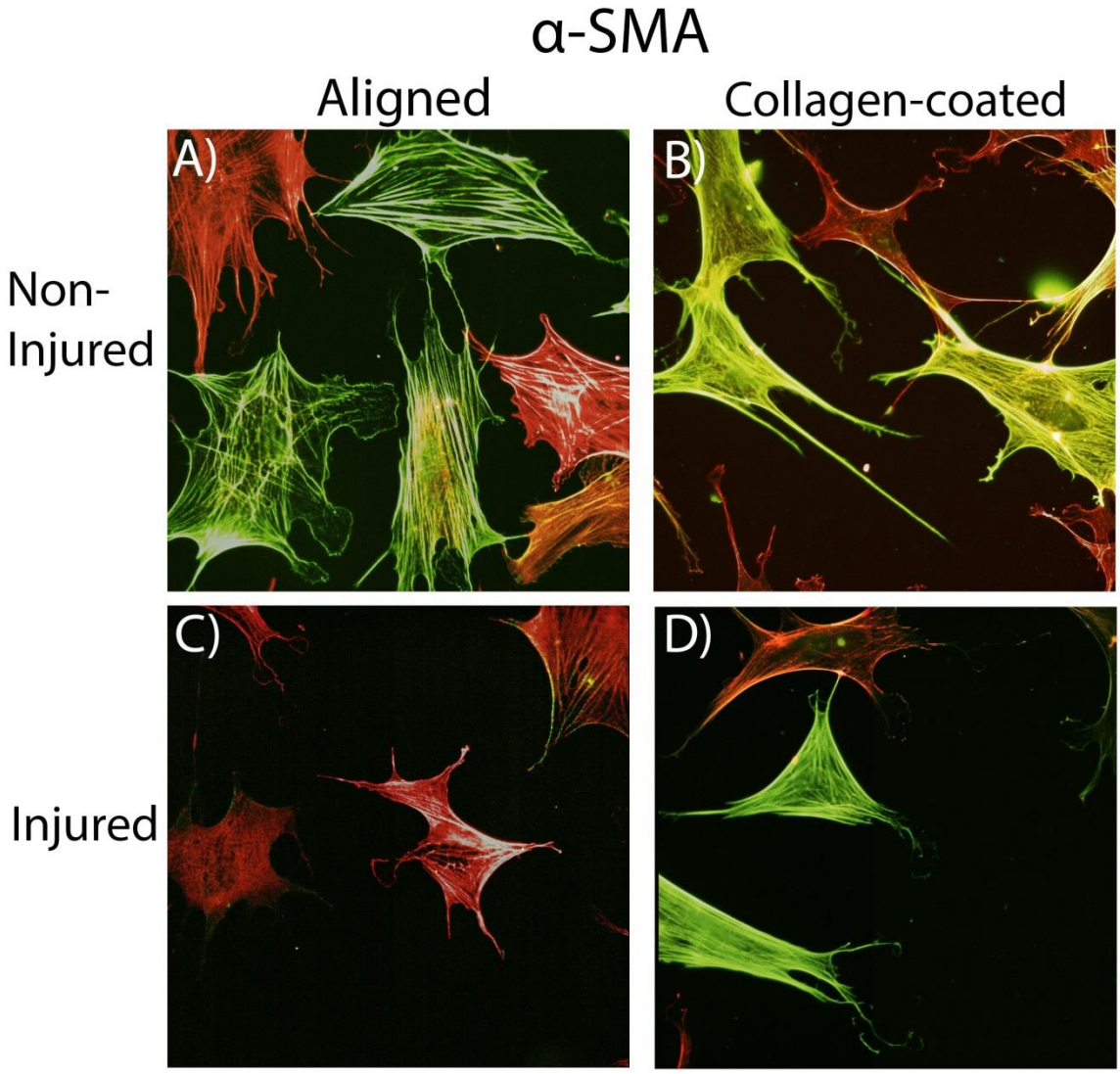

Figure 2.14. Immunocytochemistry images of α-SMA (shown in green) and phalloidin (shown in red) on primary keratocytes treated with TGF-β. Cells are shown on aligned substrates (A, C), and on collagen-coated substrates (B, D). The non-injured regions (A, B) and leading edge of injured regions (C, D) are shown. The injured regions are at the bottom of images C, D. Collagen is patterned vertically in the aligned substrates. Images are 175 μm x 175 μm.

Cells in serum-free media were quiescent, dendritic, and did not express stress fibers on either aligned or collagen-coated substrates (Figure 2.15). Cells on aligned collagen generally co-aligned to the collagen pattern in the injured region (Figure 2.15C), but were not as aligned in the non-injured region (Figure 2.15A). Cells in serum free media plated on collagen-coated dishes were randomly oriented and dendritic in both the non-injured (Figure 2.15B) and injured (Figure 2.15D) regions. Cells with serum free media also did not appear to completely repopulate the wound area in either substrate in initial experiments.

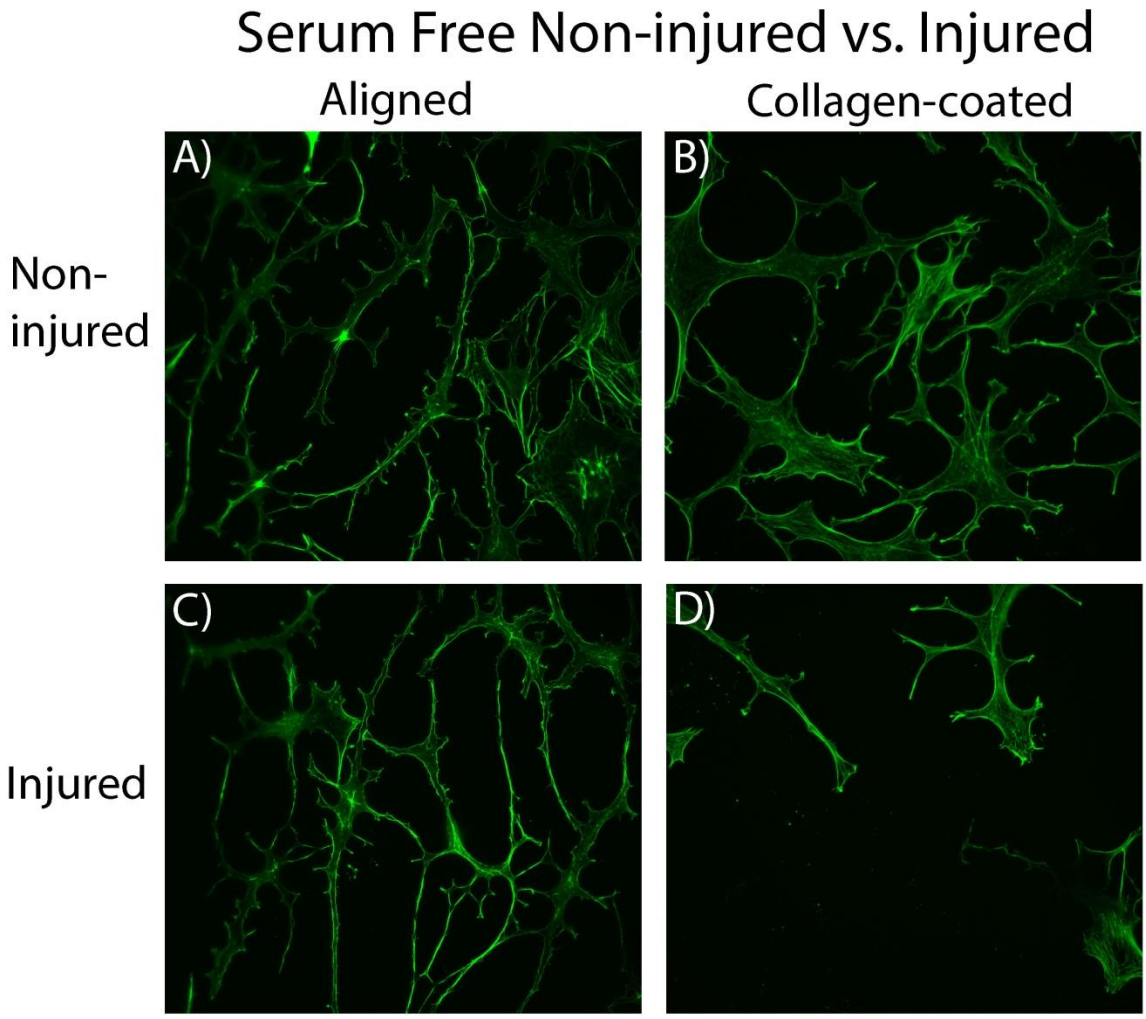

Figure 2.15. Fluorescent images of serum free primary keratocytes on aligned (A, C) and collagen-coated (B, D) substrates. The non-injured regions (A, B) and leading edge of injured regions (C, D) are shown. The injured regions are at the bottom of images C, D. Collagen is aligned vertically in the aligned substrates. Images are 200 μm x 175 μm.

2.7.4 Quantification of Cell Alignment

To quantify the extent of cell alignment in non-injured and injured regions, orientation indices were calculated. The OI refers to the extent of alignment of image content to a particular angle, with values closer to 0 having no alignment and values closer to 1 or -1 having total alignment. Here, an angle of 90° was used, based on the baseline angle of collagen fiber patterning. Using in-house MATLAB program, OI values were calculated using images from cells seeded on aligned collagen (Figure 2.16) and on collagen-coated (Figure 2.17) substrates at the leading edge of cell migration into the injured site, listed as "near wound", or in the non-injured region, listed as "outside". In each media condition on aligned substrates, the OI was higher for cells near the wound vs. outside of the wound. PDGF and TGF-β had higher orientation indices than the serum free (SF) condition for both non-injured and injured regions. In collagen-coated substrates, the OI values calculated for each growth factor condition in "outside" were centered around 0.

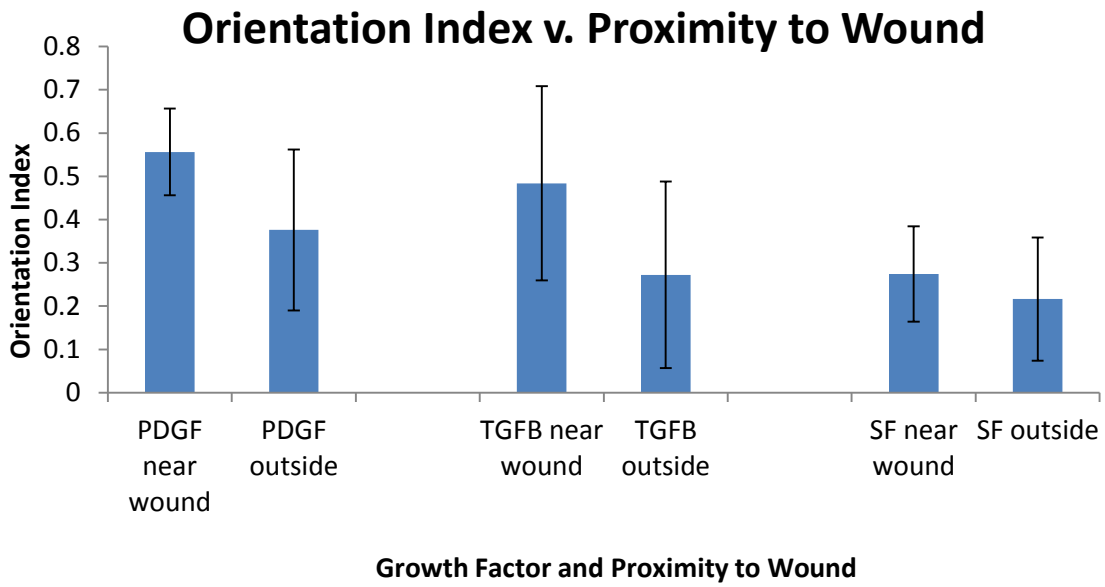

Figure 2.16. Orientation indices for each media condition on aligned substrates for injured vs. non-injured regions.

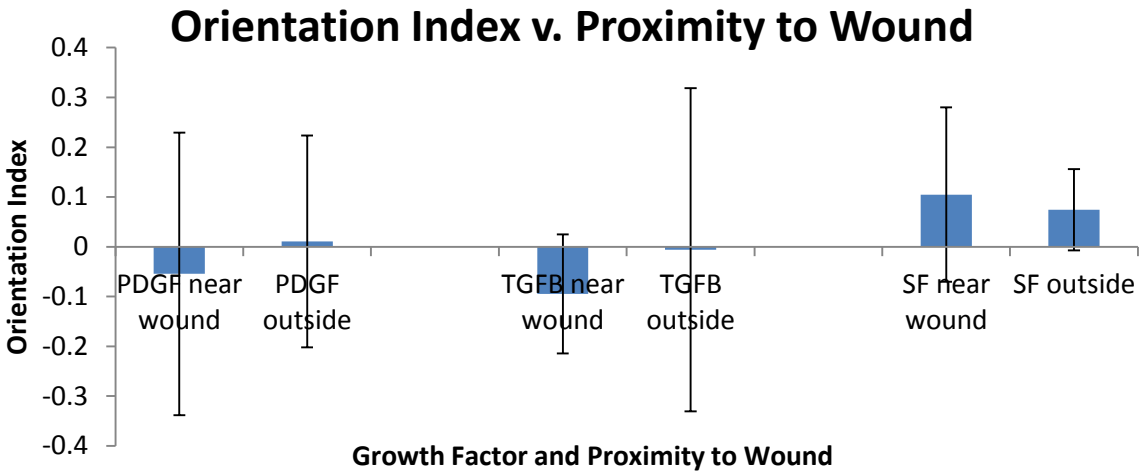

Figure 2.17. Orientation indices for each media condition on collagen-coated substrates for injured vs. non-injured regions.

2.7.5 Quantification of Cell Morphology

Cells in PDGF on aligned substrates were highly elongated compared to cells in TGF-β and serum free media. To assess cell shape quantitatively, calculations for determining length/breadth factor in MetaMorph were conducted on cell images plated on aligned substrates. A higher length/breadth factor indicates that cell shape was longer and narrower. Data generated in Figure 2.18 revealed that cells in PDGF media had a higher length/breadth factor compared to TGF-β and serum free media conditions on aligned substrates. However, the large error bars for TGF-β indicated that there was more variability in shape than measured for PDGF and serum free. This was also observed qualitatively with fluorescent images (Figure 2.13).

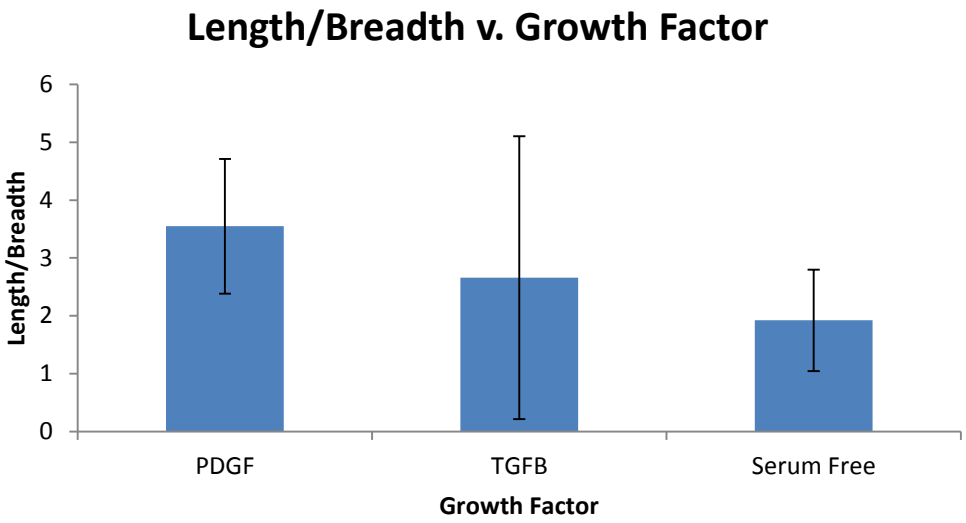

Figure 2.18. Length/Breadth for each media condition on aligned substrates.

Additionally, shape factor was calculated in MetaMorph using cell images from aligned substrates to determine the circularity of a cell. The closer the shape factor measurement was

to 1, the more circular the cell was within an image. Cells in PDGF had a lower shape factor measurement than TGF-β and serum free media conditions on aligned substrates (Figure 2.19). These results were consistent with qualitative observation from fluorescent images (Figure 2.12); cells in PDGF were more elongated and less circular than cells seen in the TGF-β and serum free media conditions.

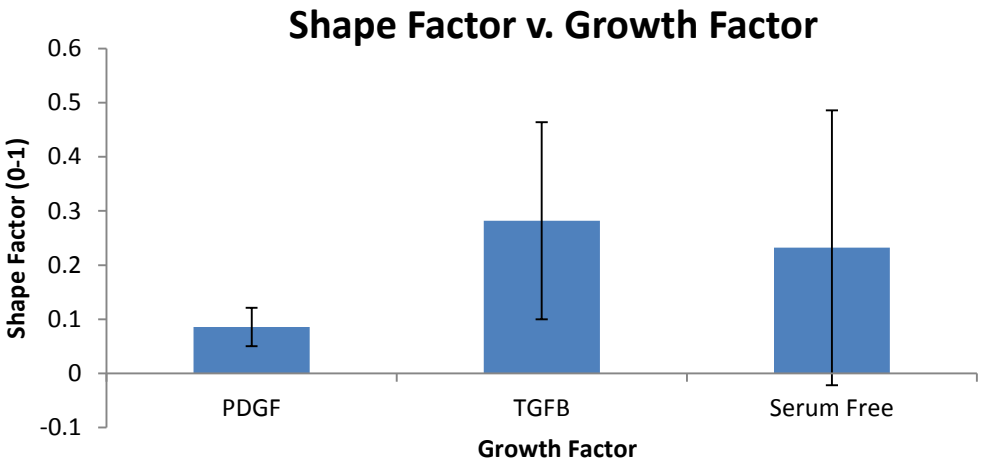

Figure 2.19. Shape Factor for each media condition on aligned substrates.

2.8 DISCUSSION OF INITIAL RESULTS

Fluorescent imaging revealed that substrate alignment affected cell patterning and morphology. Cells were more aligned on aligned substrates for all growth factor conditions compared to collagen-coated substrates. These findings were also previously shown on polyurethane substrates, where a greater topographical "pitch" size corresponded with more alignment of keratocytes, fibroblasts, and myofibroblasts.[125] However, substrate alignment was not shown to reduce TGF-β transformation in non-injured regions, which is inconsistent

from previous studies with electrospun Type I collagen fibers.[123] A difference in substrate fabrication methods could explain this finding. Although transformation was consistently observed outside of the wound site in the TGF-β condition on aligned substrates, α-SMA expression was reduced in cells at the leading edge of migration. Consistent with previous studies, motile cells were observed to have narrower morphologies and a reduction in stress fibers.[126]

Interestingly, corneal fibroblasts and myofibroblasts have been shown to migrate mostly in parallel to substrate topography and not perpendicular.[125] These findings were also observed in this study with the horizontal montages collected, where cells migrated mostly along collagen fibers. Additionally, cells were also observed to be more aligned with collagen during migration based on orientation index calculations. Growth factors were observed to influence cell morphology on aligned substrates: cells in PDGF were more elongated than cells in TGF-β and serum free media based on length/breadth and shape factor values. Further studies are needed to compare morphological changes in collagen-coated substrates. Additional studies for determining cell migratory rates and effects of 3-D ex vivo ECM environments are discussed in Chapter 5.

CHAPTER THREE
Lamellar Keratectomy

Reproduced with permission from: Kivanany, P.B., Grose, K.C., and Petroll, W.M., Exp Eye Res, 2016. 153: p. 56-64, Elsevier.

3.1 BACKGROUND

3.1.1 Significance and Imaging Modalities for Investigating Wound Healing after Keratectomy

Previous studies have assessed changes in cell phenotype, backscatter and ECM composition during stromal wound healing following keratectomy wounds;[49, 51-54] however, the temporal and spatial correlation between cell alignment and ECM patterning during the fibrosis, remodeling and/or regeneration phases of wound healing has not been established.

In this study, the temporal and spatial relationships were investigated between cell and ECM organization during healing following LK. Using the custom modified HRT-RCM in vivo confocal microscope,[127] keratocyte patterning, tissue growth, and corneal haze development was assessed throughout the full thickness of the cornea at various time points post-injury. Additionally, in situ multiphoton fluorescence and SHG imaging was used to determine the correlation between cell and ECM alignment in the migratory, fibrotic and regenerative/remodeling phases of wound healing. [128, 129]

3.2 METHODS

3.2.1 Animal Model

All animal procedures were in accordance with the ARVO statement for the Use of Animals in Ophthalmic and Vision Research as well as approved by the University of Texas Southwestern Medical Center Institutional Animal Care and Use Committee. 12 New Zealand white rabbits were anesthetized using 50 mg/kg intramuscular ketamine and 5.0 mg/kg xylazine and locally anesthetized in the left eye with 1 drop of proparacaine. LK was performed following anesthesia. A speculum was placed into the left eye and a 150 μm deep incision was made in the peripheral cornea using a diamond knife. A spatula was used at the base of the incision to separate the layers of collagen within the stroma. Once a resection plane was created, a 5 mm trephine punch was used to remove the anterior corneal tissue in the central cornea. Immediately following surgery, 0.3 mg/kg of buprenorphine SR (slow release) was injected. Gentamicin eye drops were administered as an antibiotic in the left eye twice a day for 7 days following injury.

3.2.2 In Vivo Confocal Microscopy

Rabbits were monitored using an HRT-RCM in vivo confocal microscope with CMTF software for analysis as previously described.[127, 130] Rabbits were scanned 1 week before LK (Pre-Op), and at 3, 7, 21, and 60 days after LK. Rabbits were anesthetized prior to scanning with 50 mg/kg intramuscular ketamine and 5.0 mg/kg xylazine and locally anesthetized in each eye with 1 drop of proparacaine. Since the reflection from the Tomocap can obscure images of the superficial epithelial cells, a thin PMMA washer was placed on the Tomocap to eliminate these reflections, as previously described.[131] The objective was positioned on the cornea to create a flat field-of-view image in the central cornea. CMTF scans were collected

by starting the scan in the anterior chamber and finishing above the epithelium with a constant speed of 60 µm per second. Images were acquired with the rate set to 30 frames per second. To allow quantitative assessment of haze, scans were collected using a constant gain setting, by unchecking the "auto brightness" box in the HRT software interface. Each scan was conducted using a gain of 6, which was set by moving the horizontal slider under the "auto brightness" box six mouse clicks to the right. At least 3 scans were collected within the central area of the cornea where LK was performed. Each scan contained a 3-D stack of 384 x 384-pixel images (400 x 400 µm), with a step size of approximately 2 µm between images. Additional scans were collected closer to the wound edge in some animals. In some cases, a portion of the scan was saturated when using manual gain settings due to strong cell/matrix reflectivity. In these cases, additional scans were taken using the "auto brightness" enabled so that changes in cell patterning and morphology could be documented. Only the scans taken with a gain of 6 were used for quantitative analysis.

After image acquisition, scans were saved as ".vol" files, which could be opened into in-house CMTF software to analyze the 3-D changes in cell morphology and cell/ECM reflectivity.[127] The program generates an intensity vs. depth curve, corresponding to the average pixel intensity of each image and the z-depth of that image within the scan, respectively. The relative amount of backscatter, or haze, associated with the stromal keratocytes and ECM was measured by taking the area under the curve between the location of the basal lamina peak (top of the stroma) and the endothelial peak. A baseline of 13 was chosen for haze calculations, since this value was below the baseline intensity for the normal

stroma and above the intensity of the anterior chamber. The thicknesses for the epithelial and stroma layer were calculated by the CMTF program after right clicking in the region of the curve that corresponded to the start of each layer in the cornea.

3.2.3 In Situ Multiphoton Imaging

A subset of rabbits was sacrificed at 7, 21, and 60 days to further investigate cell and matrix patterning. The corneal tissue was fixed via anterior chamber perfusion with a PBS solution containing: 1% paraformaldehyde, 1% DMSO, 1% Triton-X-100, and 5% Dextran for 5 minutes, followed by additional submersion ex vivo for 15 minutes, as previously described.[132] Tissues were washed with 1X PBS twice for 10 minutes each, then labeled in situ with Alexa Fluor 488 phalloidin (Molecular Probes, Thermo Fisher Scientific, Waltham, MA, USA) at a concentration of 1:20 in PBS for 3 hours at 37°C. Next, the tissues were washed with PBS three times for 30 minutes each.

Labeled tissues were imaged using multiphoton fluorescence and SHG imaging on a laser scanning confocal microscope (Leica SP8, Heidelberg, Germany). Corneas were blocked to localize the wound area, and placed with the epithelium facing the bottom of the MatTek dish for imaging. A glycerol:PBS solution (2:1) was used to help maintain normal corneal hydration. Multiphoton fluorescence and SHG images were generated using a wavelength of 880 nm (Coherent Chameleon Vision II, ultrafast Ti: Sapphire laser, Santa Clara, CA). SHG forward scatter, phalloidin (F-actin), and SHG backscatter images were

captured simultaneously, as described previously.[130] Stacks of optical sections were collected using a 25x water immersion objective lens (0.95 NA, 2.4 mm free working distance).

3.2.4 Image Analysis for Alignment Measurements

Cell and/or matrix alignment from both in vivo HRT-RCM scans and in situ laser confocal scans were quantified using the "Directionality" plugin in ImageJ, which uses a Fourier Transform algorithm to determine the percent of image content aligned at each radial angle within the image (http://imagej.nih.gov/ij/; provided in the public domain by the National Institutes of Health, Bethesda, MD, USA). Plots showing both cell and matrix directionality were generated from in situ F-actin and SHG images to allow direct comparison of the angle distributions. Regions for analysis were selected in the anterior and posterior stroma using the first stromal image below the epithelium and the last stromal image above the endothelium, respectively. Analysis was conducted in grid-like sub-regions in each image (256 x 256 pixel sub-regions from 1024 x 1024 pixel images) as previously described.[133] Sub-regions that did not contain cells or collagen were not included in the analysis.

3.2.5 Statistical Methods

SigmaPlot (version 12.5; Systat Software, Inc., San Jose, CA, USA) was used for statistical analysis. Linear regression analysis was used to determine the correlation coefficients between the angular distributions of F-actin and the forward scattered SHG signals, as previously described.[130] One way analysis of variance (ANOVA) was used for

comparing haze values, epithelial and stromal thicknesses, and correlation coefficients. Post-hoc analysis using the Holm-Sidak Method was conducted to compare between groups.

3.2.6 Scientific Rigor and Reproducibility

Multiple rabbits were scanned in vivo at each time point, and multiple scans were completed for each eye in different regions. Multiple rabbits were sacrificed for in situ labeling at each time point, and multiple regions were scanned in situ for SHG and multiphoton imaging. Correlation calculations were completed by two different lab members with consistent results. Negative controls were used for fibronectin and α-SMA labeling to insure positive labeling.

3.3 RESULTS

3.3.1 Time-Dependent Tracking of Cellular Changes using In Vivo Confocal Microscopy

The CMTF scans were obtained without difficulty using the HRT-RCM at all of the time points evaluated. Corneal keratocytes were quiescent and did not appear elongated in the pre-operative (Pre-Op), normal cornea; backscatter was primarily from the nuclei with only a faint signal from cell bodies (Figure 3.1A). After keratectomy, an area of keratocyte death is created directly beneath the tissue removal site within the native ECM.[49] By 3 days post-injury, elongated, reflective cells (presumably corneal fibroblasts) had migrated into this acellular wound region (Figure 3.1B), which was approximately 100 microns thick (vertical green arrows in Figure 3.1B). The epithelium was only partially resurfaced at 3 days after

injury, and significant stromal edema was present. At 7 days, elongated corneal fibroblasts were again observed throughout the anterior stromal region (Figure 3.1C). Backscattering from these cells was brightest near the surface of the injured stroma (Supplemental Movie 11 and 12). The epithelium had completely resurfaced at 7 days, and there was less stromal edema. At 21 days, a highly reflective, disorganized layer of cells was present directly beneath the epithelium (Figure 3.1D, note that automatic brightness image is shown). Below this layer, elongated cells were still present in the anterior stroma (Figure 3.1E); however, they were generally less reflective than at day 7. At 60 days, cells in both the sub-epithelial region and anterior stroma had a more quiescent phenotype, as indicated by reduced backscatter primarily originating from the cell nuclei (Figure 3.1F). Cells in the posterior stroma remained quiescent and the endothelium appeared normal at all of the time points studied (not shown).

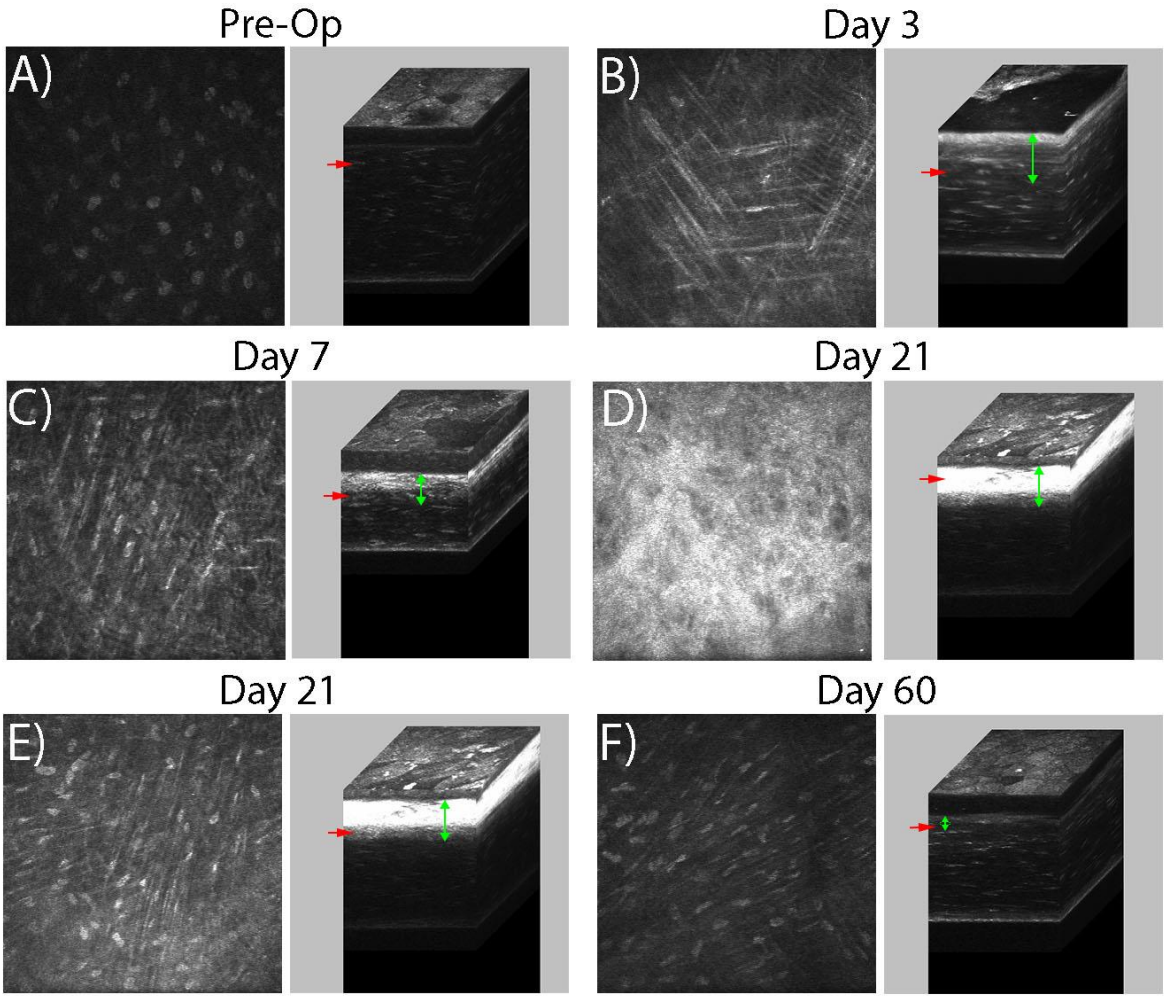

Figure 3.1. Representative images from in vivo CMTF scans (330 µm x 330 µm). The depth of each image within the cornea can be seen in the 3-D image (red arrows, immediately right of the images). Green arrows indicate the region of fibroblastic transformation and/or remodeling in the anterior stroma. (A) Pre-operative, uninjured eye, (B) 3 days post-injury, (C) 7 days post-injury, (D, E) 21 days post-injury, and (F) 60 days post-injury. A, B, C, E, and F were acquired using a manual gain of 6. (D) was acquired using auto brightness enabled, since the manual gain image was saturated.

For quantitative analysis, intensity vs. depth curves were calculated and plotted in the CMTF software (Figure 3.2). [127] In the normal cornea, 3 distinct peaks can be found in the curve (Figure 3.2A), which correspond to the boundaries of the 3 layers of the cornea (epithelial surface "Epi", basal lamina "BL", endothelium "Endo"). At 21 days, a large peak is observed in the anterior stroma due to cell activation and fibrosis (Figure 3.2B), and the haze measured (shaded region under the CMTF curve) is greater than that of uninjured corneas (compared with Figure 3.2A). These CMTF scans were used to measure the average haze for each time point (Figure 3.2C). Quantitative analysis reveals a substantial increase in backscatter post-injury at 7 days compared to the Pre-Op cornea, and maximum haze at 21 days (Figure 3.1D and 3.2C). A reduction in haze to near Pre-Op levels occurs by 60 days. There was a decrease in stromal thickness at day 7 as compared to Pre-Op due to LK; however, stromal thickness progressively increased at 21 days and 60 days (Figure 3.2D). The epithelial thickness had returned to Pre-Op values by day 7, and there were no significant changes at 21 or 60 days after injury (Figure 3.2D).

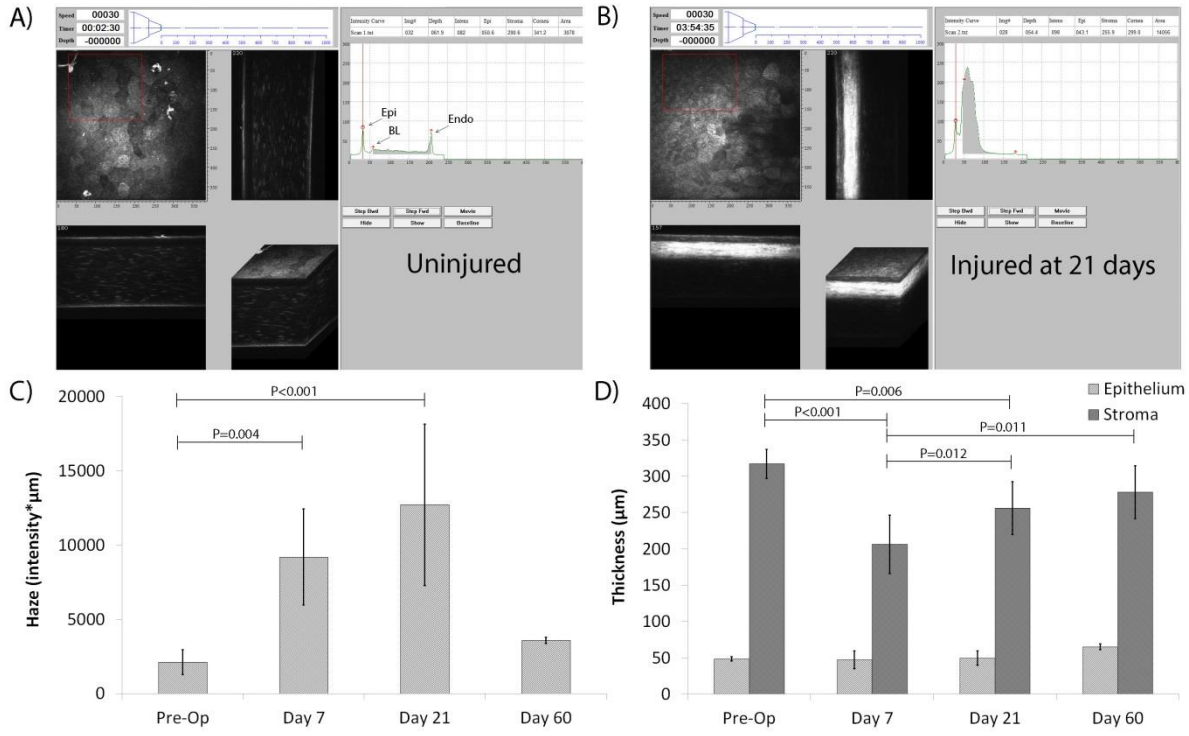

Figure 3.2. CMTF results from in vivo HRT-RCM scans. A) Example of output from a HRT-RCM scan in an uninjured cornea uploaded into CMTF. In the normal cornea, 3 distinct peaks can be found in the curve, which correspond to the boundaries of the 3 layers of the cornea (epithelium "epi", stroma "BL", endothelium "Endo"). B) Example of output from a scan in an injured cornea at 21 days post-injury. A large peak is observed in the anterior stroma due to cell activation and fibrosis (arrow). The haze measured is greater post-injury than pre-injury (shown in A). C) Haze at each time point. (* $P < 0.01$ compared to Pre-Op, ANOVA). D) Epithelial and stromal thickness at each time point (P values are shown as indicated between groups, ANOVA).

3.3.2 Assessment of In Vivo Changes in Cell Patterning

Images obtained with in vivo confocal microscopy also revealed changes in cell patterning. At 3 days post-injury, cells in the anterior stroma had an elongated morphology, and groups of cells aligned in parallel were often observed (Figure 3.1B). A similar pattern was observed at 7 days, although cells were more reflective (Figure 3.1C). At 21 days, cells that were in the reflective layer directly beneath the epithelium were not elongated or aligned in any particular pattern (Figure 3.1D). Below this layer, cells were elongated and generally aligned in interconnected, parallel lines (Figure 3.1E). By 60 days, cells directly beneath the epithelium were elongated and highly aligned with narrow processes (Figure 3.1F).

To investigate whether cell patterning could be quantified from the in vivo confocal images, the "Directionality" plugin in ImageJ (Fiji version) was used. Sequential images within in vivo confocal scans reveal that cell alignment shifts from one layer to the next (arrows, Figure 3.3A and 3.3B), consistent with the orthogonal layering of the collagen lamellae within the cornea (also see Supplemental Movies 11 and 12). Corresponding graphs for each image show the percentage of image content at each angle. As the scan progresses towards the epithelium (scan endpoint), a new layer of cells oriented at a different direction gradually comes into focus (Supplemental Movie 11 and 12), which correlates with a decrease in one peak and an increase in another (depending on the prominence of cell direction at a specific angle).

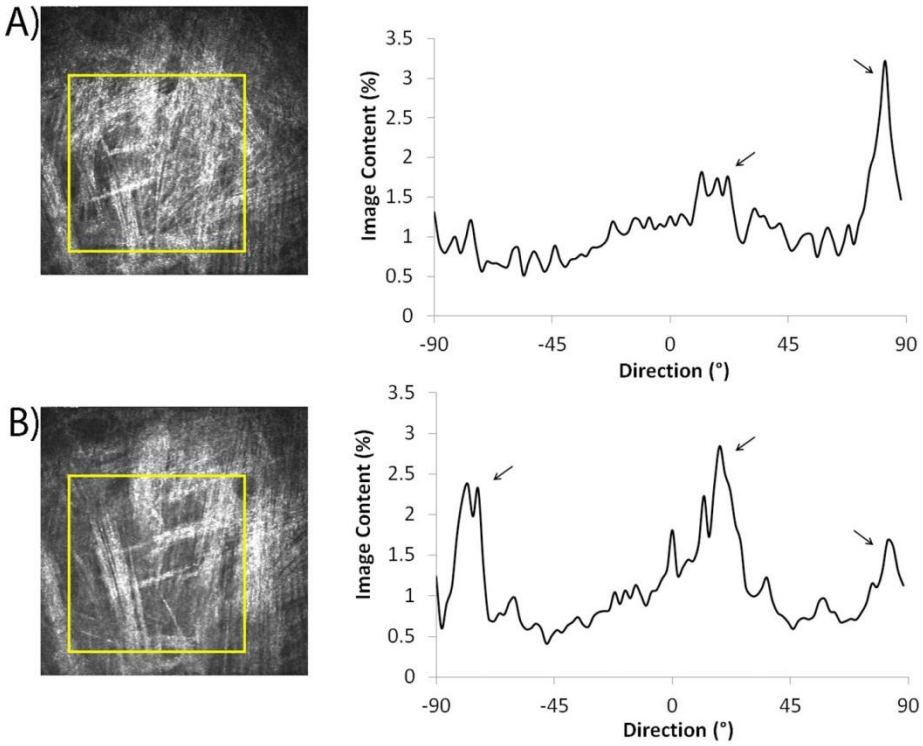

Figure 3.3. Directionality analysis using in vivo HRT-RCM scans. (A, B) Sequential images taken from an in vivo scan 7 days post-LK, and the corresponding graphs revealing the highest percentage of image content at specified angles (arrows).

3.3.3 Temporal and Spatial Analysis of Cell/ECM Alignment

In order to assess changes in keratocyte cytoskeletal organization, F-actin labeling was used. To determine if there was any co-alignment between cells and collagen lamellae, SHG images were collected simultaneously. In the control (un-operated eye), keratocytes are quiescent, and collagen fibers are interwoven in the anterior region of the uninjured stroma with no apparent cell/ECM correlation (Figure 3.4A). Consistent with a study by Young, et al., [134] dendritic processes appeared to be aligned in correlation with the collagen lamellae of the posterior stroma, although no measurable correlation was found since the cell bodies were not aligned. By 7 days, keratocytes transformed into a fibroblastic phenotype, as indicated by an elongated morphology and more intense F-actin labeling. These cells appeared to be arranged into parallel groups that were co-aligned with the collagen lamellae in the anterior stroma (Figure 3.4B).

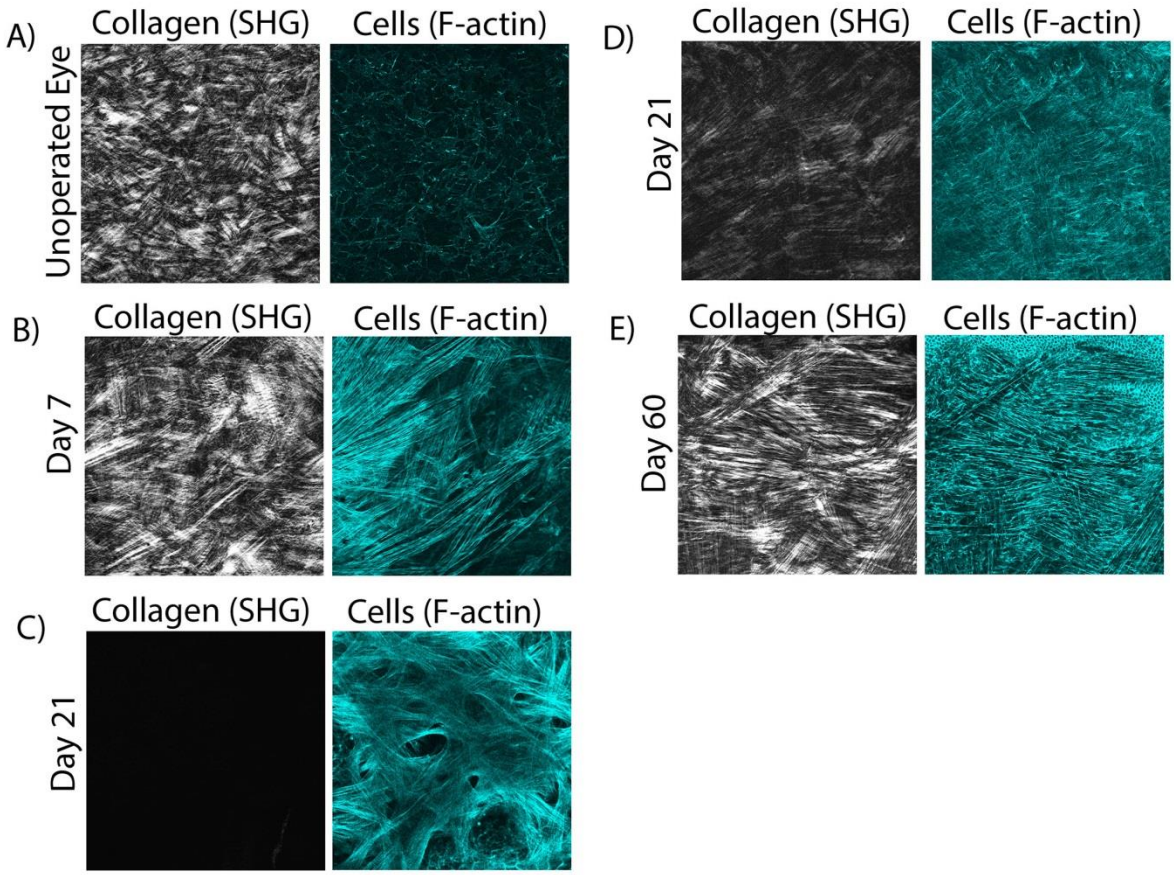

Figure 3.4. Multiphoton fluorescent and SHG images at each time point. A) Collagen and cells in an uninjured cornea (anterior stroma), at 7 days (B), at 21 days on top of the wound (C) and in the anterior stroma (D), and at 60 days (E). Images in (A, B, D, E) are 465 µm x 465 µm. Image (C) is 230 µm x 230 µm.

At 21 days, a region containing a thin additional layer of cells is present directly beneath the epithelium, where little or no SHG signal is detected (Figure 3.4C). These cells are randomly arranged with a broad morphology and prominent intracellular stress fibers. α-SMA (Figure 3.5A) and fibronectin (Figure 3.5B) labeling are also observed in this region, indicating myofibroblast transformation. In contrast, cells directly underneath this myofibroblastic layer, appear to be co-aligned with the collagen at 21 days; these cells are thinner and do not have prominent stress fibers (Figure 3.4D and Supplemental Movie 13).

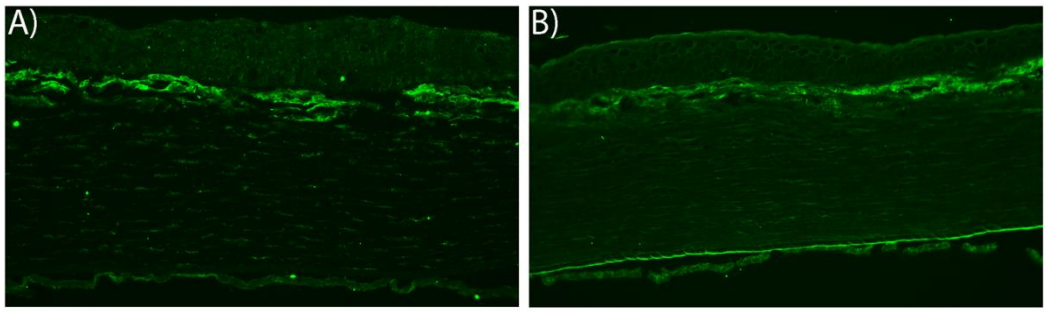

Figure 3.5. Corneal sections labeled with α-SMA (A) and fibronectin (B). Images are 520 µm x 300 µm.

By 60 days, all cells in the anterior stroma are highly aligned with the collagen. These cells are thinner, and have less intense F-actin labeling (Figure 3.4E and Supplemental Movie 14). Overall, the cell morphology and patterning observed in situ is highly comparable to that observed in vivo with the HRT-RCM.

To quantify the extent of alignment between the collagen and the keratocytes, directionality analysis was used at various sites in the cornea. The images were divided into

sub-regions for this analysis (Figure 3.6A and 3.6B), since larger images often contained multiple lamellae oriented at different angles, and could introduce uncertainty in the interpretation of cell/matrix correlations. The average correlation values from the designated regions (as specified in the Methods) indicated that cells and collagen were generally co-aligned in the anterior stroma of the injured corneas, whereas minimal cell/ECM co-alignment was observed in the posterior cornea or in uninjured control corneas (Figure 3.6C). At 7 days, there was greater cell/ECM alignment in the anterior stroma compared to the posterior stroma. Likewise, the anterior stroma had greater co-alignment of cells/ECM compared to the posterior stroma at 21 days. The greatest difference in correlation between the anterior and posterior stroma at any given time point was at 60 days, with the cell/ECM alignment also being the greatest in the anterior stroma compared to all other time points studied.

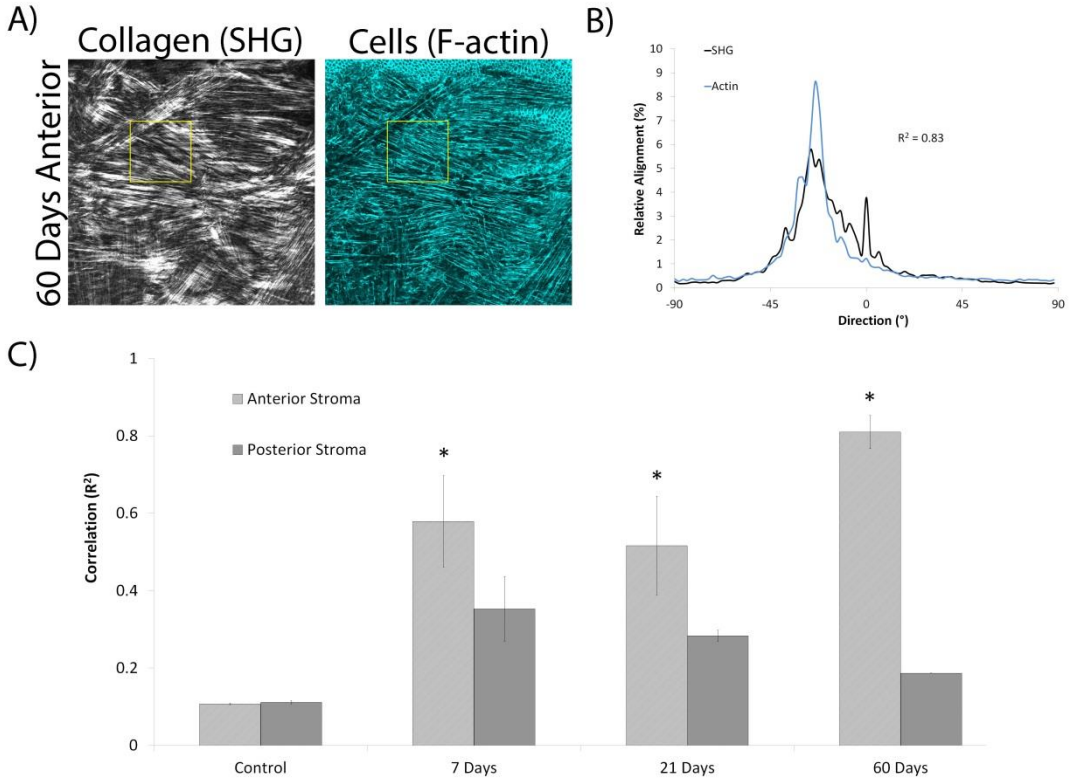

Figure 3.6. Directionality analysis was used to quantify correlation at each time point. Directionality analysis was conducted using smaller regions within an image (the yellow boxed region in (A)), which generated corresponding output shown in (B, from the yellow boxed region). C) Alignment of cells with collagen in different regions of the cornea at all time points. Images in (A-E) are 465 µm x 465 µm. (* $P < 0.05$ compared to posterior stroma and control, ANOVA).

3.4 DISCUSSION

Beginning at 3 days after injury, elongated fibroblasts within the anterior region of the native stroma were organized into groups of parallel cells, whose alignment was highly correlated with that of the collagen lamellae, consistent with observations after FI. The backscattering from these cells peaked at day 7 and gradually decreased at days 21 and 60. These results demonstrate how collagen lamellae patterning may provide topographical cues that modulate corneal fibroblast migration following injury. Supporting these findings, in vitro studies have shown that cell morphology, migration, and phenotype are directly affected by localized substrate topography.[135-137] More specifically, corneal fibroblasts have been previously found to co-align to collagen-coated substrates containing ridges and grooves aligned parallel with a pitch greater than 1 μm.[138] In contrast, on planar surfaces or on surfaces with smaller pitch sizes, fibroblasts were randomly oriented and migrated slower.

In contrast to the aligned cells observed in the stroma, a second population of cells was observed in the sub-epithelial region, beginning at 21 days following LK. This thin layer of cells formed an interconnected network that was randomly arranged, and produced significant backscatter and haze. Cells also had prominent stress fibers and expressed α-SMA and fibronectin at 21 days, suggesting myofibroblast transformation. Importantly, a substantial reduction in sub-epithelial haze between 21 and 60 days was found, as well as stromal re-thickening and a significant increase in cell/matrix co-alignment. These results suggest that there was remodeling of the fibrotic tissue and regeneration of corneal stroma at the wound site.

The EBM plays an important role in differentiation of migrating keratocytes. After LK, the EBM is removed and growth factors, such as TGF-β and PDGF (from the tears and epithelial cells), are allowed to infiltrate into the stroma and modulate keratocyte phenotype to initiate wound healing.[17, 29, 139, 140] Most notably, TGF-β induces myofibroblast transformation of corneal keratocytes, particularly in the anterior stroma.[18, 31, 141-145] These results show myofibroblast localization in the sub-epithelial layer at the wound site by 21 days. However, by 60 days, these myofibroblasts disappear and are replaced by narrow-bodied cells that do not express prominent stress fibers. The mechanism for the transition in the cell phenotype between 21 days to 60 days is unknown. One possible mechanism is that the myofibroblasts become apoptotic and are replaced by more quiescent, elongated keratocytes.[146] Some reports have shown apoptosis of myofibroblasts in the anterior stroma 4 weeks to 3 months post-PRK, likely due to reestablishment of epithelial basement membrane and decreased levels of TGF-β and PDGF.[141, 147] Maintenance of myofibroblast phenotype is dependent upon TGF-β and PDGF; [141] therefore, a phenotypic switch (transdifferentiation) to more passive fibroblasts and keratocytes is also a possibility at decreased levels of these growth factors. [16, 20, 141, 143]

As mentioned above, in addition to changes in cell morphology and phenotype, dramatic changes in cell/matrix alignment were observed between 21 and 60 days after injury. Previous studies by Jester and coworkers[49] have shown that following PRK, significant sub-epithelial haze, myofibroblast transformation and associated fibrosis initially

develops, peaking at 21 days. However, by 6 months, both stromal thickness and haze values return to near Pre-Op levels, suggesting possible regeneration and/or remodeling of corneal tissue. The results following LK are consistent with these findings, and provide new data from SHG and multiphoton imaging as well as correlation analysis, suggesting that this stromal tissue is highly aligned, similar to the native stroma. A study conducted by Wang, et al. demonstrated that cell-secreted collagen was patterned in correlation to the direction of micro-grooved silicone membranes.[148] Thus, sub-epithelial corneal fibroblasts may use the topography of the anterior collagen layer after LK as a template, and align and secrete collagen based on the native collagen patterning of this layer.[149, 150] It is also possible that at later time points, as new cells begin to fill in the tissue void, they spread and/or migrate using cell-secreted collagen from the layer beneath them as a guide, and secrete collagen that is patterned similarly to the native stroma.[87, 105, 106, 151-153] This mechanism of collagen deposition and cell alignment is a potential explanation for why the patterning at 60 days resembles the less interwoven collagen patterning observed at the mid-stroma (template layer location) of the normal cornea, instead of the highly interwoven pattern normally observed in the anterior stroma.[129] However, it is not possible in this study to definitively confirm if aligned cells and collagen seen in the sub-epithelial region at 60 days are on top of or within the native stroma and where collagen is cell-secreted. Labeling native collagen with DTAF (5([4,6-dichlorotriazin-2yl]amino)fluorescein) immediately after surgery would allow native versus newly secreted collagen to be distinguished at different time points after injury, as well as determination of cell location in either post-LK or native stroma.[154]

Remodeling of corneal collagen due to cell mechanical activity may be responsible for creating the highly aligned collagen pattern seen at 60 days. Cell contractility forces can change the orientation of collagen fibers within non-cell-derived collagen gels to match the cell alignment during spreading and migration.[116, 124, 155] In this study, fibroblasts are highly elongated at 60 days, which would result in contractile forces being exerted on the ECM parallel to the direction of the long cell axis.[156, 157]

In this study, in vivo confocal microscopy was used to measure the progress of corneal wound healing and cell activity at various time points after injury in the cornea. In vivo confocal microscopy has been used in a variety of corneal research and clinical applications since its development over 25 years ago, [56, 60, 62, 63, 65, 158-164] and is ideally suited to monitoring the cellular events of wound healing.[16, 66, 162-165] Previous studies have used HRT-RCM to investigate quantitative changes in cell morphology, density, and reflectivity.[127] Here, for the first time, cell alignment is quantified from CMTF scans obtained using the HRT-RCM in the cornea of a live rabbit using the "Directionality" plugin in ImageJ, creating a new quantitative method of characterizing cell patterning in vivo from CMTF scans.

One limitation of this study is the use of the LK model, which creates a rough wound bed due to tearing of lamellae, and is less reproducible than laser tissue ablation. The use of a clinical PRK laser to create an injury would reduce variability in the surgical procedure and would also be more clinically relevant. It would also be interesting to evaluate more extended

time points after injury, since complete re-thickening (regeneration) of the corneal stroma has been shown at 6 months after PRK surgery.[49]

CHAPTER FOUR
Photorefractive Keratectomy
4.1 BACKGROUND

Previous studies have shown that following keratectomy surgery in the rabbit, there is remodeling of fibrotic tissue and regeneration of stromal tissue over time.[166] [24, 50] Studies by Jester and coworkers showed that following PRK in the rabbit, there was an initial fibrotic response at 21 days which resulted in significant corneal haze. Over time, however, this fibrotic tissue was remodeled, and by 17 weeks, corneal transparency was restored.[24, 50] In addition, regrowth of the corneal stroma under the wound bed resulted in a gradual return towards pre-operative thickness. Cell and extracellular matrix (ECM) mechanical interactions play an important role in the development and maintenance of corneal transparency, as well as the response of the cornea to injury or refractive surgery.[50, 122] Specifically, the alignment of cells and the forces they generate has been shown to impact collagen deposition, organization and alignment.[114, 167-170] However, a detailed temporal and spatial assessment of the changes in cell and ECM patterning that may mediate long term corneal stromal remodeling and regeneration has not been reported.

In this study, this gap is addressed by using a combination of high resolution 3-D imaging techniques including in vivo confocal microscopy, in situ multiphoton fluorescence imaging, and second harmonic generation (SHG) imaging to assess changes in cell and matrix patterning during the repopulation, fibrosis, remodeling, and regenerative phases of wound healing following PRK in the rabbit. Regeneration (stromal growth) is also tracked

and quantified, stromal cell-ECM co-alignment is calculated, and specific protein markers are used to characterize stages of wound healing over time.

4.2 METHODS

4.2.1 Animals

Experiments in this study were performed using 30 New Zealand white rabbits (2.2-3.1 kg; Charles River Laboratories, Wilmington, MA, USA). All animal procedures were in compliance with the ARVO Statement for the Use of Animals in Ophthalmic and Vision Research and approved by the University of Texas Southwestern Medical Center Institutional Animal Care and Use Committee.

4.2.2 Photorefractive Keratectomy (PRK)

Rabbits were anesthetized using 2% isoflurane gas. Local anesthesia was provided using one drop of proparacaine in the affected eye. The corneal epithelium was removed using laser ablation, and PRK was performed using a VISX Star S4 IR Excimer Laser (Abbott Laboratories, Inc., Abbott Park, IL, USA). Rabbits received a monocular 8-mm diameter, 9.0 diopter PRK myopic correction, creating an approximate stromal ablation depth of ~118 μm. In a subset of rabbits, DTAF (Sigma, St. Louis, MO) was administered directly after PRK to track collagen deposition in the wound bed spatially and temporally as previously described.[154, 171] After PRK, rabbits were given 0.3 mg/kg of buprenorphine SR subcutaneously, and one drop of gentamicin was administered for 7 days following surgery in the affected eye.

4.2.3 In Vivo Confocal Microscopy

Rabbits were monitored using a modified HRT-RCM in vivo confocal microscope with CMTF software as previously described.[2, 122] Rabbits were anesthetized using an intramuscular injection of 50 mg/kg ketamine and 5.0 mg/kg xylazine cocktail, and locally anesthetized with 1 drop of proparacaine. Rabbits were scanned 1 week before PRK (Pre-Op), and at 3, 7, 21, 60, 90, and 180 days after PRK. Since the reflection from the Tomocap can obscure images of the superficial epithelial cells, a thin PMMA washer was placed on the Tomocap as previously described.[77] The objective was positioned on the cornea to create a flat field-of-view image in the central cornea. CMTF scans were collected by starting the scan in the anterior chamber and finishing above the epithelium with a constant speed of 60 μm per second. Images were acquired with the rate set to 30 frames per second. To allow quantitative assessment of haze, scans were collected using a constant gain setting, by unchecking the "auto brightness" box in the HRT software interface. Each scan was conducted using a gain of 6, which was set by moving the horizontal slider under the "auto brightness" box six mouse clicks to the right. At least 3 scans were collected within the central area of the cornea where PRK was performed. The center of the wound was located by first moving the objective around the cornea to find the borders of the ablated tissue. Each CMTF scan contained a 3-D stack of 384 × 384-pixel images (400 × 400 μm), with a step size of approximately 2 μm between images. Additional scans were collected closer to the wound edge in some animals. In some cases, a portion of the scan was saturated when using manual gain settings due to strong cell/matrix reflectivity. In these cases, additional scans were taken using a gain of 0 so that changes in cell patterning and morphology could be

documented. Only the scans taken with a gain of 6 were used for quantitative analysis. In a subset of four rabbits, slit lamp photos were obtained prior to confocal imaging for qualitative analysis of corneal haze (BM 900, Haag-Streit, Bern, Switzerland).

After image acquisition, CMTF scans were saved as ".vol" files, which could be opened into in-house software to analyze the 3-D changes in cell morphology and cell/ECM reflectivity.[2] The program generates an intensity vs. depth curve, corresponding to the average pixel intensity of each image and the z-depth of that image within the scan, respectively. The relative amount of backscatter, or haze, associated with the stromal keratocytes and ECM was measured by taking the area under the curve between the location of the basal lamina peak (or top of the stroma) and the endothelial peak. A baseline of 13 was chosen for haze calculations, since this value was below the baseline intensity for the normal stroma and above the intensity of the anterior chamber. The thicknesses for the epithelial and stromal layer were also calculated by the CMTF program using the interfaces (peaks on CMTF curve) between each layer in the cornea.

4.2.4 In Situ Multiphoton Fluorescence and SHG Imaging

At 7, 21, 60, 90, and 180 days, a subset of rabbits was sacrificed, and corneas were fixed using anterior chamber perfusion for 5 minutes with a PBS solution containing 1% paraformaldehyde, 5% dextran, 1% DMSO, and 1% Triton-X-100.[89] Corneas were dissected out of the eye, and fixed for an additional 15 minutes. Next, corneas were washed with 1X PBS twice for 10 minutes each, and labeled in situ with either Alexa Fluor 488 or 546

phalloidin (1:20) at 37°C for 3 hours. The corneas were then washed with 1X PBS three times for 30 minutes each. Corneas were then labeled for nuclei with a PBS solution containing Syto (1:1000, ThermoFisher, Waltham, MA, USA) and RNase, DNAase-free (1:100, Roche, Basel, Switzerland) for 1 hour at room temperature.

After labeling, corneas were placed in a glycerol:PBS solution (2:1) overnight to reduce swelling. Next, tissues were imaged using a laser scanning confocal microscope (Leica, SP8, Heidelberg, Germany) with multiphoton and SHG components, and using a 25x water immersion objective (0.95 NA, 2.4 mm free working distance). The central cornea was blocked out using a single edge blade, which allowed for isolation of the injured area, and placed epithelial side down for en face imaging. To capture SHG and multiphoton fluorescence images, a wavelength of 880 nm was used (Coherent Chameleon Vision II, ultrafast Ti: Sapphire laser, Santa Clara, CA). SHG forward scatter, DTAF or phalloidin (F-actin), and SHG backscatter were acquired concurrently, as previously described.[50, 122] In DTAF-labeled corneas, phalloidin and Syto were imaged simultaneously in a separate scan. In some corneas, tissues were sliced in the center of the wound and turned side-down to obtain cross sectional images.[83, 172]

4.2.5 Alignment and Correlation Analysis

Cell and/or matrix alignment from in situ laser confocal scans were quantified using an in-house MATLAB program, which uses a Fourier Transform algorithm to determine the percent of image content aligned at each radial angle within the image.[50] Specifically,

original en face images (1024 x 1024 pixels) were divided into 16 sub regions (256 x 256 pixels), as previously described. [50, 133] Regions for analysis were selected approximately 30 µm posterior to the basal lamina (anterior stroma) and approximately 65 µm anterior to the endothelium (posterior stroma). A Welch window was then applied to prevent edge effects in the discrete Fourier Transform (FT). The FT power spectrum of each image sub region was calculated, and the average intensity of each angle was calculated from the pixels that lied on the angle and those nearest to the angle in the transformed image. Using polar coordinates, line averages from the center to the periphery of the rotated FT power spectrum were calculated along the radial direction. Points close to the center of the FT power spectrum were excluded from the line averages because they represented low-frequency information (such as shading), which is not of interest. Plots showing both cell and matrix directionality were generated from in situ F-actin and SHG images to allow direct comparison of the angle distributions. Regions that lacked cells or SHG collagen signal were excluded from final calculations.

4.2.6 Immunocytochemistry

After fixing, a subset of corneas were embedded in optimal cutting temperature solution (OCTS), snap-frozen in liquid nitrogen, and stored at -80°C prior to sectioning. Using a Cryostat (CM3050 S, Buffalo Grove, IL, USA), sections of 7 µm in thickness were cut and mounted onto slides for labeling.

For fibronectin labeling, primary anti-goat fibronectin antibody (1:200, Santa Cruz, Dallas, TX, USA) was added to the slides and incubated at 37°C for 2 hours. Sections were then washed three times, 20 minutes per wash, and then incubated with secondary donkey anti-goat FITC or TRITC (1:200 or 1:150) at 37°C for 1 hour. For α-SMA labeling, primary anti-mouse α-SMA (1:600, Sigma, St. Louis, MO, USA) was added to the slides and incubated for 2 hours at 37°C. Sections were then washed three times, 20 minutes per wash, and then incubated with secondary anti-mouse FITC or TRITC (1:200 or 1:150) at 37°C for 1 hour. For double labeling with F-actin, slides were incubated with Alexa Fluor phalloidin 488 or 546 (1:100) simultaneously with the secondary antibodies. Images were captured using a fluorescent microscope with a 20x objective lens (Leica, DMI3000B, Buffalo Grove, IL, USA).

4.2.7 Statistics

SigmaPlot (version 12.5; Systat Software, Inc., San Jose, CA, USA) was used for statistical analysis. Linear regression analysis was used to determine the correlation coefficients between the angular distributions of F-actin and the forward scattered SHG signals, as previously described.[50] One way analysis of variance (ANOVA) was used for comparing sub-layer thickness, haze values, and correlation coefficients. Post-hoc analysis using the Holm-Sidak method was used for comparisons between groups.

4.2.8 Scientific Rigor and Reproducibility

PRK was performed for three separate experiments using a different set of rabbits for reproducibility. Multiple rabbits were used per time point for in vivo scanning and in situ labeling, and multiple regions within each cornea were selected for in vivo, SHG, and multiphoton assessment. Negative controls were used for immunohistochemistry experiments to verify positive labeling. Correlation measurements using in-house MATLAB software was verified using the Directionality Plugin.

4.3 RESULTS

4.3.1 In Vivo Assessment

Representative 2-D and 3-D CMTF images are shown in Figure 1. In the normal cornea, backscatter of light in the stroma came primarily from the keratocyte nuclei (Figure 4.1A). After PRK, a region of cell death is created under the photoablated surface, which was observed at day 3 (not shown).[90, 173] At 7 days, this region was repopulated by elongated and reflective cells that were often co-aligned (hereafter referred to as the *migrating* region; Figure 4.1B). By day 21, stromal haze was at a maximum, and two distinct patterns of cells were observed (Figure 4.1C and D). Cells anterior to the photoablated surface (hereafter referred to as the *fibrosis/remodeling* region) were dense, interconnected in a random pattern, and highly reflective (Figure 4.1C). Directly posterior to the photoablated surface (hereafter referred to as the *regenerative* region), cells within the stroma were thin, elongated and organized into parallel groups, and did not appear as reflective (Figure 4.1D). By day 60, cells in the *fibrosis/remodeling* region were reduced in reflectivity (Figure 4.1E), whereas cells in the *regenerative* region remained elongated and co-aligned (Figure 4.1F). By day 90

and 180, cellular backscatter was limited to the keratocyte nuclei in the *remodeling* region (Figure 4.1G and I), indicating a more normal quiescent phenotype. However, diffuse haze was observed between cells. Cells in the *regenerative* region remained highly aligned with reduced backscatter as compared to day 60 (Figure 4.1H and J). Overall stromal reflectivity also appeared to decrease at day 90 and 180 (Figure 4.1G-J; 3-D reconstruction of cornea), as compared to day 21 (Figure 4.1C and D; 3-D reconstruction of cornea).

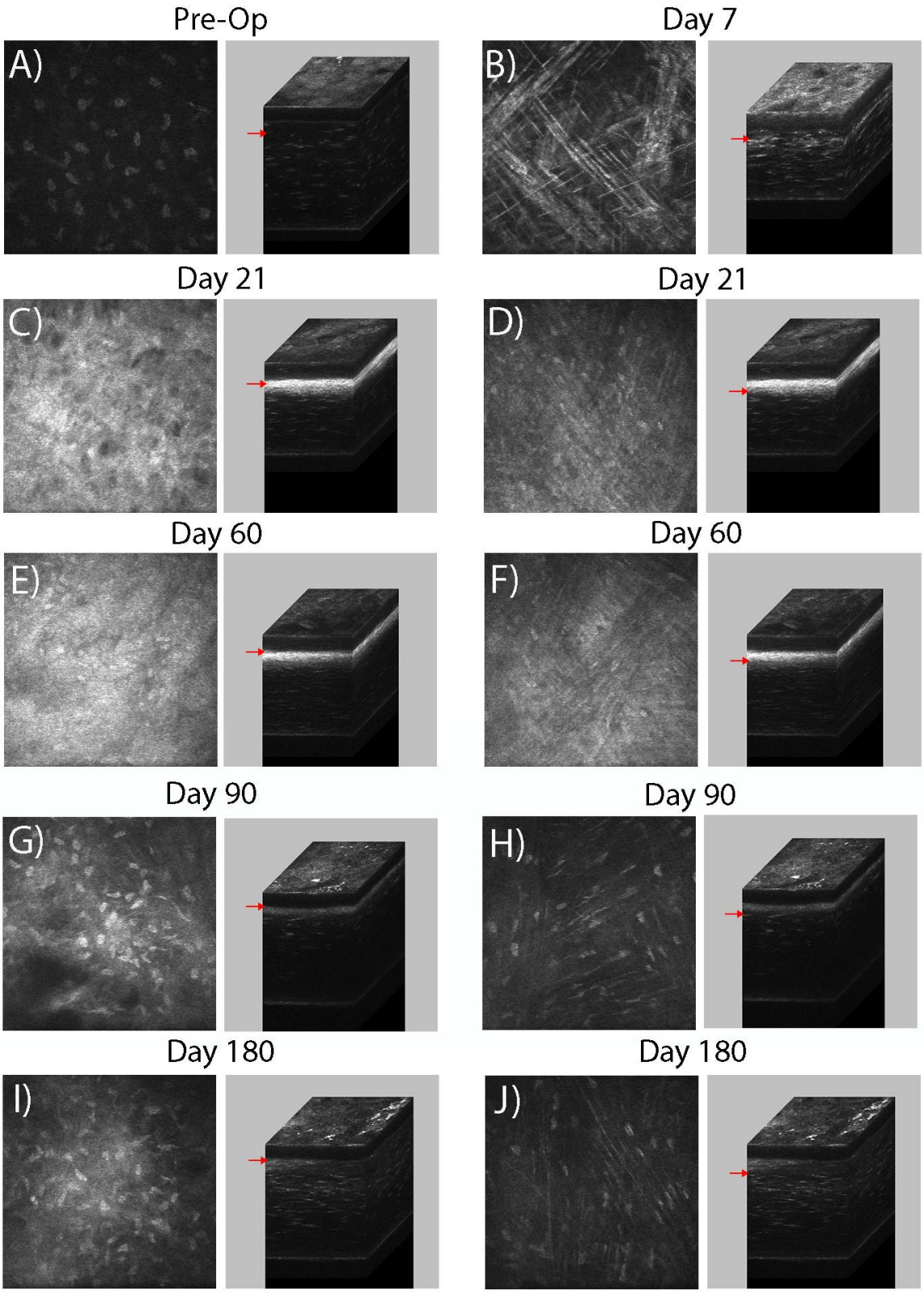
Pre-Op
A)
Day 7
B)
Day 21
C)
Day 21
D)
Day 60
E)
Day 60
F)
Day 90
G)
Day 90
H)
Day 180
I)
Day 180
J)

Figure 4.1. In vivo 2-D confocal images (left) with corresponding 3-D reconstruction of scans (right). Representative images from the (A) pre-operative (Pre-Op) cornea, (B) 7 days after PRK, (C, D) 21 days after PRK, (E, F) 60 days after PRK, (G, H) 90 days after PRK, and (I, J) 180 days after PRK. Images (A, B) are from the anterior stroma, (C, E, G, I) are from the *fibrosis/remodeling* region on top of the photoablated surface, and images (D, F, H, J) are located in the *regenerative* region just below the photoablated surface. Red arrow indicates location of the 2-D image within the 3-D stack. 2-D images are 330 µm x 330 µm.

Using in-house CMTF software for quantitative analysis, stromal haze and epithelial and stromal thicknesses were calculated at each time point (Figure 4.2) using the aforementioned intensity vs. depth curve created from 3-D scans. By day 7, the epithelium had returned to normal thickness (Figure 4.2A). Stromal thickness initially decreased by over 110 µm, as a result of the PRK procedure (day 7); however, between day 7 and day 180, stromal thickness gradually increased back to 94.5% ± 7.5 of the pre-operative value. Thickness values calculated from this study are comparable to previous PRK studies in the rabbit.[24]

Haze was quantified by calculating the area under the intensity vs. depth curve, from the basal lamina to the endothelium. Haze values were increased at 7 days following PRK, with maximum haze values calculated at day 21 (Figure 4.2B). Haze values started to decline by day 60, and decreased further to a near normal value by day 90. Moller-Pedersen and co-workers also observed a similar trend.[122] Although not statistically significant, haze was still slightly elevated at days 90 and 180, due to the diffuse ECM backscatter in the remodeled region.

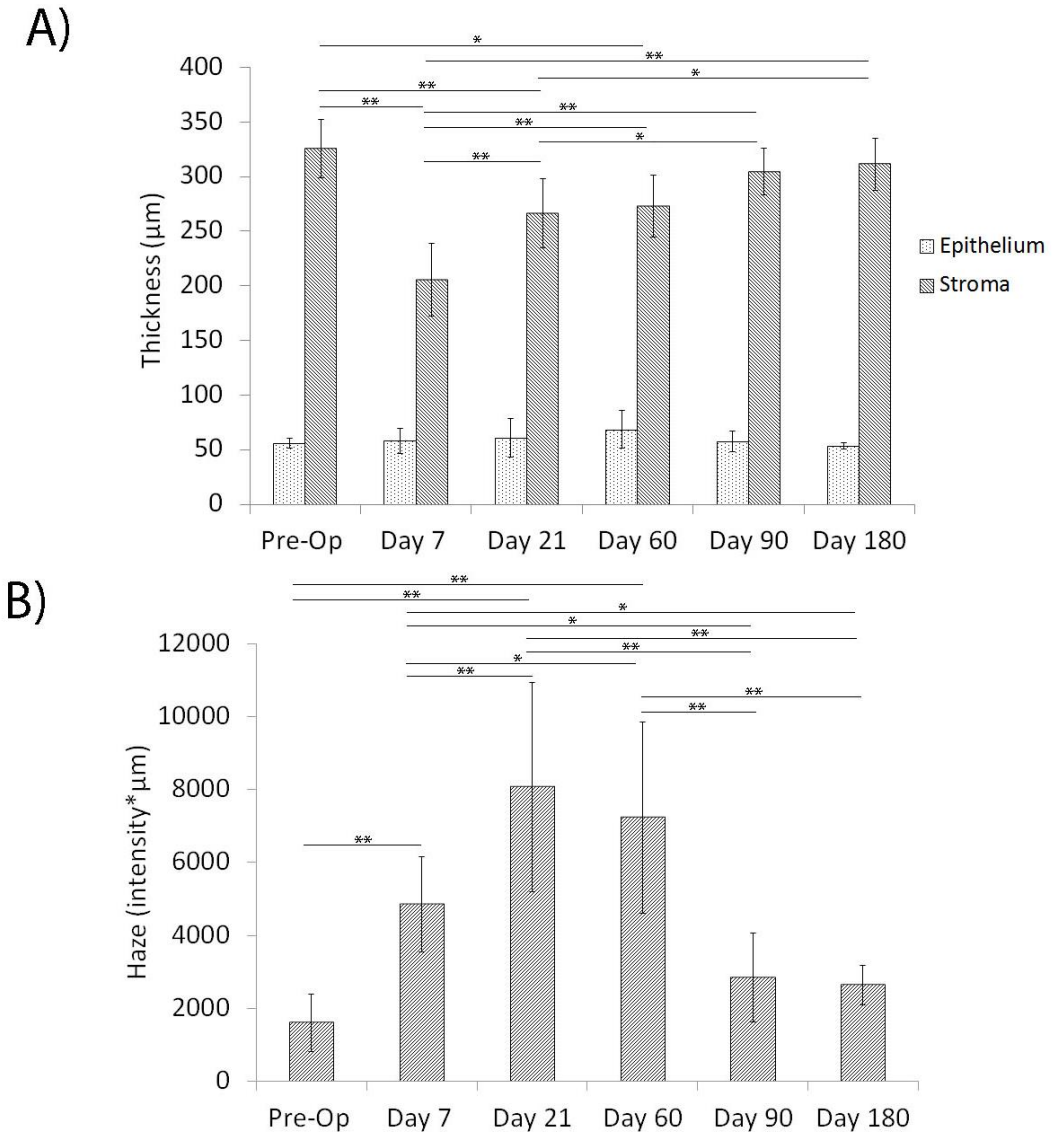

Figure 4.2. Measurements from in vivo confocal scans. (A) Epithelial and stromal thickness at each time point. (B) Stromal haze calculated at each time point. (ANOVA between groups, *P<0.05, **P<0.001).

Prior to CMTF scanning, rabbit corneas were qualitatively assessed using slit lamp microscopy (Figure 4.3). In the unoperated eye, corneas appeared transparent without haze (Figure 4.3A). At day 21, prominent haze appeared in the central cornea within the PRK location (Figure 4.3B). By day 90 (Figure 4.3C), there was little to no corneal haze seen from slit lamp examinations.

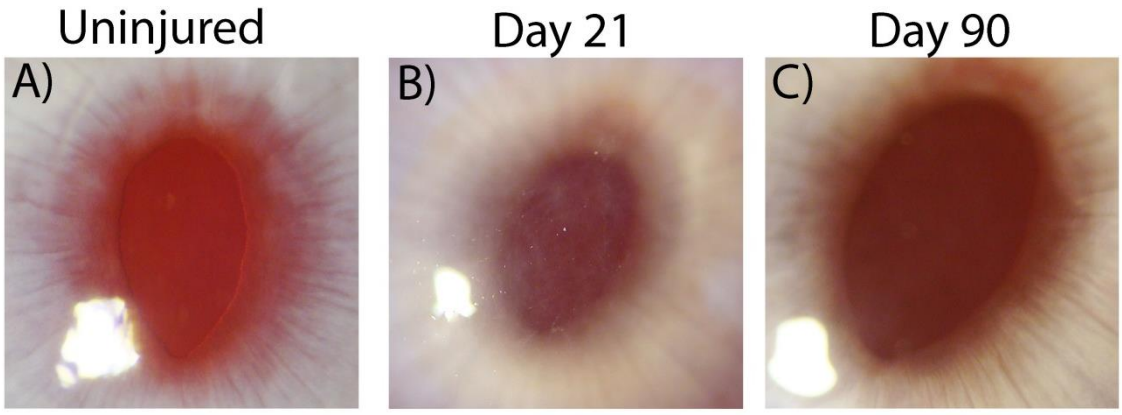

Figure 4.3. Slit lamp images of the central cornea captured pre-operatively (A), and at 21 days (B) and 90 days (C) after PRK.

4.3.2 Immunocytochemistry

Corneal cross-sections were labeled for α-SMA (Figure 4.4A-F) and fibronectin (Figure 4.4G-L) at various time points after surgery. At 7 days following PRK, there was a slight detection of α-SMA (Figure 4.4B) and fibronectin (Figure 4.4H). At 21 days, there was a drastic increase in α-SMA (Figure 4.4C) and fibronectin (Figure 4.4I). By 60 days, α-SMA (Figure 4.4D) and fibronectin (Figure 4.4J) was reduced in the wounded region of the cornea, and by day 90 and 180, no α-SMA (Figure 4.4E and F) or fibronectin (Figure 4.4K and L)

was detected. Note that when detected, fibronectin and α-SMA was always on top of the DTAF-labeled native stromal tissue (not shown).

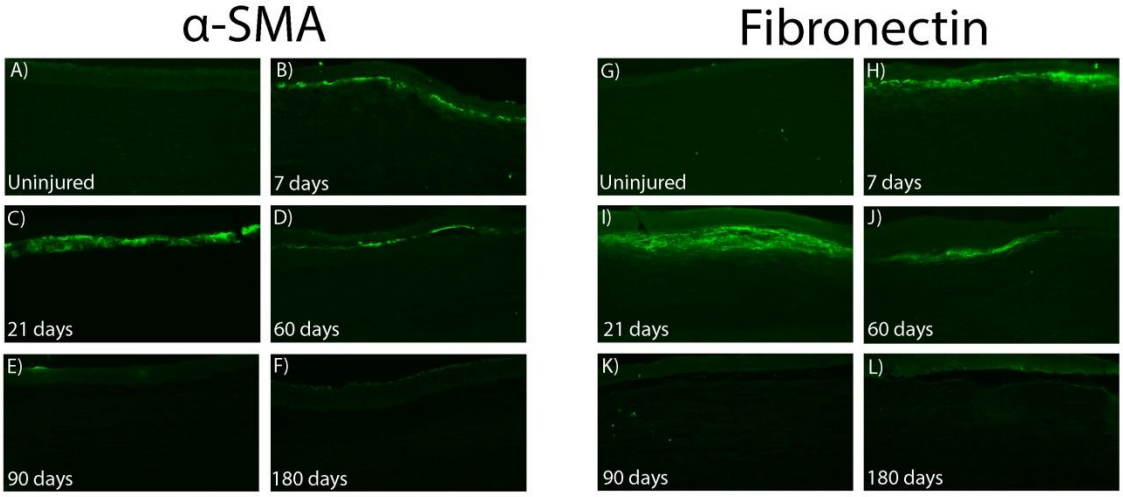

Figure 4.4. Immunohistochemistry for detection of α-SMA and fibronectin near the center of the photoablated region. (A-F) contains images from frozen sections labeled for α-SMA, and (G-L) contains images from frozen sections labeled for fibronectin at each time point. Images are from the anterior segment of the cornea. Images are 475 µm x 255 µm.

4.3.3 In Situ Multiphoton and SHG Imaging

At each time point, a subset of rabbits was sacrificed, and corneas were dissected for further analysis. Corneas were fixed and labeled in situ with phalloidin for F-actin and Syto for nuclei. Using multiphoton and SHG imaging, 3-D en face image stacks were collected from labeled tissues (Figure 4.5 and 4.6). In the unoperated eye, collagen in the anterior stroma within 20 microns of the epithelium appeared highly interwoven, and cells were quiescent with stellate morphologies, characteristic of normal keratocytes (Figure 4.5A, B). Wider lamella with less interweaving were observed deeper within the stroma (Figure 4.5A, B; taken about 128 µm below the basal lamina to allow comparison with stroma under

photoablated region).[50, 174] By 7 days, keratocytes from the wound margin had transformed into fibroblasts and migrated to the central cornea; these fibroblasts were characterized by elongated morphologies and more prominent F-actin labeling (Figures 4.5C, D and 4.6C, D). Migrating fibroblasts appeared to be co-aligned with the collagen lamellae and interconnected within parallel groups.

At day 21, myofibroblasts in the *fibrosis/remodeling* region on top of the photoablated surface contained prominent stress fibers, and were broader and more randomly arranged (Figure 4.5E, F). There was no prominent fibrillar collagen (Figure 4.5E, F) observed by SHG imaging; however, immunolabeling demonstrated that Type I collagen was present in this region (Figure 4.7A). By day 60, collagen in the *fibrosis/remodeling* region appeared to have an interwoven pattern, and cells appeared more quiescent in some areas (Figure 4.5G, H). At day 90 and 180, cells throughout the *remodeling* region were quiescent, and collagen was highly interwoven (Figure 4.5I and J, and 4.5K and L, respectively), similar to the normal sub-epithelial stroma (Figure 4.5A and B).

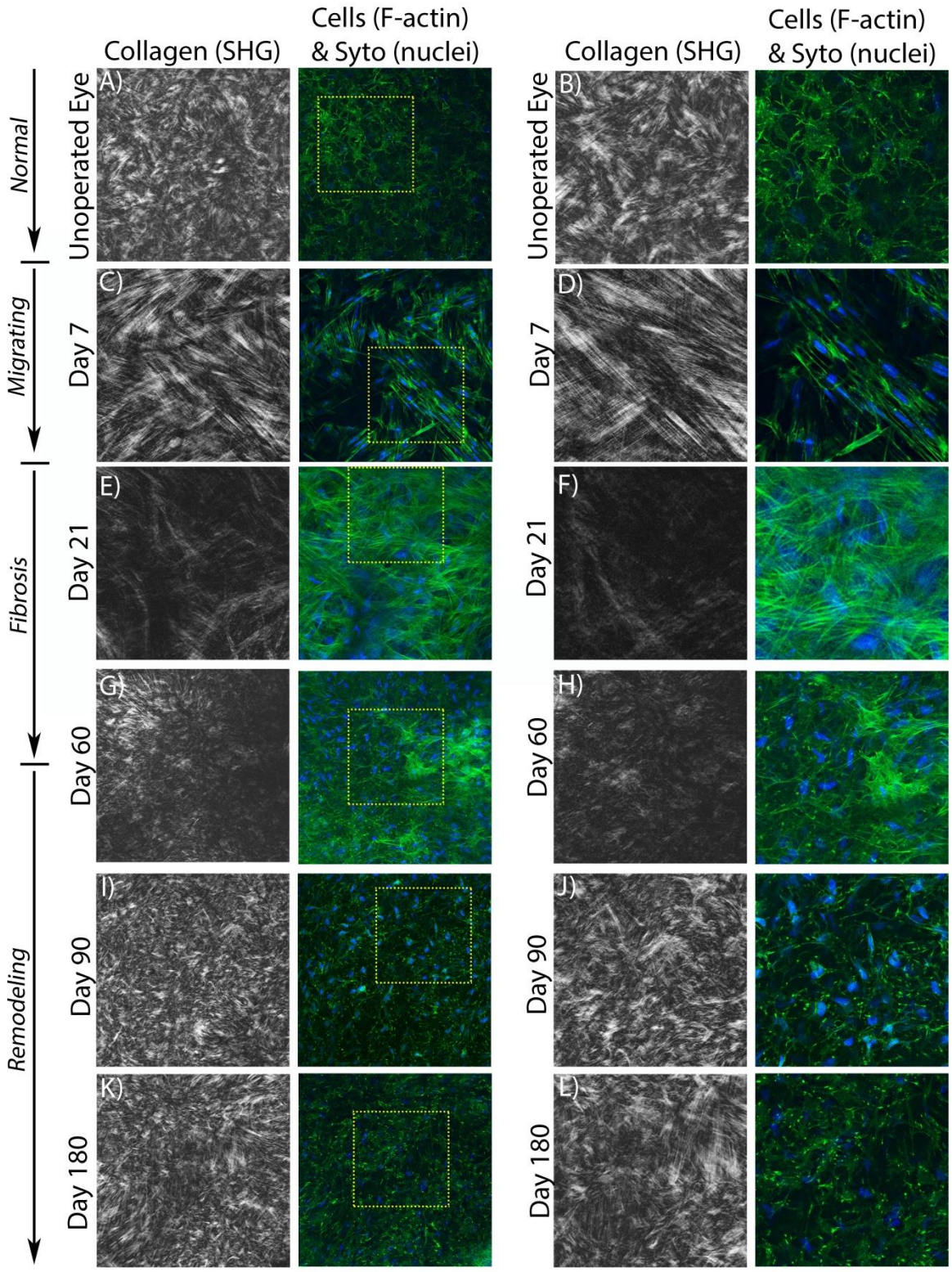
Collagen (SHG)
Cells (F-actin) & Syto (nuclei)
Collagen (SHG)
Cells (F-actin) & Syto (nuclei)
Normal
Migrating
Fibrosis
Remodeling
Unoperated Eye
Unoperated Eye
Day 7
Day 7
Day 21
Day 21
Day 60
Day 60
Day 90
Day 90
Day 180
Day 180
A)
B)
C)
D)
E)
F)
G)
H)
I)
J)
K)
L)

Figure 4.5. SHG forward scatter (collagen) and multiphoton (F-actin and nuclei) en face images. Images are from: (A, B) unoperated cornea, and (C, D) 7 days, (E, F) 21 days, (G, H) 60 days, (I, J) 90 days, and (K, L) 180 days after PRK. Images A, B were taken 20 µm posterior to the basal lamina, and C, D were collected 24 µm posterior to the photoablation site in the *migrating* region. Images E-H were collected from the *fibrosis/remodeling* region, and I-L were from the *remodeling* region. Images (B, D, F, H, J, L) are 2x zoomed-in (yellow box) images from (A, C, E, G, I, K), respectively. Images A, C, G, I, K are 465 µm x 465 µm. Images B, D, E, H, J, L are 230 µm x 230 µm. Image F is 115 µm x 115 µm.

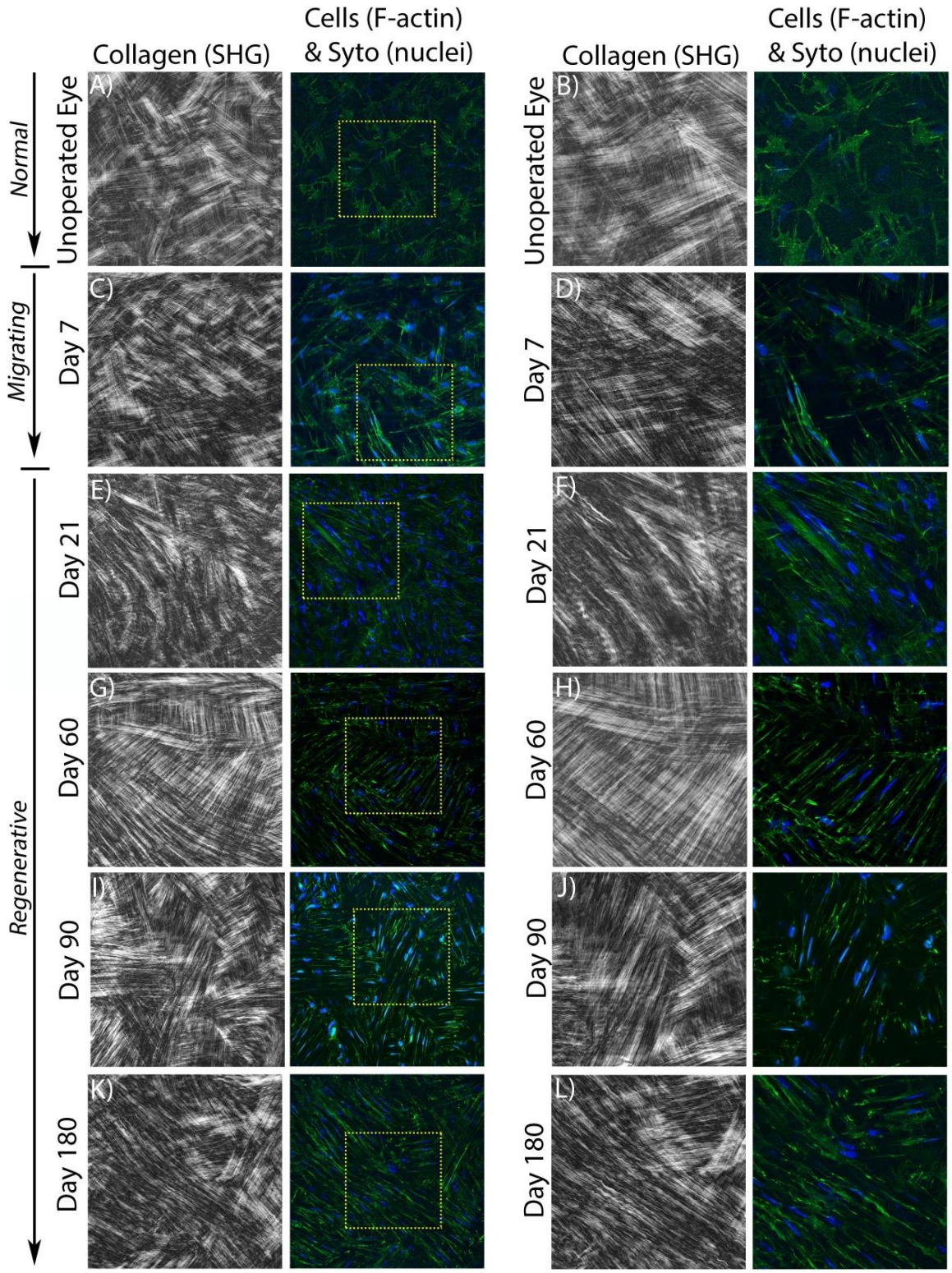
Collagen (SHG)
Cells (F-actin)
& Syto (nuclei)
Collagen (SHG)
Cells (F-actin)
& Syto (nuclei)
Normal
Migrating
Regenerative
Unoperated Eye
Unoperated Eye
Day 7
Day 7
Day 21
Day 21
Day 60
Day 60
Day 90
Day 90
Day 180
Day 180
A)
B)
C)
D)
E)
F)
G)
H)
I)
J)
K)
L)

Figure 4.6. SHG forward scatter (collagen) and multiphoton (F-actin and nuclei) en face images. Images are from: (A, B) unoperated cornea, and (C, D) 7 days, (E, F) 21 days, (G, H) 60 days, (I, J) 90 days, and (K, L) 180 days after PRK. Images A, B were taken 128 µm posterior to the basal lamina, and C, D were collected 40 µm posterior to the photoablation site in the *migrating* region. Images E-L were collected from the *regenerative* region. Images (B, D, F, H, J, L) are 2x zoomed-in (yellow box) images from (A, C, E, G, I, K), respectively. Images A, C, E, G, I, K are 465 µm x 465 µm. Images B, D, F, H, J, L are 230 µm x 230 µm.

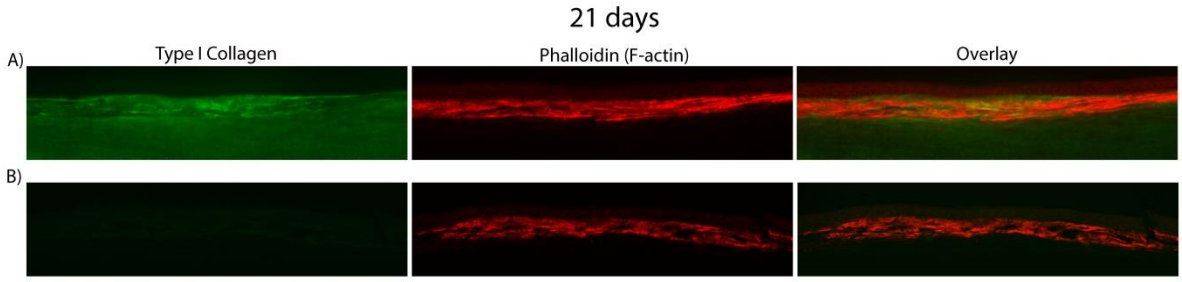

Figure 4.7. Frozen Immunohistochemistry for detection of Type I collagen (1:2000, Gibco (Thermo Fisher), Waltham, MA) and phalloidin (F-actin) in the anterior stroma at 21 days post-PRK. Images are from the anterior segment of the cornea using primary antibody (A) and negative control without primary antibody (B). Images are 645 µm x 160 µm.

In contrast to the *fibrotic/remodeling* region, collagen within the *regenerative* region underneath the photoablated surface remained highly aligned in a lamellar pattern throughout the wound healing process (Figure 4.6E-L), similar to the normal cornea (Figure 4.6A, B). Cells in the regenerative region were elongated and co-aligned with the collagen, and stress fibers were not observed.

From day 7-180, cells in the *migrating*, *remodeling*, and *regenerative* regions expressed regions of bright, punctate F-actin labeling (Figure 4.5D, H, J, L and Figure 4.6D, F, H, J, L). High magnification overlays of F-actin and forward scattered SHG images demonstrate that

the localization and alignment of punctate F-actin labeling corresponded to the pattern of collagen organization in both the *remodeling* (Figure 4.8A) and *regenerative* regions (Figure 4.8B). Punctate spots were often co-localized with collagen fibers suggesting possible sites of cell-ECM contact.

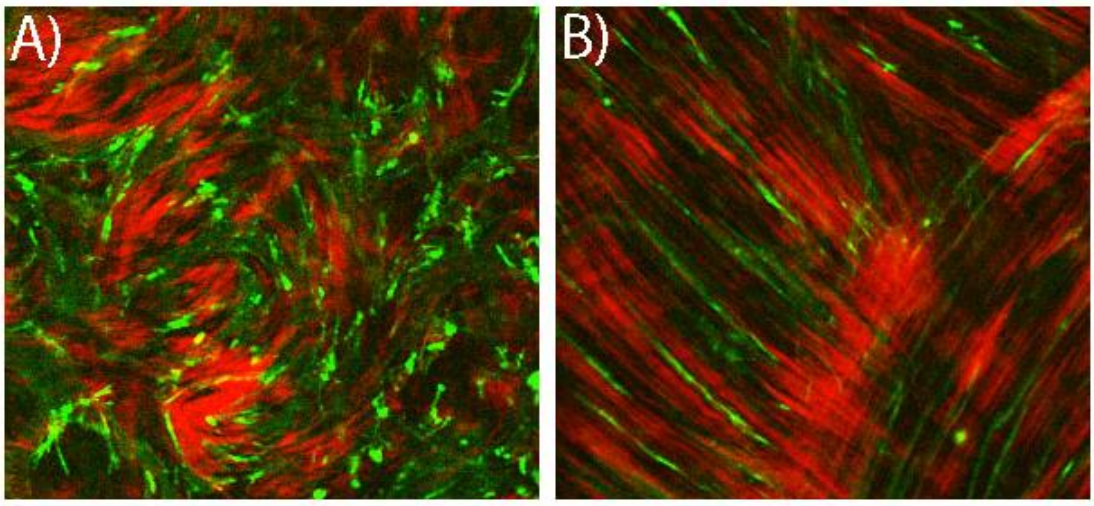

Figure 4.8. SHG and multiphoton image overlays for collagen (shown in red) and F-actin (shown in green) revealing bright punctate regions at cell ends and surfaces by day 180. (A) is taken from the *remodeling* region, and (B) is taken from the *regenerative* region. Note that the pattern of punctate F-actin labeling is highly correlated with the collagen, suggesting cell-matrix interactions. Images are 135 µm x 125 µm.

To determine the location of stromal re-growth after PRK, the thickness of the *fibrosis*/*remodeling* (non-DTAF) region, DTAF-labeled stroma (which also included the *regenerative* region), and total stroma were calculated at various time points. As shown in Figure 4.9A, growth from the *remodeling* region plateaued by day 90; however, total stromal growth progressively increased between day 7 and 180, corresponding to an increase in the thickness of DTAF labeled stroma. In situ confocal imaging revealed diffuse DTAF labeling throughout the stroma at Day 7 (shown in Figure 4.9B), with the exception of gaps

corresponding to stromal cells. In contrast, gaps in the DTAF labeling that did not correspond to stromal cells were consistently observed within the *regenerative* region of the stroma at day 21 (not shown), day 90 (Figure 4.9C, top panel), and day 180 (Figure 4.9D, top panel). There was also a transitional area in between the *remodeling* and *regenerative* regions, where DTAF labeling was discontinuous; however, forward scatter signaling was ubiquitous throughout the transition region (not shown), indicating that the *remodeling* and *regenerative* regions were continuous. In the mid-stroma, DTAF gaps were only observed where there were cells (Figure 4.9B-D, bottom panels). Within the *regenerative* region, some gaps in DTAF labeling (Figure 4.10, shown in green) corresponded to co-localization with forward scatter signaling (in blue), but not with F-actin labeling (in red). This demonstrated that the gaps contained new collagen secreted post-PRK within the *regenerative* region.

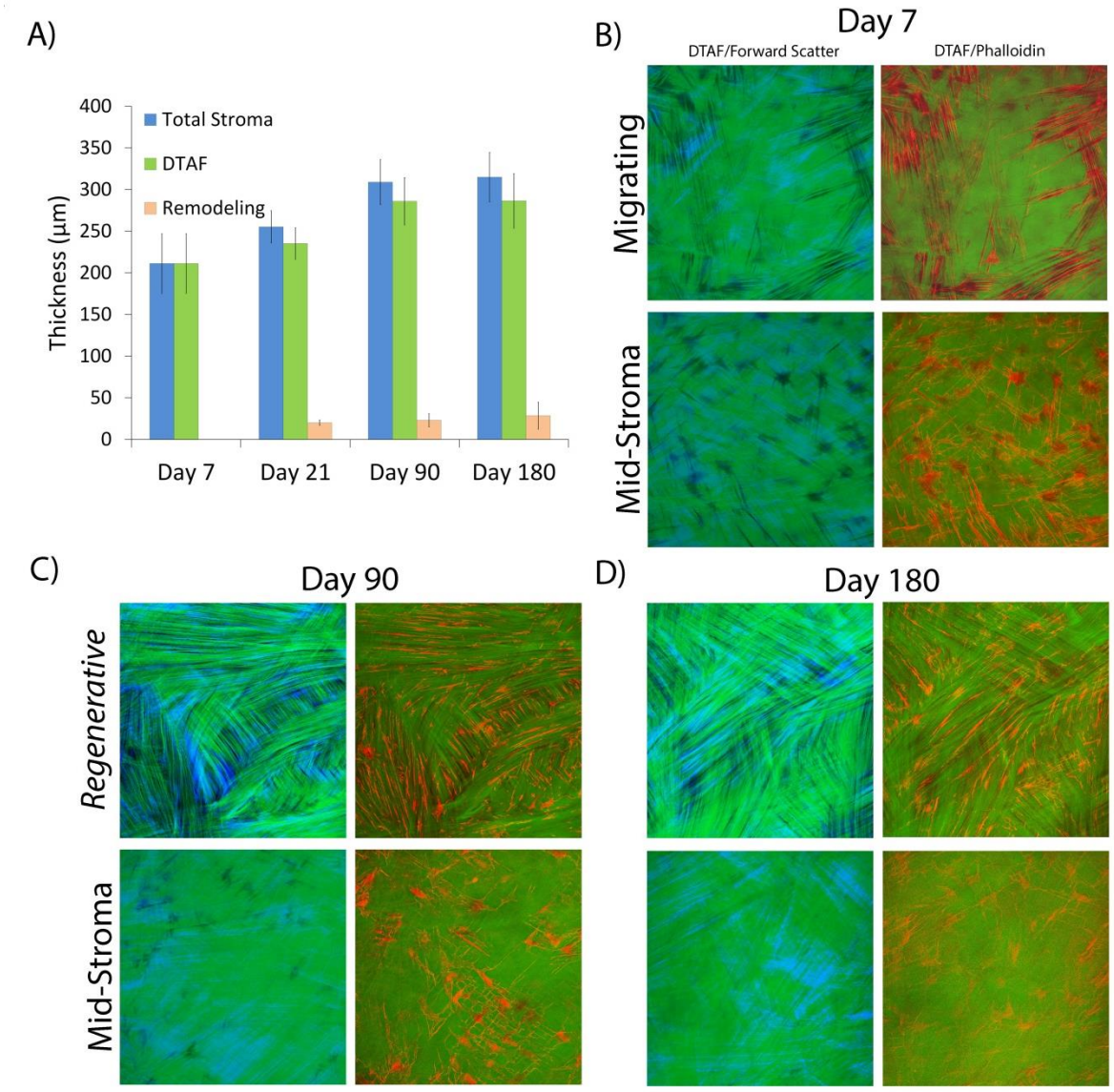

Figure 4.9. Regeneration of stromal tissue. (A) Measurements for *remodeling*, *regenerative* ("DTAF"), and total stromal thickness over time. Overlays for DTAF (green), forward scatter (blue), and phalloidin (red) en face images at (B) 7 days, (C) 90 days, and (D) 180 days. Images are 445 µm x 460 µm.

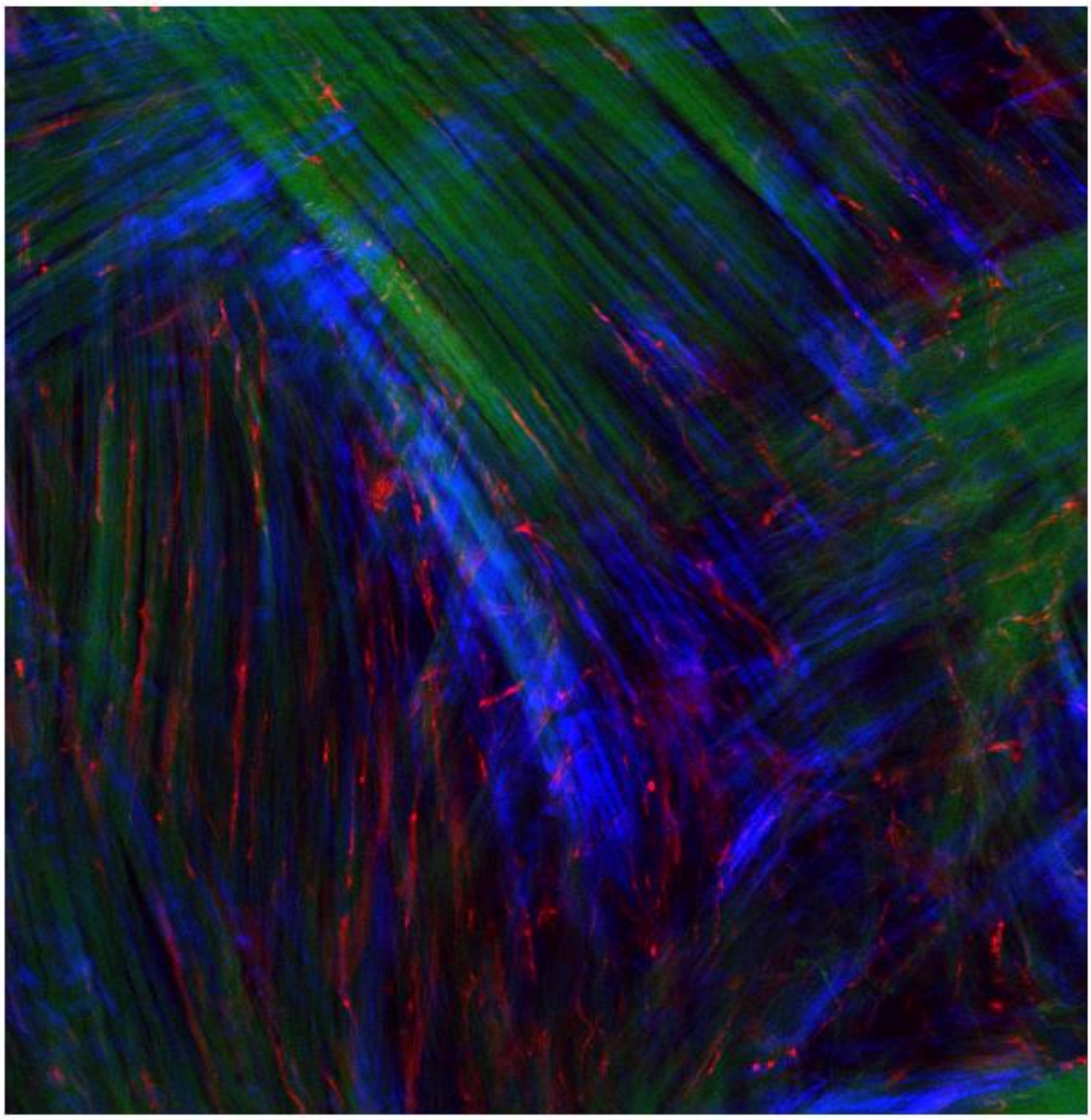

Figure 4.10. Anterior stroma in the regenerative region at day 90 showing overlay of DTAF (green), forward scatter (blue), and phalloidin (red). Image is 270 µm x 280 µm.

Cross-sectional (side view) imaging of corneas labeled in situ was conducted to further track cell patterning and collagen deposition and organization at various time points post-PRK. In control (uninjured) corneas (Figure 4.11A), backscatter (shown in blue) signaling reveals that collagen is organized in an interwoven pattern in the anterior stroma, and becomes more linear in the mid-stroma. Normal cell phenotype and patterning is observed (Figure 4.11A; F-actin in red for phalloidin) throughout the stroma. At day 21, backscatter from side view imaging suggests weak organization of collagen lamellae in the *fibrosis/remodeling* region and cells containing prominent F-actin signaling (Figure 4.11B). These cells were co-localized with Type I collagen labeling at day 21 (Figure 4.7A). By day 90 and 180, interwoven collagen containing stronger backscatter signals (Figure 4.11C, D) without DTAF co-localization (DTAF is shown in green) replaced fibrotic tissue from day 21 within the *remodeling* region, and was deposited above the *regenerative* region. In the *remodeling* region, cells appear interwoven with collagen at day 90 and 180 in zoomed-in images (Figure 4.11E, F), and this patterning is similar in appearance to the control cornea.

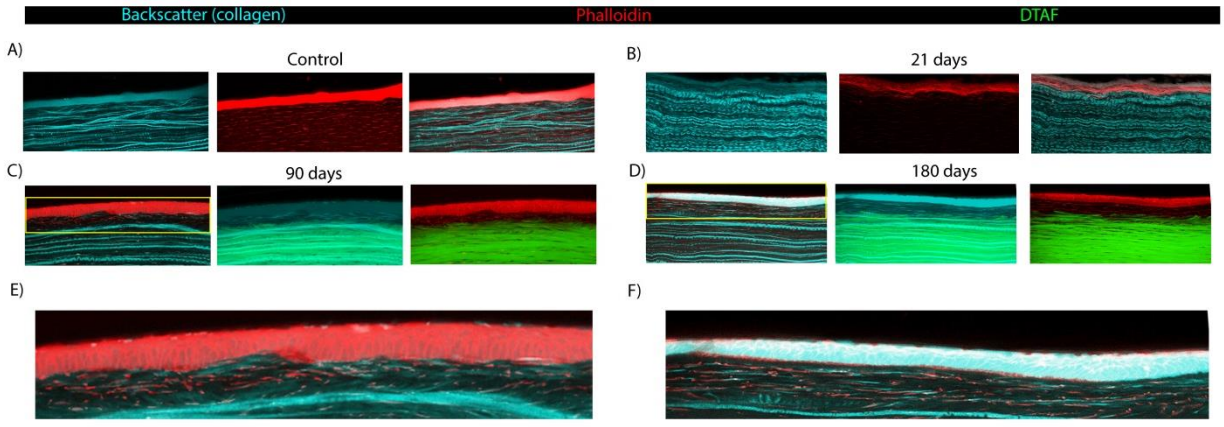

Figure 4.11. Side-view SHG and multiphoton images at various time points. (A) Images taken with a control (uninjured) cornea for backscatter, phalloidin, and backscatter/phalloidin

overlay. (B) Images taken from a 21 day post-PRK cornea for backscatter, phalloidin, and backscatter/phalloidin overlay. (C) Images taken from a 90 day post-PRK cornea for backscatter/phalloidin, backscatter/DTAF, and phalloidin/DTAF overlays. (D) Images taken from 180 days post-PRK cornea for backscatter/phalloidin, backscatter/DTAF, and phalloidin/DTAF overlays. Images are from the anterior segment of the cornea. (Phalloidin is shown in red; backscatter is shown in blue; DTAF is shown in green). (E) Zoomed-in image of the *remodeling* region of the 90 days backscatter/phalloidin overlay image shown in (C, yellow box). (F) Zoomed-in image of the *remodeling* region of the 180 days backscatter/phalloidin overlay image shown in (D, yellow box). Each image in A-D is 465 µm x 200 µm. Images E and F are 465 µm x 90 µm, zoomed-in 3x from original image (C and D, respectively).

4.3.4 Correlation Analysis

To quantify the co-alignment between cells and collagen within the stroma, correlation analysis was carried out using in-house MATLAB program. R-squared values for cell and collagen correlation were calculated at day 60, 90, and 180 in the *regenerative* region of the anterior stroma, and posterior stroma (Figure 4.12) using multiphoton and SHG images. The cells and collagen in the *regenerative* region at each time point had higher correlation (R-squared value) than the posterior stroma and control anterior stroma. These values also correlated with qualitative assessment of SHG and multiphoton images.

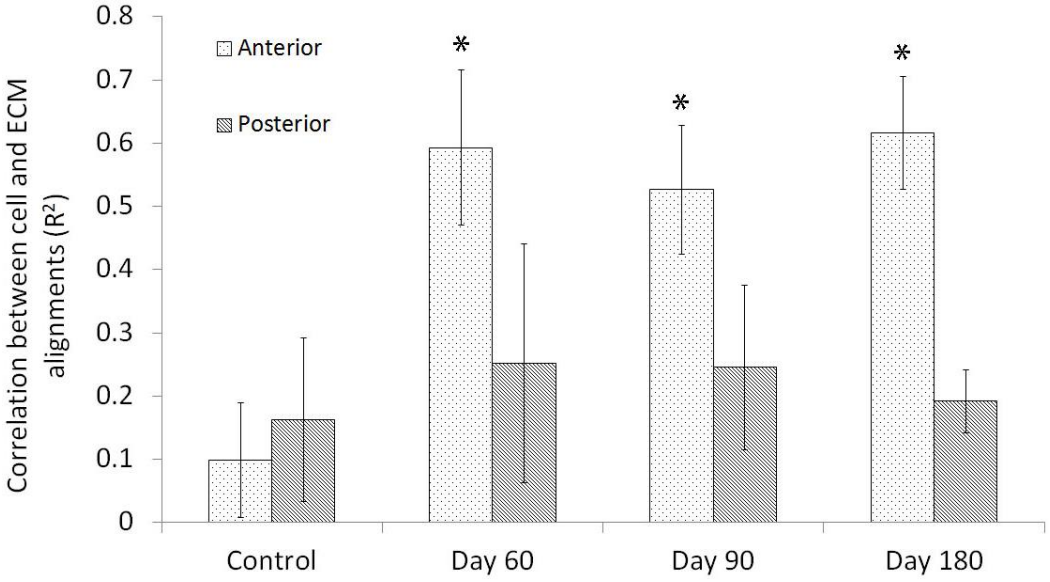

Figure 4.12. Correlation coefficients (R^2) in the pre-operative anterior control stroma (control), *regenerative* anterior stroma (day 60, 90, and 180), and posterior stroma. (*P<0.001, ANOVA, when compared to anterior control stroma).

4.4 DISCUSSION

In this study, PRK was used as a model to provide precise photoablation of the anterior cornea, yielding more consistent, clinically relevant results. In addition, rabbits were studied for up to 6 months after surgery, and DTAF was used to distinguish native collagen from new collagen secreted post-PRK. The current results provide important new insights into the underlying changes in cell and ECM patterning during the migration, fibrosis, remodeling and regenerative phases of wound healing.

4.4.1 Intrastromal Migration

Previously, cell and matrix patterning was studied following transcorneal FI, which involves intrastromal cell migration to repopulate the injured region.[122] Using SHG imaging, migrating corneal fibroblasts were aligned parallel to the stromal collagen lamellae. After PRK, there was a region of cell death within the stroma under the laser ablation site. Corneal keratocytes repopulated this injured region via intrastromal migration in parallel with the collagen lamellae, similar to the healing response following FI. In vitro studies have shown that cell morphology, migration, and phenotype are directly affected by localized substrate topography,[86, 100, 101] and corneal fibroblasts have been previously found to co-align to collagen-coated substrates containing ridges and grooves aligned in parallel.[104] Thus, lamellar patterning likely provides topographical cues that modulate corneal fibroblast migration following injury.

4.4.2 Initial Fibrosis after PRK

In contrast to cells migrating within the corneal stroma, cells that migrated on top of the wound bed were arranged randomly, and transformed into myofibroblasts, consistent with previous studies.[21, 50, 69] A sharp transition was observed starting from the fibrotic (*fibrosis/remodeling)* region into the non-fibrotic (*regenerative*) region of the stroma. Cell phenotype drastically changed from myofibroblasts on top of the ablation to elongated, non-fibrotic cells within the native stroma beneath the ablation. DTAF labeling confirmed that there were no myofibroblasts within the native stroma. Several factors may inhibit myofibroblast transformation within the native stroma. One possibility is that the stromal ECM provides topographical cues that prevent cell transformation, since aligned surface grooves have been reported to inhibit the transformation of corneal fibroblasts to myofibroblasts in vitro.[133] Additionally, cells residing in between the ECM may be protected against penetration of fibrotic-inducing growth factors, like TGF-β and PDGF, secreted by tears and the epithelium.[18, 31, 144, 145, 175-181] Finally, biochemical or matrikine signaling from other ECM components, such as proteoglycans, could inhibit myofibroblast transformation.

Myofibroblasts were most prevalent at 21 days, which was also when maximum haze was observed qualitatively with slit lamp imaging. Myofibroblasts also have decreased production of crystallin proteins and altered proteoglycan expression, which are both important for maintaining corneal transparency.[98, 182] TGF-β induces myofibroblast transformation in the cornea and suppresses interleukin (IL)-1, a cytokine that stimulates myofibroblast apoptosis; therefore, allowing longer time for myofibroblast-derived secretion of fibrotic proteins, like fibronectin and Type I collagen, to occur.[108, 183-188] The results

revealed maximum secretion of fibronectin at day 21, which was the time point with the highest calculated haze and myofibroblast accumulation (based on α-SMA labeling) in the anterior stroma.

4.4.3 Remodeling of Fibrotic Tissue

In this study, long-term resolution of fibrosis was shown in the cornea that corresponded with a reduction of corneal haze toward preoperative levels. By day 60, myofibroblasts in the *fibrosis/remodeling* region were being replaced by more quiescent-appearing cells. Previous in vitro experiments by Maltseva and associates demonstrated that fibroblast growth factor (FGF)-1 or FGF-2 can trans-differentiate myofibroblasts into fibroblasts.[189] Additionally, it has been shown that as the EBM re-forms after injury, there is a drop in TGF-β in the stroma.[190] When TGF-β levels decrease in the wound environment, IL-1 levels increase, which may be signaled in an autocrine or paracrine manner from the myofibroblasts, and induce myofibroblast apoptosis.[191, 192] Previous studies have detected myofibroblast apoptosis using TUNEL (terminal deoxynucleotidyl transferase-mediated dUTP nick end labeling) assays starting at 1 month after myopic PRK correction, which falls into the time frame of myofibroblast disappearance presented in this study.[193]

By day 90, fibrosis and haze were significantly reduced, and interwoven collagen was detected by SHG imaging. Although the precise mechanism by which fibrotic ECM is cleared from the anterior stroma has not been described fully, it is likely that a combination of cell-secreted matrix metalloproteinases (MMPs) and disappearance of myofibroblasts

(eliminating further deposition of fibrotic ECM) helps remove and eliminate further fibrosis.[142, 194, 195] The interwoven collagen organization observed from day 90 – 180 is similar to that observed in the sub-epithelial region of normal rabbit cornea. Interweaving of collagen lamellae in the anterior stroma has been described as a provider of shear strength against local environmental stresses, preventing sliding and bending of corneal sub-layers and distributing tension between lamellae.[196-200] The interwoven pattern of the sub-epithelial cornea may also be derived from an evolutionary role of maintaining corneal shape for reliable, consistent light refraction in vertebrates.[83, 201, 202] A combination of cell contractility, cell/ECM interactions, and environmental tension, forces, and pressure occurring in the eye is speculated to play an important role in the development and remodeling of interwoven collagen. It should be noted that the ECM in the remodeled region still produced slightly increased backscatter (haze) as compared to the normal cornea.

4.4.4 Regeneration

Although cells in the *remodeling* region on top of the ablation produced collagen after PRK, the majority of stromal growth occurred in the regenerative region under the wound. Moller-Pedersen et al. also reported additional tissue growth after PRK below the ablation region of the stroma, using 3-D reconstructed in vivo confocal scans and cross-sectional DTAF images.[24, 173] In this study, further insights are provided into the mechanisms for tissue re-growth below the ablation surface by using en face SHG/DTAF overlay images. Specifically, during stromal regeneration, gaps in the DTAF labeling were identified that were not co-localized with cells. Interestingly, SHG signaling was observed within these

gaps, indicating the presence of newly-secreted collagen. This new collagen was co-aligned both with the native collagen lamellae and elongated corneal keratocytes. Stromal cells have been previously shown to align in the direction of their secreted ECM, and external mechanical tension plays an important role in mediating and stabilizing the orientation of collagen assembly.[203, 204]

Punctate F-actin labeling was observed that co-aligned with collagen in both the *remodeling* and *regenerative* regions, which is a hallmark of cell-matrix mechanical interactions.[89, 170, 205] Cell contractility has been shown to influence non-cell-derived collagen patterning based on forces imposed on the local ECM environment in in vitro studies.[116, 124, 206] Additionally, the correlation between collagen and fibroblasts in the *regenerative* region may be due to cell elongation in parallel to greatest ECM stiffness within the tissue, as seen with prior studies using corneal fibroblast culture.[207] In the developing chick cornea, keratocytes in the secondary stroma have been noted to have protrusions called "keratopodia" that are co-aligned with collagen, and it has been suggested that these cells use guidance from the collagen lamellae of the primary stroma during the development of the secondary stroma.[23, 208-210] Taken together, the data suggests that cells in the *regenerative* region secrete and organize collagen in a pattern determined by the existing collagen template.

Following FI, stromal tissue is not removed; thus, there is no growth or regeneration of stromal tissue. In this model, punctate F-actin labeling is not detected during healing. Furthermore, aligned fibroblasts in the stroma revert back to a stellate, normal quiescent

morphology by day 28.[122] In contrast, following PRK, cells were elongated and co-aligned with collagen even at 180 days after injury. After keratectomy, mechanical stresses from intraocular pressure are redistributed throughout the stromal matrix, with a larger load imposed on the stromal ECM due to a decreased thickness.[196, 211] It is possible that persistent changes in the mechanical environment of the stroma may provide signals that contribute to long-term cell activation following PRK.

The PRK results provide more insight into the role of the cell/ECM interactions in wound healing, and may assist with future studies. For example, similar techniques may be used to investigate cell/ECM patterning following UV crosslinking of collagen fibrils in the stroma for treatment of keratoconus. Additionally, it could be useful to track cell/ECM interactions after steroid treatment, which is commonly used following refractive surgery in the clinic, to compare temporal and spatial cell/ECM activity during wound healing. Since the rabbits used in this model are young and have a high regenerative capacity, follow up studies should involve less regenerative animals, perhaps older rabbits, to more closely model the human eye.

CHAPTER FIVE
Conclusions and Recommendations

Portions of this chapter are reproduced with permission from: Petroll, W. M., Kivanany, P.B., Hagenasr, D., and Graham, E.K., Invest Ophthalmol Vis Sci, 2015. 56: p. 7352-7361, ARVO.

Portions of this chapter are reproduced with permission from: Kivanany, P.B., Grose, K.C., and Petroll, W.M., Exp Eye Res, 2016. 153: p. 56-64, Elsevier.

5.1 CONCLUDING DISCUSSIONS OF SPECIFIC AIMS, FUTURE WORK, AND CLOSING REMARKS

5.1.1 Conclusions for Specific Aim 1

The FI studies demonstrated that the modified HRT-RCM allows in vivo measurements of sub-layer thickness, assessment of cell morphology, alignment and connectivity, and estimation of stromal backscatter (haze) during wound healing. Interestingly, stromal cells repopulating the damaged tissue assumed an elongated and interconnected fibroblastic morphology, and parallel, interconnected streams of aligned corneal fibroblasts were often observed both in vivo and ex vivo during wound healing, particularly in the posterior cornea. This pattern of fibroblast alignment was highly correlated with the structural organization of the lamellae, suggesting contact guidance of intrastromal cell migration. This is the first demonstration known to show that ECM structure mediates the pattern of intrastromal corneal fibroblast migration during in vivo wound healing.

5.1.2 Conclusions for Specific Aim 2

Using the in vitro models for intrastromal migration with the collagen substrates, the effects of specific growth factors during wound healing could be determined. A FI was easily conducted on the substrates without altering the structure of the collagen (based on SEM imaging), which allowed for a suitable in vitro migration model. Cells in PDGF media aligned and migrated in parallel to the collagen topography. Interestingly, cells in TGF-β contained little α-SMA labeling in the leading edge of migrating cells in the injured regions of aligned substrates, but had strong α-SMA labeling in non-injured regions, which is inconsistent with previous studies that show less myofibroblast transformation on aligned polyurethane substrates.[212] Pilot studies from Dr. Petroll's lab using an ex vivo organ culture model with rabbit corneas suggested that cells within the stroma (where collagen fibers 3-dimensionally surround the cells) did not transform into myofibroblasts in TGF-β media after FI. It is unclear if the difference in these results is due to 3-D mechanical cues from the stromal collagen that prevent TGF-β induced myofibroblast transformation or if the cells within the stroma are protected from TGF-β, unlike the direct exposure in the in vitro models.

5.1.2.1 Future Work for Specific Aim 2

Additional studies are needed to further assess wound closure rates between growth factors and substrate type. Also, length/breadth and shape factor calculations will be conducted for cell images on collagen-coated substrates for comparison to the aligned substrates. Longitudinal experiments, like using time-lapse microscopy or imaging wound area daily, can be used to measure the rate of migration and extent of wound closure. Further

studies are also needed to determine if the ECM is playing a role in maintaining cell phenotype in the stroma. Ex vivo organ culture studies with PDGF and serum free media for comparison with the aforementioned pilot TGF-β results would be helpful to determine the effects of each growth factor. There are technical challenges to the organ culture model, including edema, which precludes clear imaging of collagen using SHG imaging. It is also difficult to know if the growth factors are penetrating into the cornea; therefore, a scrape injury or keratectomy could be used with or instead of FI to facilitate growth factor infiltration. Additionally, a 3-D model of aligned fibrillar collagen is warranted in order to better mimic the topographical environment of the stromal ECM and determine growth factor effects on cell behavior.

Additionally, quantifying the differences in force generation of the cells for each growth factor would provide more insight into the effects of growth factors and ECM stiffness.[213] To accomplish this, aligned collagen substrates could be patterned over polyacrylamide gels of varying stiffness. Force mapping using fluorescent beads embedded into gels allows for measurements of cell-induced deformation during migration and spreading.[214, 215] Various wound environments may also be modeled with polyacrylamide gels by patterning different types of wound healing proteins, like fibronectin or Type III collagen, and by using specific growth factors.

5.1.3 Conclusions for Specific Aim 3

New findings from the LK studies revealed that initial healing involves two distinct cell and ECM patterns and alignment by day 21. The topography and alignment of the collagen lamellae directed fibroblast patterning during repopulation of the native stroma after LK injury in the rabbit. Fibroblasts in the wound region of the stroma had an elongated morphology and were co-aligned with the collagen lamellae. In contrast, cells accumulating in the sub-epithelial region of the stroma were randomly organized, expressed stress fibers, and produced a fibrotic ECM. Interestingly, novel results from the LK study revealed that cells appeared to remodel this fibrotic ECM to produce a lamellar structure that is similar in reflectivity to the native corneal stroma. For the first time, regeneration of transparent corneal tissue was observed with respect to cell/ECM patterning after keratectomy using in vivo confocal microscopy and SHG and multiphoton imaging. This study also demonstrated that cells and ECM initially observed to be fibrotic became highly co-aligned at later time points, as indicated by correlation analysis. Although results from the PRK experiment may have indicated that the aligned pattern of cells/ECM seen in the sub-epithelial region was within the native stroma at later time points, the cell density of the aligned region was higher in the LK model at 60 days and could be located on top of the wounded stroma (not in the native ECM). A possible explanation could be a difference in wound model, but without DTAF labeling, it is difficult to determine conclusively. Additional temporal studies involving post-LK ex vivo organ culture may be useful to better understand fibroblast invasion and reorientation at multiple stages during the repopulation phase, and to assess collagen deposition and remodeling in more detail between days 21 and 60.

5.1.4 Conclusions for Specific Aim 4

The PRK studies revealed that an initial fibrotic response occurred in the *fibrosis/remodeling* region of the stroma, which was characterized by significant corneal haze, myofibroblasts, and fibronectin deposition that was organized randomly. Over time, corneal transparency and thickness were restored, and collagen in the *fibrotic* region was shown for the first time to remodel into a normal, interwoven pattern, possibly due to cell/ECM interactions at punctate sites of F-actin labeling. Cells and ECM were co-aligned in the *regenerative* region, and stromal growth came primarily from this region. Bright punctate F-actin sites observed in the *regenerative* region likely played a role in aligned collagen deposition and correlation between cells/ECM, and may have also played a role in the patterning of collagen in the *remodeling* region. These new findings may provide insight into how the collagen regenerates in a transparent manner.

5.1.5 Closing Remarks

In the aforementioned Specific Aims, temporal and spatial cell/ECM interactions and patterning have been assessed after injury, and transparency appears to be restored using the FI, LK, and PRK models. However, the long-term goals of this work are to translate these findings to the clinic, since corneal scarring is a major cause of blindness worldwide. Thus, identifying the changes in gene and protein expression that occur during the intrastromal migration and the remodeling and regenerative phases of healing in the rabbit could potentially lead to novel therapies for preventing or reversing corneal scarring in patients. The results from this work may also warrant comparative studies with other tissues

containing organized lamellar collagen in other tissues to gain further insights into corneal wound healing.

BIBLIOGRAPHY

1. Ehlers, N. and J. Hjortdal, *The Cornea: Epithelium and Stroma*, in *Advances in Organ Biology*, J. Fischbarg, Editor. 2005, Elsevier. p. 83-111.
2. Petroll, W.M., et al., *Quantitative 3-D corneal imaging in vivo using a modified HRT-RCM confocal microscope.* Cornea, 2013. **36**: p. e36-43.
3. Morishige, N., et al., *Noninvasive corneal stromal collagen imaging using two-photon-generated second-harmonic signals.* J Cataract Refract Surg, 2006. **32**: p. 1784-1791.
4. Netto, M.V., et al., *Wound healing in the cornea: a review of refractive surgery complications and new prospects for therapy.* Cornea, 2005. **24**(5): p. 509-22.
5. Meek, K.M. and C. Knupp, *Corneal structure and transparency.* Prog Retin Eye Res, 2015. **49**: p. 1-16.
6. Forrester, J.V., et al., *Chapter 1 - Anatomy of the eye and orbit*, in *The Eye (Fourth Edition)*. 2016, W.B. Saunders. p. 1-102.e2.
7. Eghrari, A.O., S.A. Riazuddin, and J.D. Gottsch, *Chapter Two - Overview of the Cornea: Structure, Function, and Development*, in *Progress in Molecular Biology and Translational Science*, J.F. Hejtmancik and J.M. Nickerson, Editors. 2015, Academic Press. p. 7-23.
8. Kruegel, J. and N. Miosge, *Basement membrane components are key players in specialized extracellular matrices.* Cell Mol Life Sci, 2010. **67**(17): p. 2879-95.
9. Tuori, A., et al., *The immunohistochemical composition of the human corneal basement membrane.* Cornea, 1996. **15**(3): p. 286-94.
10. *Adler's Physiology of the Eye*. Ninth ed, ed. W.M. Hart. 1992: Mosby-Year Book. 888.
11. Chakravarti, S., et al., *Corneal opacity in lumican-null mice: defects in collagen fibril structure and packing in the posterior stroma.* Invest Ophthalmol Vis Sci, 2000. **41**: p. 3365-3373.
12. Funderburgh, J.L., M.M. Mann, and M.L. Funderburgh, *Keratocyte phenotype mediates proteoglycan structure: a role for fibroblasts in corneal fibrosis.* J Biol Chem, 2003. **278**: p. 45629-45637.
13. Hassell, J.R. and D.E. Birk, *The molecular basis of corneal transparency.* Exp Eye Res, 2010. **91**(3): p. 326-35.
14. Ichijima, H., et al., *Actin filament organization during endothelial wound healing in the rabbit cornea. Comparison between trasncorneal freeze and mechanical scrape injuries.* Invest Ophthalmol Vis Sci, 1993. **34**: p. 2803-2812.
15. Hamada, R., et al., *[Analytical and statistical study of the lamellae, keratocytes and collagen fibrils of the central region of the normal human cornea. (Light and electron microscopy)].* Arch Ophtalmol Rev Gen Ophtalmol, 1972. **32**(8): p. 563-70.
16. Jester, J.V., W.M. Petroll, and H.D. Cavanagh, *Corneal stromal wound healing in refractive surgery: the role of myofibroblasts.* Prog Retin Eye Res, 1999. **18**(3): p. 311-56.

17. Stramer, B.M., et al., *Molecular mechanisms controlling the fibrotic repair phenotype in cornea: implications for surgical outcomes.* Invest Ophthalmol Vis Sci, 2003. **44**(10): p. 4237-46.
18. Jester, J.V., et al., *Transforming growth factor(beta)-mediated corneal myofibroblast differentiation requires actin and fibronectin assembly.* Invest Ophthalmol Vis Sci, 1999. **40**(9): p. 1959-67.
19. Blalock, T.D., et al., *Connective tissue growth factor expression and action in human corneal fibroblast cultures and rat corneas after photorefractive keratectomy.* Invest Ophthalmol Vis Sci, 2003. **44**(5): p. 1879-87.
20. Jester, J.V., et al., *The cellular basis of corneal transparency: evidence for 'corneal crystallins'*. J Cell Sci, 1999. **112 (Pt 5)**: p. 613-22.
21. Jester, J.V., et al., *Myofibroblast differentiation modulates keratocyte crystallin protein expression, concentration, and cellular light scattering.* Invest Ophthalmol Vis Sci, 2012. **53**(2): p. 770-8.
22. Meek, K.M., *The Cornea and Sclera*, in *Collagen: Structure and Mechanics*, P. Fratzl, Editor. 2008, Springer US: Boston, MA. p. 359-396.
23. Young, R.D., et al., *Three-dimensional aspects of matrix assembly by cells in the developing cornea.* Proc Natl Acad Sci U S A, 2014. **111**(2): p. 687-92.
24. Moller-Pedersen, T., et al., *Confocal microscopic characterization of wound repair after photorefractive keratectomy using in vivo confocal microscopy.* Invest Ophthalmol Vis Sci, 1998. **39**: p. 487-501.
25. Petroll, W.M. and N. Lakshman, *Fibroblastic Transformation of Corneal Keratocytes by Rac Inhibition is Modulated by Extracellular Matrix Structure and Stiffness.* J Funct Biomater, 2015. **6**(2): p. 222-40.
26. Kim, A., et al., *Corneal Stromal Cells use both High- and Low-Contractility Migration Mechanisms in 3-D Collagen Matrices.* Exp Cell Res, 2012. **318**: p. 741-752.
27. Kim, A., et al., *Growth factor regulation of corneal keratocyte differentiation and migration in compressed collagen matrices.* Invest Ophthalmol Vis Sci, 2010. **51**(2): p. 864-75.
28. Jester, J.V., et al., *Expression of alpha-smooth muscle (alpha-SM) actin during corneal stromal wound healing.* Invest Ophthalmol Vis Sci, 1995. **36**(5): p. 809-19.
29. Jester, J.V., et al., *TGFbeta induced myofibroblast differentiation of rabbit keratocytes requires synergistic TGFbeta, PDGF and integrin signaling.* Exp Eye Res, 2002. **75**(6): p. 645-57.
30. Chen, J., et al., *Rho-mediated regulation of TGF-beta1- and FGF-2-induced activation of corneal stromal keratocytes.* Invest Ophthalmol Vis Sci, 2009. **50**(8): p. 3662-70.
31. Funderburgh, J.L., et al., *Proteoglycan expression during transforming growth factor beta -induced keratocyte-myofibroblast transdifferentiation.* J Biol Chem, 2001. **276**(47): p. 44173-8.

32. Etheredge, L., B.P. Kane, and J.R. Hassell, *The effect of growth factor signaling on keratocytes in vitro and its relationship to the phases of stromal wound repair.* Invest Ophthalmol Vis Sci, 2009. **50**(7): p. 3128-36.
33. Møller-Pedersen, T., et al., *Corneal Haze Development After PRK Is Regulated by Volume of Stromal Tissue Removal.* Cornea, 1998. **17**(6): p. 627.
34. Mohan, R.R., et al., *Modulation of TNF-alpha-induced apoptosis in corneal fibroblasts by transcription factor NF-kappaB.* Invest Ophthalmol Vis Sci, 2000. **41**(6): p. 1327-36.
35. Wilson, S.E., *Analysis of the keratocyte apoptosis, keratocyte proliferation, and myofibroblast transformation responses after photorefractive keratectomy and laser in situ keratomileusis.* Trans Am Ophthalmol Soc, 2002. **100**: p. 411-33.
36. Mar, P.K., et al., *Disruption of actin filaments by gelsolin over-expression impairs matrix reorganization.* Invest Ophthalmol Vis Sci, 1998. **39**(4): p. S35.
37. Maurer, J.K., et al., *Confocal microscopic characterization of initial corneal changes of surfactant-induced eye irritation in the rabbit.* Toxicol Appl Pharmacol, 1997. **143**(2): p. 291-300.
38. Knappe, S., et al., *Results of confocal microscopy examinations after collagen cross-linking with riboflavin and UVA light in patients with progressive keratoconus.* Ophthalmologica, 2011. **225**(2): p. 95-104.
39. Mencucci, R., et al., *Effects of riboflavin/UVA corneal cross-linking on keratocytes and collagen fibres in human cornea.* Clin Experiment Ophthalmol, 2010. **38**(1): p. 49-56.
40. Wollensak, G., et al., *Keratocyte apoptosis after corneal collagen cross-linking using riboflavin/UVA treatment.* Cornea, 2004. **23**(1): p. 43-9.
41. Jester, J.V., et al., *TGFbeta induced myofibroblast differentiation of rabbit keratocytes requires synergistic TGFbeta, PDGF and integrin signalling.* Exp Eye Res, 2002. **75**: p. 645-657.
42. Stramer, B.M., et al., *Molecular mechanisms controlling the fibrotic repair phenotype in cornea: implications for surgical outcomes.* Invest Ophthalmol Vis Sci, 2003. **44**: p. 4237-4246.
43. Wilson, S.E., J.J. Liu, and R.R. Mohan, *Stromal-epithelial interactions in the cornea.* Prog Retin Eye Res, 1999. **18**: p. 293-309.
44. Wilson, S.E., et al., *The Corneal Wound Healing Response: Cytokine-mediated Interaction of the Epithelium, Stroma, and Inflammatory Cells.* Prog Retin Eye Res, 2001. **20**(5): p. 625-637.
45. Jester, J.V., et al., *Transforming growth factor(beta)-mediated corneal myofibroblast differentiation requires actin and fibronectin assembly.* Invest Ophthalmol Vis Sci, 1999. **40**: p. 1959-1967.
46. Blalock, T.D., et al., *Connective tissue growth factor expression and action in human corneal fibroblast cultures and rat corneas after photorefractive keratectomy.* Invest Ophthalmol Vis Sci, 2003. **44**: p. 1879-1887.
47. Lanfer, B., et al., *Aligned fibrillar collagen matrices obtained by shear flow deposition.* Biomaterials, 2008. **29**(28): p. 3888-95.

48. Saeidi, N., E.A. Sander, and J.W. Ruberti, *DYNAMIC SHEAR-INFLUENCED COLLAGEN SELF-ASSEMBLY.* Biomaterials, 2009. **30**(34): p. 6581-6592.
49. Moller-Pedersen, T., et al., *Confocal microscopic characterization of wound repair after photorefractive keratectomy.* Invest Ophthalmol Vis Sci, 1998. **39**(3): p. 487-501.
50. Kivanany, P.B., K.C. Grose, and W.M. Petroll, *Temporal and spatial analysis of stromal cell and extracellular matrix patterning following lamellar keratectomy.* Exp Eye Res, 2016. **153**: p. 56-64.
51. Latvala, T., et al., *Expression of cellular fibronectin and tenascin in the rabbit cornea after excimer laser photorefractive keratectomy: a 12 month study.* The British Journal of Ophthalmology, 1995. **79**(1): p. 65-69.
52. Rawe, I.M., et al., *A morphological study of rabbit corneas after laser keratectomy.* Eye, 1992. **6**(6): p. 637-642.
53. Fitzsimmons, T.D., et al., *Hyaluronic acid in the rabbit cornea after excimer laser superficial keratectomy.* Invest Ophthalmol Vis Sci, 1992. **33**(11): p. 3011-6.
54. Farid, M., et al., *Detection of corneal fibrosis by imaging second harmonic-generated signals in rabbit corneas treated with mitomycin C after excimer laser surface ablation.* Invest Ophthalmol Vis Sci, 2008. **49**(10): p. 4377-83.
55. Efron, N., *Contact lens-induced changes in the anterior eye as observed in vivo with the confocal microscope.* Prog Retin Eye Res 2007. **26**: p. 398-436.
56. Zhivov, A., R.F. Guthoff, and O. Stachs, *In vivo confocal microscopy of the ocular surface: from bench to bedside and back again.* Br J Ophthalmol, 2010. **94**(12): p. 1557-8.
57. Labbe, A., et al., *Contribution of in vivo confocal microscopy to the diagnosis and management of infectious keratitis.* The Ocular Surface, 2009. **7**: p. 41-52.
58. Dhaliwal, J.S., S.C. Kaufman, and A.G.Y. Chiou, *Current applications of clinical confocal microscopy.* Curr Opin Ophthalmol, 2007. **18**: p. 300-307.
59. Villani, E., et al., *In vivo confocal microscopy of the ocular surface: from bench to bedside.* Curr Eye Res, 2014. **39**(3): p. 213-31.
60. Zhivov, A., et al., *In vivo confocal microscopy of the ocular surface.* Ocul Surf, 2006. **4**(2): p. 81-93.
61. Petroll, W.M., H.D. Cavanagh, and J.V. Jester, *Confocal Microscopy,* in *Cornea*, J. Krachmer, M. Mannis, and E. Holland, Editors. 2011, Elsevier, Inc.: St. Louis. p. 205-220.
62. Erie, J.C., J.W. McLaren, and S.V. Patel, *Confocal microscopy in ophthalmology.* Am J Ophthalmol, 2009. **148**(5): p. 639-46.
63. Patel, D.V. and C.N. McGhee, *Quantitative analysis of in vivo confocal microscopy images: a review.* Surv Ophthalmol, 2013. **58**(5): p. 466-75.
64. Petroll, W.M., J.V. Jester, and H.D. Cavanagh, *Clinical confocal microscopy.* Curr Opinion Ophthalmol, 1998. **9**(IV): p. 59-65.
65. Petroll, W.M. and D.M. Robertson, *In vivo confocal microscopy of the cornea: New developments in image acquisition, reconstruction, and analysis using the HRT-Rostock Corneal Module.* Ocul Surf, 2015. **13**(3): p. 187-203.

66. Bouheraoua, N., et al., *Optical coherence tomography and confocal microscopy following three different protocols of corneal collagen-crosslinking in keratoconus.* Invest Ophthalmol Vis Sci, 2014. **55**(11): p. 7601-9.
67. Tervo, T. and J. Moilanen, *In vivo confocal microscopy for evaluation of wound healing following corneal refractive surgery.* Prog Retin Eye Res, 2003. **22**: p. 339-358.
68. Kaufman, S.C. and H.E. Kaufman, *How has confocal microscopy helped us in refractive surgery?* Curr Opin Ophthalmol, 2006. **17**: p. 380-388.
69. Jester, J.V., W.M. Petroll, and H.D. Cavanagh, *Corneal stromal wound healing in refractive surgery: the role of the myofibroblast.* Prog. Retinal. Eye. Res., 1999. **18**: p. 311-356.
70. Lemp, M.A., P.N. Dilly, and A. Boyde, *Tandem scanning (confocal) microscopy of the full thickness cornea.* Cornea, 1986. **4**: p. 205-209.
71. Cavanagh, H.D., et al., *Confocal microscopy of the living eye.* CLAO J, 1990. **16**: p. 65-73.
72. Petroll, W.M., H.D. Cavanagh, and J.V. Jester, *3-Dimensional reconstruction of corneal cells using in vivo confocal microscopy.* J Microsc, 1993. **170**: p. 213-219.
73. Masters, B.R. and A.A. Thaer, *Real-time scanning slit confocal microscopy of the in vivo human cornea.* Appl Optics 1994. **33**: p. 695-701.
74. Brakenhoff, G.J. and K. Visscher, *Confocal imaging with bilateral scanning and array detectors.* J Microsc, 1992. **165**: p. 139-146.
75. Guthoff, R.F., C. Baudouin, and J. Stave, *Atlas of confocal laser scanning in vivo microscopy in ophthalmology*. 2006, Berlin: Heidelberg/Springer.
76. Erie, E.A., et al., *Corneal subbasal nerve density: A comparison of two confocal microscopes.* Eye Contact Lens, 2008. **34**: p. 322-325.
77. Zhivov, A., et al., *In vivo three-dimensional confocal laser scanning microscopy of corneal surface and epithelium.* Br J Ophthalmol, 2009. **93**: p. 667-672.
78. Li, H.F., et al., *Epithelial and corneal thickness measurements by in vivo confocal microscopy through focusing (CMTF).* Curr Eye Res, 1997. **16**: p. 214-221.
79. Li, J., et al., *On-line 3-dimensional confocal imaging in vivo.* Invest Ophthalmol Vis Sci, 2000. **41**: p. 2945-2953.
80. Wiegand, W., et al., *Optical sectioning of the cornea with a new confocal in vivo slit-scanning video-microscope.* Ophthalmology 1993. **100(9A)**: p. 128.
81. Mohler, W., A.C. Millard, and P.J. Campagnola, *Second harmonic generation imaging of endogenous structural proteins.* 2003. **29**: p. 97-109.
82. Hochheimer, B.F., *Second harmonic light generation in the rabbit cornea.* Appl Opt, 1982. **21**(8): p. 1516-8.
83. Winkler, M., et al., *A Comparative Study of Vertebrate Corneal Structure: The Evolution of a Refractive Lens.* Investigative Ophthalmology & Visual Science, 2015. **56**(4): p. 2764-2772.
84. Williams, R.M., W.R. Zipfel, and W.W. Webb, *Multiphoton microscopy in biological research.* Curr Opin Chem Biol, 2001. **5**(5): p. 603-8.

85. Myrna, K.E., et al., *Substratum topography modulates corneal fibroblast to myofibroblast transformation.* Invest Ophthalmol Vis Sci, 2012. **53**(2): p. 811-6.
86. Teixeira, A.I., P.F. Nealey, and C.J. Murphy, *Responses of human keratocytes to micro- and nanostructured substrates.* J Biomed Mater Res A, 2004. **71A**(3): p. 369-376.
87. Karamichos, D., et al., *A role for topographic cues in the organization of collagenous matrix by corneal fibroblasts and stem cells.* PLoS One, 2014. **9**(1): p. e86260.
88. Petroll, W.M., et al., *ZO-1 reorganization and myofibroblast transformation of corneal endothelial cells after freeze injury in the cat.* Exp Eye Res, 1997. **64**: p. 257-267.
89. Jester, J.V., et al., *Corneal keratocytes: In situ and in vitro organization of cytoskeletal contractile proteins.* Invest Ophthalmol Vis Sci, 1994. **35**: p. 730-743.
90. Moller-Pedersen, T., et al., *Corneal haze development after PRK is regulated by volume of stromal tissue removal.* Cornea, 1998. **17**: p. 627-639.
91. Ichijima, H., et al., *In vivo confocal microscopic studies of endothelial wound healing in rabbit cornea.* Cornea, 1993. **12**: p. 369-78.
92. Gordon, S.R., *Cytological and immunocytochemical approaches to the study of corneal endothelial wound repair.* Prog Histochem Cytochem, 1994. **28**(2): p. 1-64.
93. Gordon, S.R. and C.A. Staley, *Role of the cytoskeleton during injury-induced cell migration in corneal endothelium.* Cell Motil Cytoskeleton, 1990. **16**(1): p. 47-57.
94. Kay, E.D., et al., *Type I collagen and fibronectin synthesis by retrocorneal fibrous membrane.* Invest Ophthalmol Vis Sci, 1982. **22**(2): p. 200-12.
95. Waring, G.O., 3rd, *Posterior collagenous layer of the cornea. Ultrastructural classification of abnormal collagenous tissue posterior to Descemet's membrane in 30 cases.* Arch Ophthalmol, 1982. **100**(1): p. 122-34.
96. Michels, R.G., K.R. Kenyon, and A.E. Maumence, *Retrocorneal fibrous membrane.* Invest Ophthalmol, 1972. **11**(10): p. 822-31.
97. Jester, J.V., et al., *Myofibroblast differentiation modulates keratocyte crystallin protein expression, concentration,, and cellular light scattering.* Invest Ophthalmol Vis Sci, 2012. **53**: p. 770-778.
98. Jester, J.V., et al., *The cellular basis of corneal transparency: evidence for 'corneal crystallins'.* J Cell Sci, 1999. **112**: p. 613-622.
99. Thomasy, S.M., et al., *Elastic modulus and collagen organization of the rabbit cornea: epithelium to endothelium.* Acta Biomater, 2014. **10**(2): p. 785-91.
100. Ghibaudo, M., et al., *Substrate topography induces a crossover from 2D to 3D behavior in fibroblast migration.* Biophys J, 2009. **97**: p. 357-368.
101. Teixeira, A.I., et al., *Epithelial contact guidance on well-defined micro- and nanostructured substrates.* J Cell Sci, 2003. **116**(10): p. 1881-1892.
102. He, S., et al., *Dissecting Collective Cell Behavior in Polarization and Alignment on Micropatterned Substrates.* Biophys J, 2015. **109**(3): p. 489-500.

103. Pepose, J.S. and J.L. Ubels, *The Cornea*, in *Adler's Physiology of the Eye*, W.M. Hart, Editor. 1992, Mosby Year book: St. Louis. p. 29-70.
104. Pot, S.A., et al., *Nanoscale topography-induced modulation of fundamental cell behaviors of rabbit corneal keratocytes, fibroblasts, and myofibroblasts.* Invest Ophthalmol Vis Sci, 2010. **51**(3): p. 1373-81.
105. Guillemette, M.D., et al., *Surface topography induces 3D self-orientation of cells and extracellular matrix resulting in improved tissue function.* Integr Biol (Camb), 2009. **1**(2): p. 196-204.
106. Saeidi, N., et al., *Disorganized collagen scaffold interferes with fibroblast mediated deposition of organized extracellular matrix in vitro.* Biotechnol Bioeng, 2012. **109**(10): p. 2683-98.
107. Guo, X.Q., et al., *Morphologic characterization of organized extracellular matrix deposition by ascorbic acid-stimulated human corneal fibroblasts.* Invest Ophthalmol Vis Sci, 2007. **48**: p. 4056-4060.
108. Karamichos, D., et al., *Human corneal fibrosis: an in vitro model.* Invest Ophthalmol Vis Sci, 2010. **51**(3): p. 1382-8.
109. Ren, R., et al., *Human primary corneal fibroblasts synthesize and deposit proteoglycans in long-term cultures.* Dev Dyn, 2008. **237**: p. 2705-2715.
110. Friedl, P., et al., *Migration of highly aggressive MV3 melanoma cells in 3-dimensional collagen lattices results in local matrix reorganization and shedding of alpha2 and beta1 integrins and CD44.* Cancer Res, 1997. **57**: p. 2061-2070.
111. Provenzano, P.P., et al., *Collagen reorganization at the tumor-stromal interface facilitates local invasion.* BMC Med, 2006. **4**(1): p. 38.
112. Gaggioli, C., et al., *Fibroblast-led collective invasion of carcinoma cells with differing roles for RhoGTPases in leading and following cells.* Nat Cell Biol, 2007. **9**(12): p. 1392-400.
113. Provenzano, P.P., et al., *Contact guidance mediated three-dimensional cell migration is regulated by Rho/ROCK-dependent matrix reorganization.* Biophys J, 2008. **95**: p. 5374-5384.
114. Grinnell, F. and W.M. Petroll, *Cell motility and mechanics in three-dimensional collagen matrices.* Annu Rev Cell Dev Biol, 2010. **26**: p. 335-61.
115. Petroll, W.M., et al., *Dynamic assessment of fibroblast mechanical activity during Rac-induced cell spreading in 3-D culture.* J Cell Physiol, 2008. **217**: p. 162-171.
116. Guido, S. and R.T. Tranquillo, *A methodology for the systematic and quantitative study of cell contact guidance in oriented collagen gels. Correlation of fibroblast orientation and gel birefringence.* J Cell Sci, 1993. **105 (Pt 2)**: p. 317-31.
117. Raeber, G.P., M.P. Lutolf, and J.A. Hubbell, *Part II: Fibroblasts preferentially migrate in the direction of principal strain.* Biomech Model Mechanobiol, 2008. **7**(3): p. 215-25.
118. Friedl, P. and K. Wolf, *Plasticity of cell migration: a multiscale tuning model.* J Cell Biol, 2009. **199**: p. 11-19.
119. Miron-Mendoza, M., et al., *The role of thrombin and cell contractility in regulating clustering and collective migration of corneal fibroblasts in different ECM environments.* Invest Ophthalmol Vis Sci, 2015. **56**(3): p. 2079-90.

120. Miron-Mendoza, M., et al., *Individual versus collective fibroblast spreading and migration: regulation by matrix composition in 3D culture.* Exp Eye Res, 2012. **99**: p. 36-44.
121. Miron-Mendoza, M., E. Graham, and W.M. Petroll. *Fibronectin as a regulator of collective migration and clustering of corneal fibroblasts in 3D fibrin matrices*. in *ARVO Annual Meeting*. 2015.
122. Petroll, W.M., et al., *Corneal fibroblast migration patterns during intrastromal wound healing correlate with ECM structure and alignment.* Invest Ophthalmol Vis Sci, 2015. **56**: p. 7352–7361.
123. Phu, D., et al., *Effect of substrate composition and alignment on corneal cell phenotype.* Tissue Eng Part A, 2011. **17**(5-6): p. 799-807.
124. Kim, A., N. Lakshman, and W.M. Petroll, *Quantitative assessment of local collagen matrix remodeling in 3-D culture: the role of Rho kinase.* Exp Cell Res, 2006. **312**(18): p. 3683-92.
125. Pot, S.A., et al., *Nanoscale Topography–Induced Modulation of Fundamental Cell Behaviors of Rabbit Corneal Keratocytes, Fibroblasts, and Myofibroblasts.* Investigative Ophthalmology & Visual Science, 2010. **51**(3): p. 1373-1381.
126. Pellegrin, S. and H. Mellor, *Actin stress fibres.* Journal of Cell Science, 2007. **120**(20): p. 3491-3499.
127. Petroll, W.M., et al., *Quantitative 3-dimensional corneal imaging in vivo using a modified HRT-RCM confocal microscope.* Cornea, 2013. **32**(4): p. e36-43.
128. Han, M., G. Giese, and J. Bille, *Second harmonic generation imaging of collagen fibrils in cornea and sclera.* Opt Express, 2005. **13**(15): p. 5791-7.
129. Morishige, N., et al., *Noninvasive corneal stromal collagen imaging using two-photon-generated second-harmonic signals.* J Cataract Refract Surg, 2006. **32**(11): p. 1784-91.
130. Petroll, W.M., et al., *Corneal Fibroblast Migration Patterns During Intrastromal Wound Healing Correlate With ECM Structure and Alignment.* Invest Ophthalmol Vis Sci, 2015. **56**(12): p. 7352-61.
131. Zhivov, A., et al., *In vivo three-dimensional confocal laser scanning microscopy of corneal surface and epithelium.* Br J Ophthalmol, 2009. **93**(5): p. 667-72.
132. Jester, J.V., et al., *Corneal keratocytes: in situ and in vitro organization of cytoskeletal contractile proteins.* Invest Ophthalmol Vis Sci, 1994. **35**(2): p. 730-43.
133. Sivaguru, M., et al., *Quantitative analysis of collagen fiber organization in injured tendons using Fourier transform-second harmonic generation imaging.* Optics Express, 2010. **18**(24): p. 24983-24993.
134. Young, R.D., et al., *Three-dimensional aspects of matrix assembly by cells in the developing cornea.* Proc Natl Acad Sci U S A, 2014. **111**(2): p. 687-92.
135. Ghibaudo, M., et al., *Substrate topography induces a crossover from 2D to 3D behavior in fibroblast migration.* Biophys J, 2009. **97**(1): p. 357-68.
136. Teixeira, A.I., et al., *Epithelial contact guidance on well-defined micro- and nanostructured substrates.* J Cell Sci, 2003. **116**(Pt 10): p. 1881-92.

137. Teixeira, A.I., P.F. Nealey, and C.J. Murphy, *Responses of human keratocytes to micro- and nanostructured substrates.* J Biomed Mater Res A, 2004. **71**(3): p. 369-76.
138. Pot, S.A., et al., *Nanoscale Topography–Induced Modulation of Fundamental Cell Behaviors of Rabbit Corneal Keratocytes, Fibroblasts, and Myofibroblasts.* Invest Ophthalmol Vis Sci, 2010. **51**(3): p. 1373-81.
139. Wilson, S.E., J.J. Liu, and R.R. Mohan, *Stromal-epithelial interactions in the cornea.* Prog Retin Eye Res, 1999. **18**(3): p. 293-309.
140. Wilson, S.E., et al., *The corneal wound healing response: cytokine-mediated interaction of the epithelium, stroma, and inflammatory cells.* Prog Retin Eye Res, 2001. **20**(5): p. 625-37.
141. Mohan, R.R., et al., *Apoptosis, necrosis, proliferation, and myofibroblast generation in the stroma following LASIK and PRK.* Exp Eye Res, 2003. **76**(1): p. 71-87.
142. Fini, M.E., *Keratocyte and fibroblast phenotypes in the repairing cornea.* Prog Retin Eye Res, 1999. **18**(4): p. 529-51.
143. Masur, S.K., et al., *Myofibroblasts differentiate from fibroblasts when plated at low density.* Proc Natl Acad Sci U S A, 1996. **93**(9): p. 4219-23.
144. Jester, J.V., et al., *Inhibition of corneal fibrosis by topical application of blocking antibodies to TGF beta in the rabbit.* Cornea, 1997. **16**(2): p. 177-87.
145. Petridou, S., et al., *TGF-beta receptor expression and smad2 localization are cell density dependent in fibroblasts.* Invest Ophthalmol Vis Sci, 2000. **41**(1): p. 89-95.
146. Torricelli, A.A., et al., *The corneal fibrosis response to epithelial-stromal injury.* Exp Eye Res, 2016. **142**: p. 110-8.
147. Torricelli, A.A., et al., *Transmission electron microscopy analysis of epithelial basement membrane repair in rabbit corneas with haze.* Invest Ophthalmol Vis Sci, 2013. **54**(6): p. 4026-33.
148. Wang, J.H., et al., *Cell orientation determines the alignment of cell-produced collagenous matrix.* J Biomech, 2003. **36**(1): p. 97-102.
149. Gouveia, R.M., et al., *Bioactive films produced from self-assembling peptide amphiphiles as versatile substrates for tuning cell adhesion and tissue architecture in serum-free conditions.* Journal of Materials Chemistry B, 2013. **1**(44): p. 6157-6169.
150. Gouveia, R.M., et al., *New Self-Assembling Multifunctional Templates for the Biofabrication and Controlled Self-Release of Cultured Tissue.* Tissue Eng Part A, 2015. **21**(11-12): p. 1772-84.
151. Guo, X., et al., *Morphologic characterization of organized extracellular matrix deposition by ascorbic acid-stimulated human corneal fibroblasts.* Invest Ophthalmol Vis Sci, 2007. **48**(9): p. 4050-60.
152. Karamichos, D., et al., *Human Corneal Fibrosis: An In Vitro Model.* Invest Ophthalmol Vis Sci, 2010. **51**(3): p. 1382-8.
153. Ren, R., et al., *Human primary corneal fibroblasts synthesize and deposit proteoglycans in long-term 3-D cultures.* Dev Dyn, 2008. **237**(10): p. 2705-15.

154. Jester, J.V., et al., *Radial keratotomy. 1. The wound healing process and measurement of incisional gape in two animal models using in vivo confocal microscopy.* Invest Ophthalmol Vis Sci, 1992. **33**(12): p. 3255-70.
155. Eastwood, M., et al., *Effect of precise mechanical loading on fibroblast populated collagen lattices: morphological changes.* Cell Motil Cytoskeleton, 1998. **40**(1): p. 13-21.
156. Wang, N., et al., *Cell prestress. I. Stiffness and prestress are closely associated in adherent contractile cells.* Am J Physiol Cell Physiol, 2002. **282**(3): p. C606-16.
157. Karamichos, D., N. Lakshman, and W.M. Petroll, *Regulation of corneal fibroblast morphology and collagen reorganization by extracellular matrix mechanical properties.* Invest Ophthalmol Vis Sci, 2007. **48**(11): p. 5030-7.
158. Efron, N., *Contact lens-induced changes in the anterior eye as observed in vivo with the confocal microscope.* Prog Retin Eye Res, 2007. **26**(4): p. 398-436.
159. Labbe, A., et al., *Contribution of in vivo confocal microscopy to the diagnosis and management of infectious keratitis.* Ocul Surf, 2009. **7**(1): p. 41-52.
160. Dhaliwal, J.S., S.C. Kaufman, and A.G. Chiou, *Current applications of clinical confocal microscopy.* Curr Opin Ophthalmol, 2007. **18**(4): p. 300-7.
161. Villani, E., et al., *In Vivo Confocal Microscopy of the Ocular Surface: From Bench to Bedside.* Current eye research, 2014. **39**(3): p. 213-231.
162. Petroll, W., H. Cavanagh, and J. Jester, *Confocal microscopy.* Cornea. St. Louis: Elsevier, Inc, 2011: p. 205-220.
163. Petroll, W.M., H.D. Cavanagh, and J.V. Jester, *Clinical confocal microscopy.* Curr Opin Ophthalmol, 1998. **9**(4): p. 59-65.
164. Tervo, T. and J. Moilanen, *In vivo confocal microscopy for evaluation of wound healing following corneal refractive surgery.* Prog Retin Eye Res, 2003. **22**(3): p. 339-58.
165. Kaufman, S.C. and H.E. Kaufman, *How has confocal microscopy helped us in refractive surgery?* Curr Opin Ophthalmol, 2006. **17**(4): p. 380-8.
166. Cintron, C. and C.L. Kublin, *Regeneration of corneal tissue.* Dev Biol, 1977. **61**(2): p. 346-57.
167. Flynn, B.P., et al., *Mechanical strain stabilizes reconstituted collagen fibrils against enzymatic degradation by mammalian collagenase matrix metalloproteinase 8 (MMP-8).* PLoS One, 2010. **5**(8): p. e12337.
168. Bhole, A.P., et al., *Mechanical strain enhances survivability of collagen micronetworks in the presence of collagenase: implications for load-bearing matrix growth and stability.* Philos Trans A Math Phys Eng Sci, 2009. **367**(1902): p. 3339-62.
169. Karamichos, D., N. Lakshman, and W.M. Petroll, *Extracellular matrix mechanical properties regulate corneal fibroblast morphology and collagen remodeling in 3-D culture.* Invest Ophthalmol Vis Sci, 2007. **48**: p. 5030-5037.
170. Petroll, W.M. and M. Miron-Mendoza, *Mechanical interactions and crosstalk between corneal keratocytes and the extracellular matrix.* Exp Eye Res, 2015. **133**: p. 49-57.

171. Moller-Pedersen, T., et al., *Neutralizing antibody to TGFbeta modulates stromal fibrosis but not regression of photoablative effect following PRK.* Curr Eye Res, 1998. **17**(7): p. 736-47.
172. Jester, J.V., et al., *Evaluating corneal collagen organization using high-resolution nonlinear optical macroscopy.* Eye Contact Lens, 2010. **36**(5): p. 260-4.
173. Moller-Pedersen, T., et al., *Neutralizing antibody to TGFβ modulates stromal fibrosis but not regression of photoablative effect following PRK.* Curr Eye Res, 1998. **17**: p. 736-737.
174. Lakshman, N., A. Kim, and W.M. Petroll, *Characterization of corneal keratocyte morphology and mechanical activity within 3-D collagen matrices.* Exp Eye Res, 2010. **90**(2): p. 350-9.
175. Jester, J.V., et al., *TGFβ Induced Myofibroblast Differentiation of Rabbit Keratocytes Requires Synergistic TGFβ, PDGF and Integrin Signaling.* Experimental Eye Research, 2002. **75**(6): p. 645-657.
176. Wilson, S.E., et al., *The Corneal Wound Healing Response:: Cytokine-mediated Interaction of the Epithelium, Stroma, and Inflammatory Cells.* Progress in Retinal and Eye Research, 2001. **20**(5): p. 625-637.
177. Wilson, S.E., J.J. Liu, and R.R. Mohan, *Stromal-epithelial interactions in the cornea.* Progress in Retinal and Eye Research, 1999. **18**(3): p. 293-309.
178. Stramer, B.M., et al., *Molecular Mechanisms Controlling the Fibrotic Repair Phenotype in Cornea: Implications for Surgical Outcomes.* Investigative Ophthalmology & Visual Science, 2003. **44**(10): p. 4237-4246.
179. Fini, M.E., *Keratocyte and fibroblast phenotypes in the repairing cornea.* Progress in Retinal and Eye Research, 1999. **18**(4): p. 529-551.
180. Masur, S.K., et al., *Myofibroblasts differentiate from fibroblasts when plated at low density.* Proceedings of the National Academy of Sciences of the United States of America, 1996. **93**(9): p. 4219-4223.
181. Mohan, R.R., et al., *Apoptosis, necrosis, proliferation, and myofibroblast generation in the stroma following LASIK and PRK.* Experimental Eye Research, 2003. **76**(1): p. 71-87.
182. Funderburgh, J., et al., *Proteoglycan expression during transforming grwoth factor beta-induced keratocyte-myofibroblast transdifferentiation.* J Biol. Chem., 2001. **276**: p. 44173-44178.
183. Gao, X., et al., *Connective tissue growth factor stimulates renal cortical myofibroblast-like cell proliferation and matrix protein production.* Wound Repair Regen, 2008. **16**(3): p. 408-15.
184. Carrington, L.M., et al., *Differential regulation of key stages in early corneal wound healing by TGF-beta isoforms and their inhibitors.* Invest Ophthalmol Vis Sci, 2006. **47**(5): p. 1886-94.
185. Huh, M.I., et al., *Distribution of TGF-beta isoforms and signaling intermediates in corneal fibrotic wound repair.* J Cell Biochem, 2009. **108**(2): p. 476-88.
186. Karamichos, D., A.E. Hutcheon, and J.D. Zieske, *Transforming growth factor-beta3 regulates assembly of a non-fibrotic matrix in a 3D corneal model.* J Tissue Eng Regen Med, 2011. **5**(8): p. e228-38.

187. Reneker, L.W., et al., *Induction of corneal myofibroblasts by lens-derived transforming growth factor beta1 (TGFbeta1): a transgenic mouse model.* Brain Res Bull, 2010. **81**(2-3): p. 287-96.
188. Singh, V., et al., *Effect of TGFbeta and PDGF-B blockade on corneal myofibroblast development in mice.* Exp Eye Res, 2011. **93**(6): p. 810-7.
189. Maltseva, O., et al., *Fibroblast growth factor reversal of the corneal myofibroblast phenotype.* Invest Ophthalmol Vis Sci, 2001. **42**(11): p. 2490-5.
190. Marino, G.K., et al., *Epithelial basement membrane injury and regeneration modulates corneal fibrosis after pseudomonas corneal ulcers in rabbits.* Exp Eye Res, 2017. **161**: p. 101-105.
191. Barbosa, F.L., et al., *Stromal interleukin-1 expression in the cornea after haze-associated injury.* Exp Eye Res, 2010. **91**(3): p. 456-61.
192. Kaur, H., et al., *Corneal myofibroblast viability: opposing effects of IL-1 and TGF beta1.* Exp Eye Res, 2009. **89**(2): p. 152-8.
193. Wilson, S.E., S.S. Chaurasia, and F.W. Medeiros, *Apoptosis in the Initiation, Modulation and Termination of the Corneal Wound Healing Response.* Experimental eye research, 2007. **85**(3): p. 305-311.
194. Fini, M.E. and B.M. Stramer, *How the cornea heals: cornea-specific repair mechanisms affecting surgical outcomes.* Cornea, 2005. **24**(8 Suppl): p. S2-s11.
195. Girard, M.T., et al., *Stromal fibroblasts synthesize collagenase and stromelysin during long-term tissue remodeling.* Journal of Cell Science, 1993. **104**(4): p. 1001-1011.
196. Dupps, W.J., Jr. and S.E. Wilson, *Biomechanics and wound healing in the cornea.* Exp Eye Res, 2006. **83**(4): p. 709-20.
197. Smolek, M.K., *Interlamellar cohesive strength in the vertical meridian of human eye bank corneas.* Invest Ophthalmol Vis Sci, 1993. **34**(10): p. 2962-9.
198. Dupps, W.J., Jr. and C. Roberts, *Effect of acute biomechanical changes on corneal curvature after photokeratectomy.* J Refract Surg, 2001. **17**(6): p. 658-69.
199. Roberts, C., *The cornea is not a piece of plastic.* J Refract Surg, 2000. **16**(4): p. 407-13.
200. Roberts, C., *Biomechanics of the cornea and wavefront-guided laser refractive surgery.* J Refract Surg, 2002. **18**(5): p. S589-92.
201. Smolek, M.K. and B.E. McCarey, *Interlamellar adhesive strength in human eyebank corneas.* Invest Ophthalmol Vis Sci, 1990. **31**(6): p. 1087-95.
202. Payrau, P., et al., *[Ultrastructure of the sutural fibers of the cornea of Elasmobranch fishes].* Arch Ophtalmol Rev Gen Ophtalmol, 1965. **25**(8): p. 745-54.
203. Paten, J.A., et al., *Flow-Induced Crystallization of Collagen: A Potentially Critical Mechanism in Early Tissue Formation.* ACS Nano, 2016. **10**(5): p. 5027-40.
204. Zareian, R., et al., *Human Corneal Fibroblast Pattern Evolution and Matrix Synthesis on Mechanically Biased Substrates.* Tissue Eng Part A, 2016. **22**(19-20): p. 1204-1217.

205. Miron-Mendoza, M., et al., *Techniques for assessing 3-D cell-matrix mechanical interactions in vitro and in vivo.* Exp Cell Res, 2013. **319**(16): p. 2470-80.
206. Eastwood, M., et al., *Effect of prcise mechanical loading on fibroblast populated collagen lattices: Morphological changes.* Cell Motil Cytoskel, 1998. **40**: p. 13-21.
207. Karamichos, D., N. Lakshman, and W.M. Petroll, *Regulation of Corneal Fibroblast Morphology and Collagen Reorganization by Extracellular Matrix Mechanical Property.* Invest Ophthalmol Vis Sci, 2007. **48**(11): p. 5030-5037.
208. Coulombre, A., Coulombre, JL, *The development of the structural and optical properties of the cornea*, in *The Structure of the Eye*, G. Smelser, Editor. 1961, Academic Press: New York.
209. Trelstad, R.L. and A.J. Coulombre, *Morphogenesis of the collagenous stroma in the chick cornea.* J Cell Biol, 1971. **50**: p. 840-858.
210. Coulombre, J. and A. Coulombre, *Corneal development. V. Treatment of five-day-old embryos of domestic fowl with 6-diazo-5-oxo-L-norleucine (DON).* Dev Biol, 1975. **45**(2): p. 291-303.
211. Ruberti, J.W., A. Sinha Roy, and C.J. Roberts, *Corneal biomechanics and biomaterials.* Annu Rev Biomed Eng, 2011. **13**: p. 269-95.
212. Myrna, K.E., et al., *Substratum Topography Modulates Corneal Fibroblast to Myofibroblast Transformation.* Investigative Ophthalmology & Visual Science, 2012. **53**(2): p. 811-816.
213. Tse, J.R. and A.J. Engler, *Preparation of hydrogel substrates with tunable mechanical properties.* Curr Protoc Cell Biol, 2010. **Chapter 10**: p. Unit 10.16.
214. Martiel, J.-L., et al., *Chapter 15 - Measurement of cell traction forces with ImageJ*, in *Methods in Cell Biology*, E.K. Paluch, Editor. 2015, Academic Press. p. 269-287.
215. Style, R.W., et al., *Traction force microscopy in physics and biology.* Soft Matter, 2014. **10**(23): p. 4047-55.